Volume 68C
Number 3
July–Sept. 1964

Engineering and Instrumentation

U.S. DEPARTMENT OF COMMERCE

SECTION C

JOURNAL OF RESEARCH

NATIONAL BUREAU OF STANDARDS

Journal of Research
of the
National Bureau of Standards

C. Engineering and Instrumentation

JULY–SEPT. • 1964

VOLUME • 68C

NUMBER • 3

Editor: Martin Greenspan

Associate Editors: G. F. Montgomery, Thomas N. Flynn

Publication dates:
Feb. 15, May 15, Aug. 15, Nov. 15, 1964

JOURNAL OF RESEARCH

The National Bureau of Standards Journal of Research reports research and development in the fields of activity shown at right. Also included from time to time are survey articles on topics closely related to the Bureau's scientific and technical program.

The Journal is published in four separate sections as follows:

A. Physics and Chemistry

Contains papers of interest primarily to scientists working in these fields. Issued six times a year. Annual subscription: domestic, $4.00; foreign, $4.75. Single copy 70¢.

B. Mathematics and Mathematical Physics

Presents studies and compilations designed mainly for the mathematician and the theoretical physicist. Issued quarterly. Annual subscription: domestic, $2.25; foreign, $2.75. Single copy 75¢.

C. Engineering and Instrumentation

Reports research and development results of interest chiefly to the engineer and the applied scientist. Issued quarterly. Annual subscription; domestic, $2.25; foreign, $2.75. Single copy 75¢.

D. Radio Science (formerly Radio Propagation)

Published in cooperation with U.S. National Committee of URSI. Presents papers in radio propagation, communications, and radio science generally. Issued monthly. Annual subscription: domestic, $9.00; foreign, $11.50. Single copy $1.00.

U.S. DEPARTMENT OF COMMERCE
Luther H. Hodges, Secretary
NATIONAL BUREAU OF STANDARDS
A. V. Astin, Director

The National Bureau of Standards is a principal focal point in the Federal Government for assuring maximum application of the physical and engineering sciences to the advancement of technology in industry and commerce. Its responsibilities include development and maintenance of the national standards of measurement, and the provisions of means for making measurements consistent with those standards; determination of physical constants and properties of materials; development of methods for testing materials, mechanisms, and structures, and making such tests as may be necessary, particularly for government agencies; cooperation in the establishment of standard practices for incorporation in codes and specifications; advisory service to government agencies on scientific and technical problems; invention and development of devices to serve special needs of the Government; assistance to industry, business and consumers in the development and acceptance of commercial standards and simplified trade practice recommendations; administration of programs in cooperation with United States business groups and standards organizations for the development of international standards of practice; and maintenance of a clearinghouse for the collection and dissemination of scientific, technical, and engineering information.

Institute for Basic Standards. Electricity. Metrology. Heat. Radiation Physics. Mechanics. Applied Mathematics. Atomic Physics. Physical Chemistry. Laboratory Astrophysics.* Radio Standards Laboratory: Radio Standards Physics; Radio Standards Engineering.** Office of Standard Reference Data.

Institute for Materials Research. Analytical Chemistry. Polymers. Metallurgy. Inorganic Materials. Reactor Radiations. Cryogenics.** Office of Standard Reference Materials.

Central Radio Propagation Laboratory.** Ionosphere Research and Propagation. Troposphere and Space Communications. Radio Systems. Upper Atmosphere and Space Physics.

Institute for Applied Technology. Textiles and Apparel Technology Center. Building Research. Industrial Equipment. Information Technology. Performance Test Development. Instrumentation. Transport Systems. Office of Technical Services. Office of Weights and Measures. Office of Engineering Standards. Office of Industrial Services.

*NBS Group, Joint Institute for Laboratory Astrophysics at the University of Colorado.
**Located at Boulder, Colo.

Order all publications from the Superintendent of Documents
U.S. Government Printing Office, Washington, D.C., 20402.

Use of funds for printing this publication approved by the Director of the Bureau of the Budget (June 19, 1961).

JOURNAL OF RESEARCH of the National Bureau of Standards—C. Engineering and Instrumentation
Vol. 68C, No. 3, July-September 1964

Response of Highly Precise Balances to Thermal Gradients[1]

L. B. Macurdy [2]

(February 11, 1964)

As small thermal gradients often cause large instabilities in the indications of more precise balances, an investigation was made of the effects of various types of thermal gradients on several such balances. It was found that the largest instabilities result when the top of the balance case is cooler than the bottom, and further that the best performance is obtained when air at the top is warmer, rather than in thermal equilibrium throughout the case. The desired thermal gradients, i.e., top warmer than the bottom, can be achieved through proper insulation of the balance case, with provision for some flow of heat in through the lower front of the case and entrapment of warm air at the top of the case. These results apply directly to the equal-arm type of balance; a separate study would be required for balances of different configuration. However, the general nature of the effects of thermal gradients is applicable to some degree to all types of more precise balances.

1. Introduction

It is a common observation that the rest points of more precise balances may change for no apparent reason. Often the changes are so large that weighing must be discontinued until more stable conditions exist. These changes may be caused by a variety of factors, as has now been semi-quantitatively determined from experimental observations (fig. 1). An obvious approach to improved balance performance is to eliminate or reduce as many of the disturbances as possible, starting with the largest; that is, the effects of certain temperature gradients. This paper therefore reports the results of investigations, and contains recommendations for insulating balance cases so as to create the desired thermal conditions. Previous papers have dealt with the effects of humidity [1] [3] on balance performance, with oscillation of the pan assembly [2], and with means of reducing errors arising from the arrestment mechanism [3]. Carmichael [4] has studied the effects of heat on fused silica microbalances.

The changes that may occur in the rest point of a balance are illustrated by figure 2, plots of mean successive rest points of a variety of balances. Long-term (½ hr or more) periodic effects can clearly be seen; short-term fluctuations, with a period of about 8.5 sec, have also been observed. No explanation, prior to this study, had been given for these periodic effects, other than to ascribe them to air currents, thermals, transient effects, or to refer to them as random errors. It is shown that the periodic effects are primarily the result of air currents caused by thermal gradients, and are especially severe when the top of the balance case is cooler than air at the bottom. These currents may affect a 200-g balance by rapid erratic changes as large as 0.6 mg.

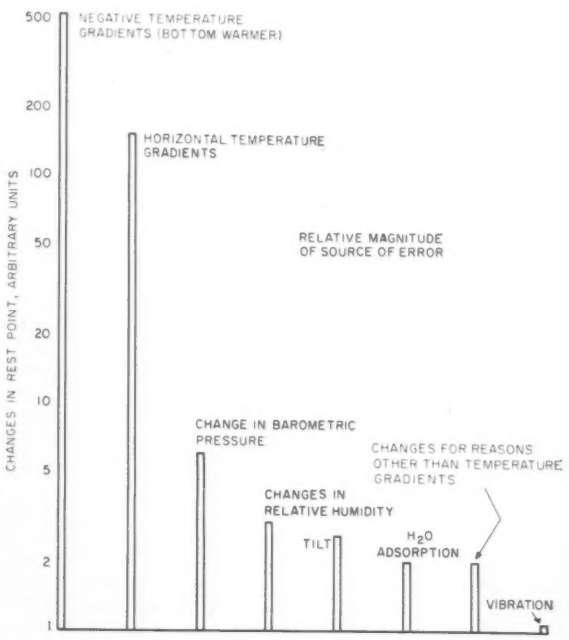

FIGURE 1. *Residual sources of error after normal precautions to insure weighing precision.*

Changes in sensitivity were made very small.

[1] An oral discussion of this material was presented at the NBS Mass Measurement Seminar, June 21, 1962.
[2] Present address: Mettler Instrument Corp., Princeton, N.J.
[3] Figures in brackets indicate the literature references at the end of this paper.

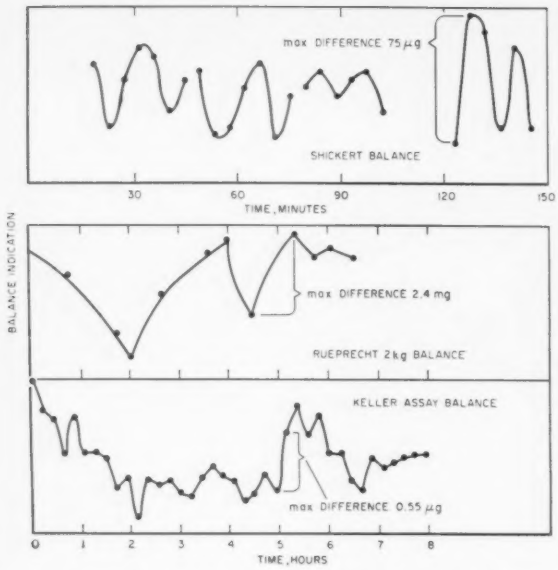

FIGURE 2. *Changes in rest point during weighings in air show periodic effects.*

Data for the Reuprecht and Keller balances are from the NBS Mass Laboratory; the curve for the Shickert balance is from an elaborate treatment of data by Thiesen, Etudes sur la Balance, Traveaux et Memoires du Bureau International des Poids et Mesures 5, 1886.

The present studies were conducted with balances of the equal-arm type, and are not directly applicable to the single-pan two-knife-edge type. Single-pan balances are generally asymmetric in both geometry and mass distribution. Because of this more complicated arrangement, some modification of the tests described below would be required to evaluate quantitatively the response of single-pan balances to thermal gradients.

2. Preliminary Studies

Preliminary experiments were conducted to establish the nature of the effects of thermal gradients on balance performance. The use of "sails" and different attitude of the pans showed that disturbances from the movement of the air within the balance case caused a large portion of the effects observed with changes in thermal gradients. Relatively large effects were associated with small departures from nearly isothermal conditions.

Complex transient motions of air, initially stable within the balance case, occur when the balance is exposed to a thermal gradient (arbitrary in direction and magnitude) external to the balance. Initial stability within the balance case is achieved if and only if the density is constant in every horizontal layer and a vertical temperature gradient exists which is more positive (temperature increasing with height) than that required for adiabatic stratification [5]. While heat flow (as a result of external gradients) in the vertical direction may increase the stability [6], heat flow into the case through the side walls results in motion of the air within the case. The nature of this motion is a function of many variables, including the magnitude of the vertical gradient, the magnitude of the horizontal gradient, the manner and duration in which the horizontal gradient is applied, the transport properties of the air enclosed, the materials and surfaces of the sides, etc. The motion can vary from minor oscillations to violent circulatory flow, which may be either periodic or steady, periodic effects arising from either normal oscillations associated with a disturbed stable system returning to equilibrium or the reaction of the flow with the boundaries [7].

Because the movement of air can fluctuate between the various principal modes of motion, the thermal conditions within the balance case in these experiments were limited to horizontal end-to-end and top-to-bottom thermal gradients, front-to-back gradients being eliminated by careful control of the environment. This created rather simple air motions, and allowed analysis of the effects of the established gradients. In these experiments the horizontal end-to-end gradients were parallel to the longer side of the balance. It is in this direction that the effects of thermal gradients appear to be most severe.

3. Steady State Tests

A microchemical balance having a glass case with wooden frame was selected for the steady state tests. The period of the beam was about 30 sec, averaging out the effects of high-frequency air movements. Thermal changes of longer periods were controlled by manual adjustment of the voltage to lamps used as heat sources.

The basic experimental arrangement used in this phase of the study is shown in figure 3. Multiple-junction copper-versus-constantan thermocouples were arranged within the balance case to indicate back-to-front, end-to-end, and top-to-bottom air-temperature differences. The front-to-back and end-to-end gradients were measured about one-third of the way up the case. A potentiometer-galvanometer system was used to determine the electromotive forces developed by the various thermocouples. Temperature gradients as small as 0.002 °C could be detected with this system.

Light bulbs were located at the sides and top of the balance, and the voltage to the bulbs was varied so as to establish and maintain the desired thermal gradients. A series of measurements at any set of thermal conditions consisted of four sets of consecutive readings of the turning points of the balance indicator and readings of the various thermocouples. Four sets of readings were taken to insure that a relatively steady relationship was being maintained. The balance pans were not loaded during the measurements.

FIGURE 3. *Apparatus for thermal studies and for tests for balance response to relative humidity* [1].

During runs the aluminum shield (upper left) is located in front of the balance to avoid disturbances from the observer.

The results of these tests are summarized in figure 4. At the bottom of this figure are shown the horizontal end-to-end and vertical thermal gradients; the rest points in response to the changing thermal conditions are shown at the top. The response of the balance to the horizontal gradient is shown for three levels of the vertical gradient. On the left the horizontal gradient was varied while the top of the balance was about 0.1 °C warmer than the base; in the center the horizontal gradient was varied over a similar range while the vertical gradient was held at zero; and on the right the horizontal gradient was changed while the bottom was slightly warmer than the top. It is obvious from the curves that under these controlled conditions the balance responds systematically to changes in the horizontal end-to-end gradient, and that the magnitude of the response depends on the vertical gradient. When the top of the balance was warmer (left) the range in rest points as the end-to-end gradient was changed was 38 μg. With no vertical gradient (center) a similar change in end-to-end gradient produced a 68 μg range, and when the bottom was warmer than the top (right) the range increased to 139 μg. It should be noted that these relatively large effects are produced by rather small thermal gradients, and would be sufficient to stop any precise weighing on a balance intended to weigh to a few micrograms.

To correlate the thermal gradients with the creation of air currents inside the balance case, data were taken with three different pan areas as the horizontal gradient was increased from near zero to 0.6 °C. As the total pan area was increased from 2.5 to 21.5 in.², the balance deflection increased markedly. The results of this test, shown in figure 5, indicate that the balance response resulting from thermal gradients is related mainly to movement of air within the balance case, and not to thermal effects on the beam.

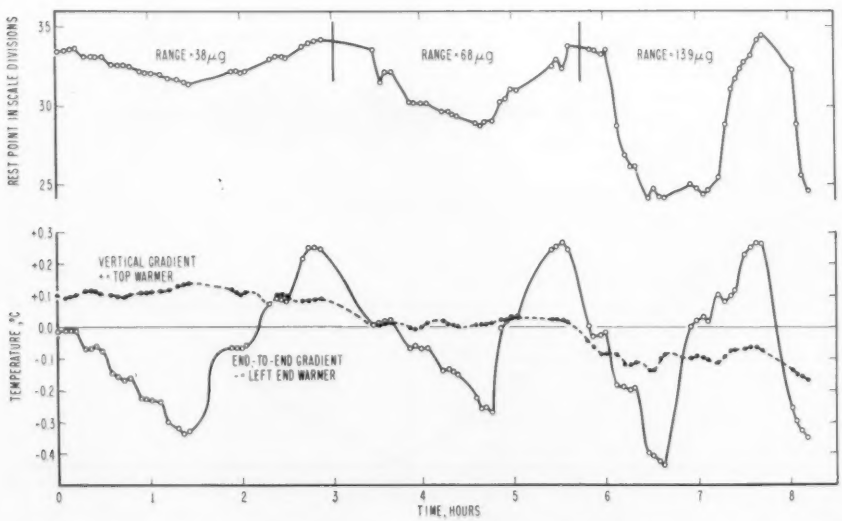

FIGURE 4. *Curves showing the change in rest point (top) as the thermal gradients changed.*

As the top went from warmer to cooler than the bottom (l. to r.) the balance response to the same horizontal gradient increased.

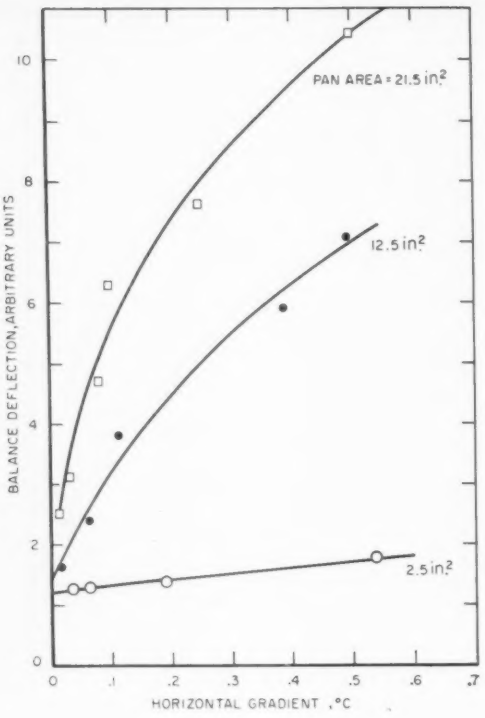

FIGURE 5. *Changes in indication with change in pan area indicates a "sail" effect.*

Tests were also made in which the top of the balance was first cooled and then allowed to return to a condition with the top warmer. The results of this type of test are shown in figure 6. At the left the top of the balance is warmer, and the balance indication is stable. As the vertical gradient decreased to zero, instabilities commenced which reached a peak when the top was about 0.4 °C cooler than the bottom. As the top was allowed to warm, the instabilities decreased, and stability was reached when once again the top was warmer than the base. End-to-end gradients were eliminated as far as possible during these tests. The time represented is about 4 hr, and full scale of the tracing is 0.6 mg.

4. Heat Pulse Tests

Pulse techniques are widely used in the testing of physical systems. In a balance the response to a disturbance will consist of one or more components each having its own amplitude and frequency. At the start of the pulse all amplitudes are zero; that is, the phase difference is zero at time zero. The separate components will show peaks in the response depending on their frequency.

In these tests a standard 5 min heat pulse was provided by two 75-w bulbs with reflectors placed 6 in. from the left end of the balance. A servo following system recorded the balance indication. Components with periods shorter than 5 min would be obscured in this test, but longer periods would be recorded as peaks. The reproducibility of the heat pulse test is clearly demonstrated by figure 7, showing the tracings produced by three consecutive pulses applied to a balance completely covered with black poster paper and the top half insulated with cork.

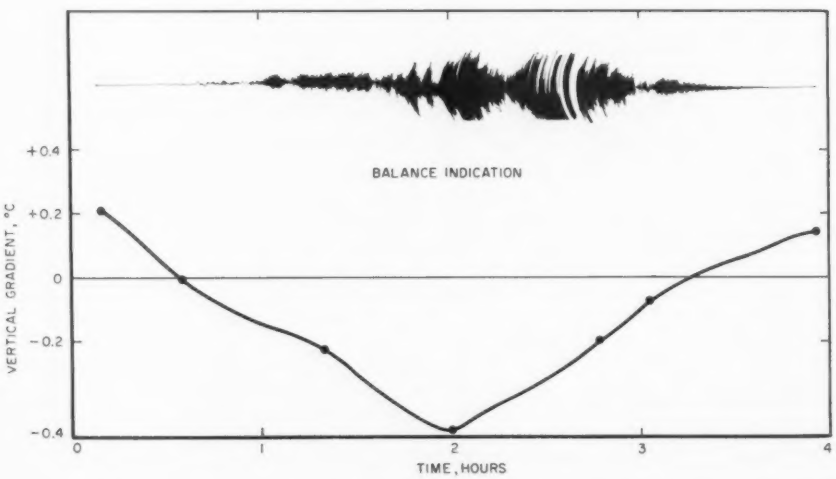

FIGURE 6. *The servo-recorded balance indication starts with the top warmer. As the top is cooled, disturbances begin, reaching a maximum in excess of the 0.6 mg range of the recorder. As the top of the balance is allowed to warm and the vertical gradient becomes positive again, the disturbance disappears. Temperature differences between top and bottom are shown in the lower curve, top warmer being labeled positive.*

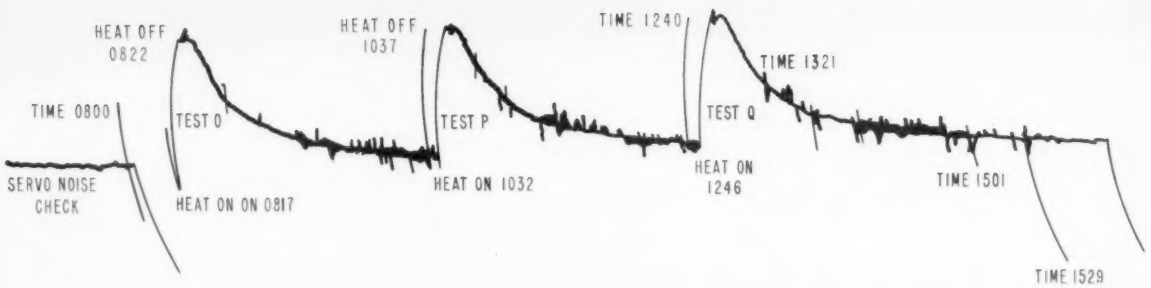

FIGURE 7. *Three successive 5-min heat pulses produced similar response in the balance indication.*

The response of the balance to the heat pulse while covered with various insulations is shown in figure 8. Curve A represents the balance without insulation. The indicator went off scale in 1.25 min and when the heat was removed it returned to equilibrium quite rapidly. B is with the entire case covered with black paper, C with black paper over the entire balance and 0.25-in.-thick cork on the top and halfway down the sides, D with black paper over the entire balance, and cork full length on the two ends and halfway down the front and back and over the entire top. Curve E represents a balance completely covered with black paper and cork; F, cork on the top and sides and halfway down the front and back; G, a balance completely covered with aluminum foil; and H, completely covered with cork and aluminum foil.

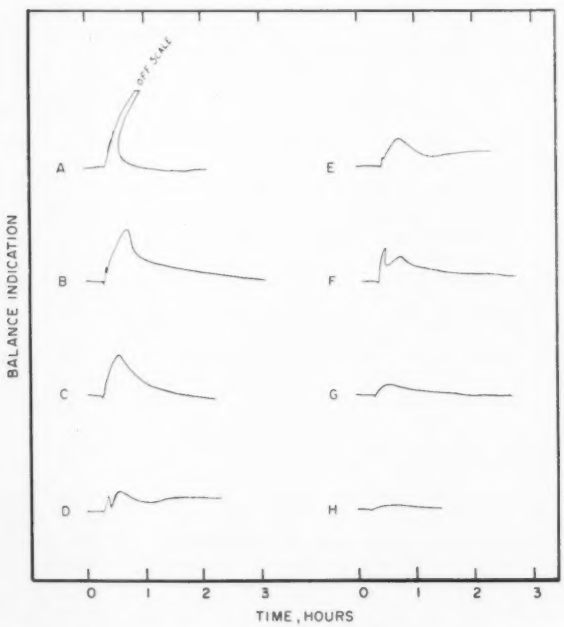

FIGURE 8. *Typical curves showing the response of the same balance with different insulations to the heat-pulse test.*
See text for description of the insulations.

Curve F is of particular interest in that it has a pronounced component of somewhat longer period than that of the initial response with the result that the interaction damps the amplitude. This configuration of insulation is used in the NBS Mass Laboratory because of its marked attenuation of disturbances.

While curves G and H show a reduction in response, this amounts to a reduction in the amount of heat entering the balance. Such insulation has the disadvantage that it tends to bring the balance into an isothermal condition, rather than the more favorable situation with the top of the balance warmer.

5. Conclusions and Recommendations

The presence of adverse thermal gradients can cause major instabilities in the performance of precise equal-arm balances. The effects of horizontal end-to-end gradients are intensified when there is no vertical gradient, or when the top of the balance is cooler than the bottom. Ideally, no horizontal gradients should be present, and air at the top should be somewhat warmer than at the bottom. From curves representing the performance of three different balances it appears that a vertical gradient (top warmer) of at least 0.3 °C/m, or 0.1 °C for a small analytical balance, provides increased stability. Creation of the proper thermal conditions reduces the possibility of weighing being disrupted or halted by rapid changes in rest point.

Elaborate and costly precautions need not be taken to provide the desired thermal gradients. Inexpensive insulations can be used, and fitting the insulation to the balance can be done with minimum effort. As mentioned, the scheme used at the NBS Mass Laboratory consists of cork over the top and down the sides of the balance, and down only the top half of the front and back. This arrangement provides ready viewing of the pans and pointer, and allows ample heat flow inward from the observer as well as reducing heat flow out from the top of the balance. When the observer remains in front of the balance, the heat coming in from the observer warms some of the air, which rises to the top of the case and establishes the desired thermal conditions. It was found that when more than half of the front and

back was covered the stability decreased. With the recommended arrangement of insulation, high-grade measurements can be made under crowded conditions without noticeable effects from persons walking about near the balance. For many years prior to the use of insulation it had been necessary to prohibit activity in the room during weighing.

As already mentioned, it was found necessary during this study to shield the balance from unequal radiation from the walls. Other thermal conditions within the room can also affect the balance. Rapid influx of cool air from an air-conditioning unit could impress an undesired thermal gradient upon the balance. The traditional arrangement of the equal-arm balance operates most advantageously during conditions when the temperature of the room is rising slowly, and the temperature of the balance lags slightly behind.

This observation follows directly from the conclusions on vertical temperature gradients. Because most of the mass and therefore heat capacity is at the bottom of a balance, it is the bottom that has the greater time lag to ambient room temperature changes. This discussion explains equally that serious disturbances occur as the temperature of the room falls below that of the balance.

Small light bulbs that are placed within or close to some balances to illuminate the scale probably should be removed, as should the transformers associated with these lights. Balances having metallic corner posts should have these posts insulated on the inside to reduce the gradual release of heat from the posts to air within the case. Symmetrical design in general reduces the effects of various disturbances, and pans should be located midway between the front and back.

The heat-pulse test was suggested by Horace A. Bowman of the Mass Laboratory, who devised the instrumentation and conducted the experiment. H. E. Almer performed some of the remaining experiments. The author is also indebted to D. Baker for editorial assistance.

6. References

[1] Response of microchemical balances to changes in relative humidity, H. E. Almer, J. Res. NBS **64C** (Eng. and Instr.) 281–285 (Oct.–Dec. 1960).

[2] Gimbal device to minimize the effects of off-center loading on balance pans, H.A. Bowman and L. B. Macurdy, J. Res. NPS **64C** (Eng. and Instr.) 277–279 (Oct.–Dec. 1960).

[3] Minimization of the arrestment error in one-pan, two-knife balance systems, H. A. Bowman and H. E. Almer, J. Res. NBS **67C** (Eng. and Instr.) 227–235 (July–Sept. 1963).

[4] Design and performance of a fused silica microbalance, Hugh Carmichael, Can. J. Phys. **30,** 524–555 (Sept. 1952).

[5] Essentials of Fluid Dynamics, Ludwig Prandtl, Blackie & Son, London, 1953, pp. 7, 17, 383.

[6] Boundary Layer Theory, Hermann Schlicting, McGraw-Hill Book Co., N.Y. 1960, p. 431.

[7] Ibid., ch. 11.

(Paper 68C3–158)

JOURNAL OF RESEARCH of the National Bureau of Standards—C. Engineering and Instrumentation
Vol. 68C, No. 3, July–September 1964

A Direct-Reading Two-Knife 50-Pound Balance of High Precision Suitable for State Weights and Measures Laboratories

H. E. Almer, H. A. Bowman, M. W. Jensen, L. B. Macurdy,[1] H. S. Peiser, and B. Wasko[2]

Performance requirements are detailed for robust fast-operating 50-pound balances precise to 1 part in about 500,000, under less than ideal weighing conditions.

Careful studies of design and configuration of large-capacity balances lead to the conclusion that the type of balance that can most easily be designed to fulfill these requirements is the one-pan, two-knife, constant-load balance.

The detailed design and construction of such a balance is described. Performance tests demonstrate that this balance conforms to the requirements. Under good operating conditions precisions of a few parts in 10,000,000 can be achieved.

1. Introduction

The National Bureau of Standards has been advocating systems for accurate rapid mass measurement, including highly constant mass standards[3] and precise quick-weighing balances. In response to requests for cooperation, two manufacturers (the Mettler Instrument and Voland Corporations) have built balances of 50-lb and smaller capacities. Since it is the 50-lb balance that extends the high-precision direct-reading balance into a new range of capacities where no such instruments were previously available, it has been selected for the subject of this paper.

The primary purpose of this paper is to describe the design and construction of a robust but precise balance for loads up to 50 lb. The intention in section 4 below is to give all relevant details of the balance as built by the Voland Corporation so that a similar instrument can be constructed by others.

To some readers, however, details of construction may not be so interesting as the considerations on which unconventional features of configuration and design are based. To give a clear, if mostly qualitative, statement of these considerations is the purpose of section 3. Detailed features of these considerations are presented in individual specialized papers referred to in the text to the extent that these have appeared in the literature.

The stimulus to test new design schemes came from the need for large-capacity, robust, precise balances to be used for weight calibration in weights and measures offices of States. The performance requirements for balances intended for this purpose are therefore given in section 2 with a brief introductory statement on responsibilities in the regulation of trade. It is not the intention of the authors, however, to suggest that the balance here described has no other potential uses. On the contrary, the need to measure large masses precisely is probably even greater in, for example, space-age industries concerned with missiles and satellites. Moreover, the new balance with its greater precision is able to provide data on mass inconstancy, evaporation rates, and adsorption or corrosion reactions within shorter test intervals.

The final short section 5 (Performance Test) describes work at the National Bureau of Standards, where not only was the adjustment carried out with considerable care, but weighing conditions are better than can be expected to prevail routinely in industry or State offices of weights and measures. It is proper that a far higher precision has been demonstrated to be obtainable with the balance than is specified in the performance requirements (sec. 2). The favorable results are indicative of the inherent soundness of the considerations on design and configuration (sec. 3). More important to many readers will be the authors' opinion that the balance as built is a robust simple stable device which a technician can learn to operate easily and quickly and on which the mass value can be read directly without intermediate observations or computations.

2. Performance Requirements

2.1. Background

The Organic Act of the National Bureau of Standards (31 Stat. 1449, as amended) includes the authorization for "The custody, maintenance, and development of the national standards of measurement, and the provision of means and methods for making measurements consistent with those standards . . . ".

[1] Present address Mettler Instrument Corporation, Princeton, N.J.
[2] Vice President, Engineering, Voland Corporation, New Rochelle, N.Y.
[3] In connection with the program, the NBS itself and two States (Hawaii and Alaska) have been supplied with highly constant mass standards of new design in series with decimal-fractional weights down to one millionth of a pound.

Consistency of measurement in trade and commerce throughout the Nation has been maintained through the activities of the several State weights and measures offices. The weights and measures statute of practically every State requires that the basic measurement standards of the State be submitted at least once in 10 years for evaluation by the National Bureau of Standards. The responsibility of relating these standards to the field testing equipment is assumed by the weights and measures laboratory of a State.

2.2. The State Weights and Measures Laboratory

The values of State mass standards are reported by the National Bureau of Standards to each of the States which in turn relates these standards to the measurements in trade and commerce within that State. Efforts of the Bureau have recently been directed toward the refinement of laboratory instruments and the simplification of their operation at the weights and measures laboratories of States.

Because the 50-lb standard is the largest mass standard normally submitted to the National Bureau of Standards by a State, even though 500-, 1,000-, and 2,500-lb test weights are in regular field use (these larger weights are compared against an accumulation of 50-lb weights), special attention has been directed to the development of a 50-lb capacity, high-precision balance that would afford excellent and repeated results with a minimum of operational technicalities and calculations.

To this time, the State laboratory has been capable of making measurements at the 50-lb range to a part in about 175,000. Such measurements are being made on a traditional and unadorned equal-arm balance, normally through substitution comparison.

2.3. A Direct-Reading Balance

For a number of years there has been on the market and in laboratory use a one-pan, two-knife balance that offers high precision, direct reading, and rapid operation through a damping device. Such balances have been of comparatively small capacity, but the simplicity of design seemed to be adaptable to a capacity of 50 lb, where the advantage of eliminating calculation could increase the accuracy of the values obtained for the 500-, 1,000-, and 2,500-lb test weights, and the advantage of speed of operation could encourage more frequent calibration of these large weights.

Following studies at the Bureau, design and performance characteristics of a prototype direct-reading 50-lb balance were established as follows:

a. Beam Design

One-pan, two-knife construction with a 50-lb counterpoise fixed to the beam so all weighings would be made at the balance capacity.

b. Operating Range

To operate normally at loads of 50, 30, 25, 20, and 10 lb, but with provision to operate at any load above 5 pounds and up to and including 50 pounds.

c. Knife-Edge Parallelism

Adjustable or fixed knife edges to provide highly precise parallelism for a period up to 10 years under normal use.

d. Balance Weights

Standard weights, either built-in or appropriate for hand application, to meet NBS Class S–1 requirements, such weights

(1) to be of such denominations as to approximately equal the difference between the nominal test load and 50 lb, and

(2) to be applied to that side of the balance to which the test load is applied, and, if built-in, with the weight value thus applied to be indicated on the balance dial in pounds and decimal fractions of the pound.

e. Indicating Element

An indicating element which, through an optical read-out with vernier, provides −70 to +70 scale divisions, readable to 0.1 division, where the 0.1 division equals 10^{-5} lb or 4.5 mg.[4]

f. Scale Adjustment

Means of adjusting the scale reading by at least 0.0005 lb.

g. Damping

A damping mechanism to bring about beam stability for a precise reading within 50 seconds of beam release.

h. Arrestment

An appropriate arrestment mechanism so designed as to prevent damage to the mechanism itself or to any other balance component under normal conditions of loading up to 60 lb.

i. Balance Pan

A weight-receiving balance pan so constructed as to provide at least 100 $in.^2$ of area for weight accommodation with at least 7 in. of clear height, so marked as to facilitate centering of the load, yet so designed as to present a minimum surface to be acted upon by air currents.

j. Weight-Transfer Mechanism

A weight-transfer mechanism to be provided by which the standard weight (or summation weight) is moved into a storage position inside the balance case and a test weight is transported from outside the balance onto the balance pan, or vice versa.

k. Balance Case

The balance to be enclosed in a case that provides adequate isolation from drafts and thermal dis-

[4] Compare sections 4.5 and 5 below.

turbances and, through windows or doors, convenient access to the pan; the case to be of good appearance and of such material and design as to provide protection for at least 20 years.

l. Limit of Extraneous Effects

Balance shifts caused by extraneous magnetic effects, change in air density up to 2 percent, and change in relative humidity up to 10 percent to be within the limits of precision prescribed for the balance.

m. Precisicn

Standard deviation of repeated mass measurements at time of delivery to the National Bureau of Standards to be not greater than 1.6×10^{-5} lb or 7 mg.

n. Readability

Readable unit to be not greater than 1×10^{-5} lb or 4.5 mg.

o. General Design Requirement

The balance to be so constructed as to demonstrate the perfection expected of high-precision balance manufacture, and, at the same time, to be sufficiently simple of operation and rugged of construction as to give excellent results over a long period of time under conditions of use and manipulation that are less than ideal for precision weighing.

3. Considerations on Design and Configuration of Large-Capacity Balances of High Precision

3.1. General

The work performed by Gould [1][5] on the perfected design of the conventional two-pan, three-knife type kilogram balance raised the state of the art to a height not previously achieved by weighing instruments intended for use at the maximum-attainable level of precision. Nevertheless, the improvement in precision obtained over previously existing instruments of this type was modest, compared with the magnitude of the effort and unsurpassed skill expended. One suspects, therefore, that the design of the two-pan, three-knife balance may be near its optimum, and that additional developmental effort would produce little improvement in precision. In the view of the present authors, it has appeared probable, at least, that any major improvement to be achieved in the near future will follow a careful study of residual weighing errors. Such a study should certainly be concerned with methods of elimiaating or quantitatively correcting these errors. It is equally desirable to determine whether there is greater resistance to such errors inherent in a balance configuration different from the conventional two-pan, three-knife type. Naturally, in discussions of alternative systems it is essential to make due allowance for new or enhanced weighing errors. Moreover, because of the possibility of unsuspected new weighing errors being introduced by a change in configuration, it is most desirable to accompany such studies with early experimental verification.

Many good studies of errors have been made and reported in the literature [2]. They are not, however, addressed to the question of configuration. In this section, therefore, some of the recent studies conducted at the National Bureau of Standards, with the primary aim of solving problems of configuration, will be described. As will be seen, these are relevant to larger-capacity balances. Moreover, their basic applicability and correctness could more easily be tested experimentally on a 50-lb balance than on a 1-kg instrument that necessarily involves the construction of parts of great precision and delicacy.

The principal alternative to the two-pan, three-knife balance configuration is the one-pan, two-knife substitution balance [3]; its general principle of operation is well known. A fixed counterweight rigidly attached to one end of the beam balances a loaded suspension coupled to the opposite end of the beam by means of conventional end-knife assembly. The beam oscillates about a knife located between the end knife and the center of gravity of the counterweight. Ordinarily such an instrument has a group of small weights hung on the suspension. These "built-in" weights are of such magnitude that their summed moment about the center knife precisely balances the moment of the counterweight. When an unknown weight is added to the pan, the system becomes unbalanced and balance is restored by removing from the suspension an appropriate number of the "built-in" weights. The mass of "built-in" weights removed from the suspension to regain balance approximately equals that of the unknown weight. The residual mass difference is indicated on a scale calibrated directly in terms of mass.

3.2. Errors Due to Varying Ambient Conditions

It has been shown that variations in relative humidity [4] and temperature [5] inside balance cases may result in instrumental drift systematic with these two parameters. Housings for high-precision balances are designed to inhibit changes in temperature and humidity. Such changes thereby are made to progress slowly so that any associated motion of the beam will occur slowly. It should be noted that a precise weighing consists of the determination of a difference in load so that the absolute value of any one balance indication has no direct effect on the result [6]. The stability of the balance is a requirement only over the time taken to complete the observations constituting one weighing. A general tendency in modern instrumentation is to combat slow instrument drift by measurement systems with fast response. Existing balances of maximum attainable precision suffer from slow response. Frequencies of 10^{-2} c/s are not unusual for the oscillations of the beams of such balances.

[4] Figures in brackets indicate the literature references at the end of this paper.

It has been pointed out [7] that a major portion of the experimental interval is taken up by these very low-frequency oscillations. The balance designer must therefore carefully consider how much he can increase the beam frequency of a balance without introducing new overriding weighing errors.

In an idealized knife-edge balance, oscillating about its center knife edge, $\omega=\sqrt{K/I}$, where ω is 2π times the frequency of oscillation of the system, I is its moment of inertia, and K is the stiffness, which is inversely proportional to the balance sensitivity. The fast response system desired can be achieved by making ω much larger than in presently existing high-precision balances. Ideally, this should be accomplished without sacrificing sensitivity. Thus the aim is for both a large ω and a small K. Contrary to opinions often loosely expressed, these are not contradictory requirements. Minimizing I in the design of a balance assures a maximum ω for any given stiffness. A large reduction of I can be achieved by reducing the arm length. Most of the other effects of arm-length reduction, discussed below, are beneficial, but new demands arise on knife-edge parallelism. Before elaborating on these demands the discussion on ambient conditions will be concluded.

There are many methods of combating the effects of varying ambient conditions on balance operation. The housing may be insulated and thermostated; the relative humidity may be controlled; the balance itself may be constructed of nonhygroscopic materials and materials of very low coefficients of thermal expansion. All of these contrivances, and many more, have virtues and should be carefully considered by the balance builder. However, besides the importance of a fast-response measuring system, as discussed above and best achieved by a short-arm length, a most significant requirement for reducing the adverse influences from changes in ambient condition is that of rapid temperature equilibration along the beam. Any change in horizontal temperature gradient will change the effective arm ratio; to minimize such changes is another important reason for building beams with short-arm lengths. High thermal conductivity and large cross-sectional areas are also beneficial, so that the horizontal gradient will always be so small as to maintain an arm-ratio precision greater than that of the balance precision desired. It is acknowledged that this analysis differs from those of many previous balance designers who have sought high sensitivity by long, light-weight beams that are sensitive to very slight changes in temperature gradients and even mechanically deform under load. The lack of reproducibility of such deformations is a serious additional source of error in long-beam balances, and is further discussed below.

Vertical temperature differences or gradients will not be discussed in this paper, partly because they are believed to affect all beam balances similarly, and partly because they are the subject of an adjoining paper [5]. Without proof or experimental demonstration, it can be stated here that a positive vertical-height gradient (top of balance warmer) or equivalent temperature difference of the order of 10^{-3} to 10^{-2} °C/cm is thought to be desirable for optimum performance of all balances.

3.3. Errors Due to Knife Edges

For a high-precision system, one attempts to develop the best quality knives. However, not even knives of highest quality are ideally perfect, and it is these slight departures from perfection that are of concern. Careful distinction should, in the authors' opinion, be made between errors from noncylindrical edges and those from curvature of the edge itself.

It should also be pointed out that in our discussion we assume that rigidly joined parts cannot move discontinuously relative to one another. For example we assume that knife edges do not move in their mountings. The assumptions can be illustrated by another example: in this discussion elastic or plastic deformation are considered, but relative movements at bolts are not. Inasmuch as real balances might be subject to engineering deficiencies permitting movements of the excluded kind, the following discussion can not be successfully applied.

The National Physical Laboratory [8] states that "in practical use the edge assumes transversely a rounded form of fairly regular curvature." Although the actual radius of this curvature may be disputed, its "regular" characteristics are universally recognized as a requirement for satisfactory balance operation. The knife behaves much like a right circular cylinder rolling on a plane surface [9], and gravimetric methods have been worked out for the measurement of the effective radius of this "regular" radius. When the knife does not remain cylindrical, it may assume an elliptical profile. The effect of elliptical knives is to change the effective arm length of the beam; in addition Corwin [10] has demonstrated that rest points calculated from observed turning points will be in error by an amount related to the amplitude of the oscillations of the beam that occur while turning points are being observed. This portion of the ellipticity error would be eliminated if the balance were always observed at zero amplitude. This could be accomplished by damping the oscillating system, and making observations on a near-motionless beam. The new error of starting friction on the knife is introduced by this type of operation. For all good knife-plane combinations tested, this error could not be measured and must therefore be less than 1 in 10^{-10} in weighing precision. The relevant tests for starting friction consist of an analysis of the deflection/time curves taken from a swinging balance with a highly sensitive read-out device [7]. Starting friction causes nonsinusoidal motion which has not been observed to the precision stated. (See also 3.6.3 below.)

Since a real knife edge is not ideally straight [10], the axis about which it rotates is not uniquely defined by the edge. It is partially defined by the longitudinal profile of the gross curvature and the load. Thus, the "regular" characteristics referred to in the foregoing paragraph may be distorted by this curvature. Damped operation will not assist here,

but use of a constant load balance will to some extent, because the loading of a curved surface against a hard flat surface will tend to straighten out the curve by an amount dependent upon the load. In making gravimetric measurements on knife-edge radii, Hodsman and Chapell [11] found the calculated radius to be smaller under conditions of larger loads. It is believed that they were experimenting on curved knives, and that the true explanation of the phenomena was that the knives were merely straightening out under load against the flat.

So far discussion has centered on errors arising from imperfection of the knife edges themselves. At least equally important in practice are those errors arising from the imperfection of mounting of the knife edges on the balance.

In conventional balance design, the center knife in the beam points downward, and the two end knives point upward. The pan assemblies in the simplest balances are suspended by vertical rods from flats (polished on their lower side) which rest on the upward-pointing end knives. The arm length of the balance is the perpendicular distance from the center knife edge to the point on the end knife at which the suspended pan assembly load is effectively concentrated. The vertical rods connecting the pan assembly to the load flat above may be shifted from their intended vertical position by, for example, a slight error in centering when placing the load on the pan. When such a shift occurs, the effective point of support then moves along the end knife in one direction or the other. If the end knife is parallel to the center knife, no error occurs; but if it is not, motion of that point causes a change in effective arm length.

The knife-edge error just described is measured by suspending the same load, first from one end of the terminal knife and then from the other end, and noting the variation in response of the balance to the action of the load at the two different moment arms. This test is sensitive because circumstances cannot arise in which the effective point of suspension traverses more than a small fraction of the length of the end knife. Nevertheless, no practicable method is known for adjusting knives so that the parallelism error is less than the attainable sensitivity of 1 in 10^8.

Thiesen [12] solved this problem by a device referred to as the Thiesen compensator which immobilizes the effective point of suspension on the end knife regardless of the verticality (or lack of it) in the suspension rods. He devised a universal coupling by placing two knife edges at right angles, one pointing upward, the other, downward. The lines of the knives mutually bisect in space; interference is avoided by removing the center sections of one knife and its associated plane. All bearing planes are mechanically constrained to coplanarity. The upward-pointing knife is the end knife on the beam, and the downward-pointing knife is attached to the suspension. The compensator, when installed, permits the suspension to swing in any horizontal direction without causing intolerable motion of the effective point of suspension on the end knife. Gould [1] and one or two other designers failed to utilize this principle because of various mechanical difficulties; however, we firmly believe that almost any one of numerous modern versions of the Thiesen compensator should be made a part of any high precision balance.

In the two-knife balance, parallelism errors are further reduced simply because the counterpoise is rigidly and permanently connected to the center knife. The instrumental condition of providing three parallel lines is thus eliminated, at least to a first approximation. In this type of balance a center-line knife edge and an effective point of terminal suspension are provided. A Thiesen compensator is still required to prevent movement of the effective point of support.

3.4. Symmetry

If one asks a metrologist to state a few general maxims for the science and art of precise measurement, he will probably include reference to symmetry; not only for the scheme of measurement, but for the design of measuring instruments. The two-pan, three-knife balance is perhaps the most perfect example of such a symmetrical measuring instrument. It may well be that it is for this reason that scientists have not seriously questioned the conventional configuration of a balance. Indeed, the loss of symmetry inherent in the one-pan, two-knife balance would make it inferior to the two-pan, three-knife arrangement, if there did not exist methods discussed elsewhere [6] for regaining symmetry conditions in successive readings.

In practice, the designer of two-arm, three-knife balances suffers from a serious handicap which, unfortunately, continues to divert his attention from more important features. Users demand that a balance for operation near the maximum attainable precision should give fairly accurate, direct weighings. Symmetrical distribution of masses on the two sides of the central knife edge then becomes important to the proper operation of conventional two-arm, three-knife balances. Hence, in the construction of such instruments, every effort is exerted to achieve precisely equal-arm lengths and precisely equal masses of the two suspensions, although this is not an important requirement in high-precision weighing. Even if these objectives could be achieved, they could never be maintained in practice, but the resultant error affects only direct weighings. Transposition weighing schemes are needed, although these tend to be time consuming.

Some substitution weighing procedures adapted for two-knife, one-pan balances [6] are faster than those for two-pan balances but there is a loss in sensitivity compared with two-pan transposition schemes. This loss is not serious so long as the readout sensitivity can be increased in compensation. Modern instrument-readout systems (see, for instance, [7]) permit effective sensitivities to be increased well beyond residual weighing errors.

The symmetry problem must be discussed in one other respect. Temperature may change the rest point and sensitivity of a one-pan balance. Such a temperature effect is not easy to demonstrate and most of such effects reported to the authors could be caused by temperature gradients (see 3.2 above). A one-pan balance can, in any event, be temperature compensated. This effect, however, is not relevant here where balances are described for precise weight calibration, that is, for weighing schemes in which the effects of slow drifts are eliminated.

3.5. Errors Associated With the Arrestor [10]

Despite its name, the arrestor of a balance is not concerned only with arresting the motion of the beam, but has several additional functions. One of these is confusingly called "arrestment," by which the knives and flats are protected from damage during the relatively rough process of pan loading. "Arrestment" is conventionally accomplished by removing the knives from physical contact with their planes. The inverse function, called "release," is to re-engage knives and flats after pan loading. Precisely the same contact configuration that existed prior to arrestment has to be re-established. Failure to reproduce contact characteristics results in important changes in arm length and sensitivity that arise from a variety of causes, including the motion of the effective point of suspension described above, and causes gross errors in the data. Such errors are collectively referred to as the "arrestment error;" it is often the largest mechanical error associated with balance operation. The major part of the arrestment error occurs during the "release" part of the operating cycle. This operation places great demands on the arrestor, since moving parts must change positon smoothly and without vibration. Smooth operation demands that clearances between moving parts be of the "slip-fit" magnitude. Yet errors of a few microns in the placement of knives and flats during release may result in intolerably large weighing errors. Hence, these clearances no longer are in the category of "working clearance," but appear to the balance operator to be an inordinately large amount of "play." Gould [1] has demonstrated that arrestment by knife-flat separation is not a requirement for satisfactory balance operation, but he and his collaborators had great difficulty in timing the beam-swing arrestment.

In the two-pan, three-knife configuration, errors generally may occur due to imperfect-release synchronization of the two end-knife assemblies. In a configuration in two-knife balances in which there is only one end knife, the magnitude of the arrestment error is statistically reduced to $1/\sqrt{2}$ of its usual magnitude. However, far more important is the fact that for two-knife balances it is relatively simple to design a system wherein the terminal knife as well as the center knife is kept in contact by a constant force. Pan loading then must be a careful smooth operation.

It is entirely feasible, although the need for it has not been demonstrated, to design a balance whose beam and bearings would be kept under approximately constant load throughout the entire life of the balance. Such a design would also overcome most of the problems of flexure further discussed in the following paragraphs.

3.6. Short Arm Length

A short-arm length has been demonstrated to be essential because of the desirability of low moment of inertia and rapid temperature equilibration along the beam (sec. 3.2). It is well to emphasize that the reduction of beam flexure is a further advantage of short beams that may be equally or even more important than the previously discussed considerations. In long-arm conventional balances, the design of the beam is such that all material not essential for the elastic support of the load must be removed. This results in filigree-type truss structures in which, first, heat flows at different rates along the various members of the structure, with the resultant establishment of temperature gradients within the beam causing distortion of the very important knife-edge adjustment (sec. 3.3); and, second, the load causes greater beam flexure. The reproducibility in the magnitude of flexure is an essential demand that is inadequately met by many conventional balances.

The beam proposed here is a short, thick, solid structure without the usual "lightening holes." Such a structure would have an equal or greater thermal capacity than conventional beams, but it would have a much lower ratio of surface area to mass. As a result, the temperature changes in such a beam would occur at a greatly reduced rate. Since the structure is solid, the establishment of nonsymmetrical distortion-causing temperature gradients is greatly reduced. These circumstances, ensure the maintenance of parallelism of the two knives (see 3.3 above). Flexure of the beam under load in short beams becomes tolerably small, and the assumption that the remaining flexure is truly reproducible and elastic becomes safe, provided a careful choice of beam material is made.

Under these circumstances the constancy of beam loadings, one of the long recognized advantages of substitution-balance configurations (often, but not exclusively, associated with one-pan balances), loses some of its importance. In other words, short beams in general will show much less variation of sensitivity with load as a result of beam flexure, an advantage that is associated with short beams as such rather than with one of the rival configurations discussed in paragraphs 3.6.1, 3.6.2, and 3.6.3 below.

Three major difficulties are encountered in an attempt to use a "very" short arm length in a conventional balance of the two-pan, three-knife configuration. Two of these are resolved in the one-pan, two-knife configuration, and the last is virtually eliminated by damping.

3.6.1. Thermal and gravimetric considerations dictate against the placement of the two balance

pans in different horizontal planes [5]. This being the case, the overall length of the beam must exceed the diameter of one pan or else the two pans would interfere with one another. With only one pan this limitation is completely removed, but the danger of errors from differences in height between pan and counterweight caused by changing ambient conditions is still present.

3.6.2. Knife-edge adjustment becomes more difficult and critical as the arm length becomes shorter. In the conventional balance configuration, the three knives must be made parallel and the end knives must be at equal distances from the center knife. In addition, the three knives must be made coplanar, or, rather, the departure of the center knife from the plane established by the two terminal knives must be fixed and constant in magnitude. Even with a "long" beam, these requirements are difficult to achieve. In the one-pan configuration, there are only two knives and the requirements of adjustment are far more readily satisfied.

3.6.3. When excited, the pan-hanger assembly (hangdown) may swing like a pendulum about the effective point of suspension with a frequency determined by the vertical mass distribution. As the hangdown swings, the vertical force on the end knife is modulated with a frequency twice that of the hangdown. The amplitude of force modulation is proportional to the total mass of the hangdown multiplied by the square of the angular amplitude.

In passing it should be pointed out that weighing errors arising from unwanted swing of the two hangdowns do not cancel but rather add (as two independent errors) in two-pan as compared with one-pan balances. More important it is immediately clear that a most critical, feature of a balance design is a pan-release mechanism that will minimize the pan swing. For a typical balance a swing of 10^{-3} radians can be shown to introduce a variation in the knife-edge load of 10^{-7} of the total load.

It must also be considered that during a weighing the hangdown is free to pick up oscillations from the swinging beam, to an extent dependent upon the damping and resonant characteristics of the system. The amount of resonant oscillations that will be induced in the hangdown decreases as the ratio of the hangdown frequency to that of the beam decreases. Practical considerations limit the reduction in hangdown frequency, if only because of the physical height of the weights which must be accommodated. One is therefore faced with an important requirement not to reduce beam arm length so much that its frequency of swing approaches that of the hangdown. (For suppression of resonance the ratio of the frequencies should also not be that of simple integers.)

Discussion with several older balance craftsmen has taught the authors that this limitation to shortening the beam has been understood in the past. However, it was always assumed that balance readings must be taken "on the fly," when the hangdown oscillations produce an uncertainty of turning points, the magnitudes of which are not easily recognized, unless very low beam frequencies are used.

In section 3.3 above, the conclusion was reached that it is advantageous to weigh with a damped beam. An additional major advantage gained from damping is that the readings taken with the beam at the equilibrium rest point automatically eliminate, by averaging, any residual error due to swing of the hangdown. Incidentally, optical magnification of balance deflection [7] at the rest point clearly shows that oscillations due to pan swing are still observable, and that a good knife edge does not "stick" because of starting friction which must be less than about $\pm 10^{-10}$ of the load force. The damping system used need not be further discussed here as simple trials have shown that for large-capacity balances, nearly the optimum damping (about 0.7 critical) can be achieved by several devices without otherwise disturbing the balance appreciably. Damping systems, however, do become more difficult in smaller balances of high precision, and should receive further study.

3.7. The Sail Effect

Even in a well-designed balance case under operating conditions in which the vertical temperature gradient is carefully controlled, there will be thermal gradients in the contained air which will set up convective air currents. The resulting adverse effects of convection can be reduced by keeping to a minimum areas on beam and pan assemblies exposed to possible air currents.

These air currents are often rotary within the balance case so that their effect on two-pan balances may be additive (i.e., "up" on one pan and "down" on the other). With only one pan on which the current can act, the effect is significantly reduced. If this one pan is centrally placed in the balance case so that it hangs in relatively quiescent air, there is an even greater reduction of this "sail effect" error.

3.8. Conclusion

On the basis of the above discussion it can be concluded that a simple robust one-pan, two-knife balance of high precision can be built, provided it is a fast response, damped, short-arm instrument. The beam should have a large cross-sectional area and be made of mechanically strong material of high thermal conductivity. A Thiesen compensator in the suspension, a good pan-release mechanism, and a gently operating weight-transfer system would also be needed. High quality knife edges rigidly mounted in the beam and many other features of high-precision balances, such as a good optical read-out system, would require great care. The demand for a short arm led to the suggestion of a horizontal cylindrical counterweight at right-angles to and bisected by the beam plane. In this way, an effective arm ratio of unity could be achieved, integral fabrication with the beam seemed feasible, and the moment of inertia for any given restoring moment required of the counterweight could be kept small.

4. Design and Construction

4.1. Introduction and General Comments

The unique requirements of exceptional precision coupled with previously unattained stability, ruggedness, and suitability for use by personnel having relatively little training, have been met by novel design based on the analysis outlined above and considerable experimentation during development. The one-pan, two-knife balance stands in its case with its beam perpendicular to the front panel. It can be operated by means of three major controls. (See fig. 1.) The first is the control lever which operates the turntable (fig. 1a) for weight transfer and the beam arrestment. The second rotates the turntable (fig. 1b). The third is the pan-arrest lever (fig. 1c). All these controls are at the front of the case and readily accessible to the operator. The optical image screen presenting the balance reading and the associated microvernier also appear in front of the balance case.

Materials were chosen to provide long life and to require minimum maintenance. All shafts rotate in either porous bronze bearings or in ball bearings.

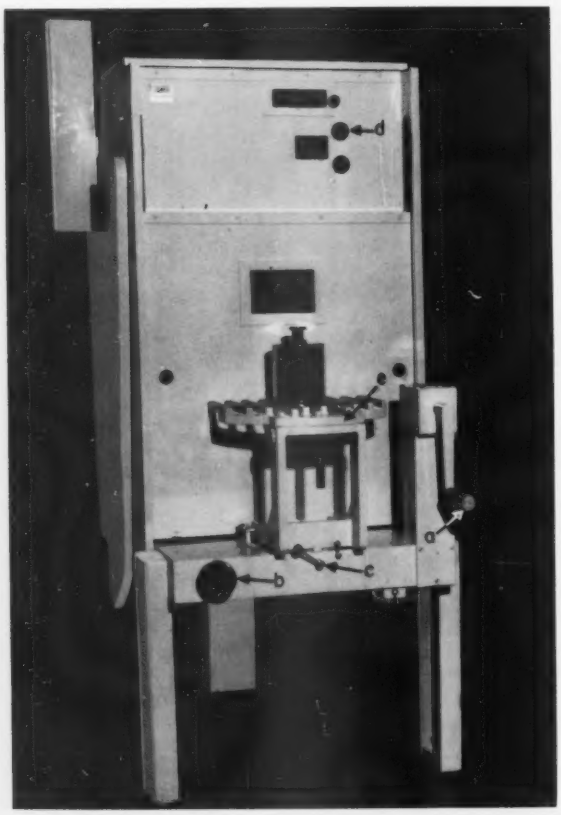

FIGURE 1. *General view of 50-lb balance.*

The knife edges are of Tantung G and the bearings of Brazilian agate. This combination seems to provide excellent life. The beam material is manganese bronze to provide a combination of adequate strength, rigidity and conductivity, and to give a counterweight density of approximately 7.9 g/cm^3 to match the stainless steel weights that are most likely to be used.

4.2. The Beam With Fixed Counterweight

The beam is short (arm length, 2¾ in.) and of low moment of inertia with an effective arm ratio of about unity (fig. 2). The fixed cylindrical counterweight (fig. 2a) is cast as an integral part of the beam. The axis of the counterweight is horizontal and perpendicularly bisected by the beam plane.[6] The beam and counterweight weigh about 70 pounds. In manufacture, the counterweight is machined to a true cylinder within ± 0.0005 in. to serve as a reference for further machining.

The effects of alinement errors and dimensional instability of the knife edges increase with decreasing arm length (see sec. 2.3). A novel and improved knife-mounting system has therefore been found essential. The beam is prepared for the center knife by a 90° inverted groove with horizontal axis perpendicularly bisected by the beam plane. The sides of the V-grooves which serve as the knife-locating surfaces are inclined by about 45° to the beam axis (fig. 2b). A clearance slot is machined into the top of the groove. The knife itself is a rectangular bar having a length of 2 in. and square cross section of side ½ in. Opposite faces are lapped parallel and adjacent faces are approximately at 90°, opposite angles being equal. One pair of angles is matched with the groove angle of the beam so that the intersections of the four rectangular optically flat faces form two interchangeable knife edges. Clamps (fig. 2c) prevent sliding only; screw adjustments are not needed. In this way stresses due to screws and other beam strains can be avoided. The short beam can be built rigidly enough to make groove spread under load negligible. The load knife is shorter (1¼ in.), but otherwise it and its groove are of a design identical with that for the center knife.

Screw trimming weights (fig. 2d) for balance and sensitivity are conventional as is a 100 in.^{2} air damper (fig. 2e) 13 in. from the center knife operating in a 5 × 20 in. tray with vertical walls.

4.3. The Beam Arrestment

Whereas the load-supporting terminal knife edge is not separated from its flat during a weighing series, a carefully designed arrestment system for the center knife has been provided. With it the usual arrestment errors, arising to a substantial part at the terminal knife edge (see sec. 3), are at least reduced.

[6] Vertical plane containing the beam axis normal to knife edges.

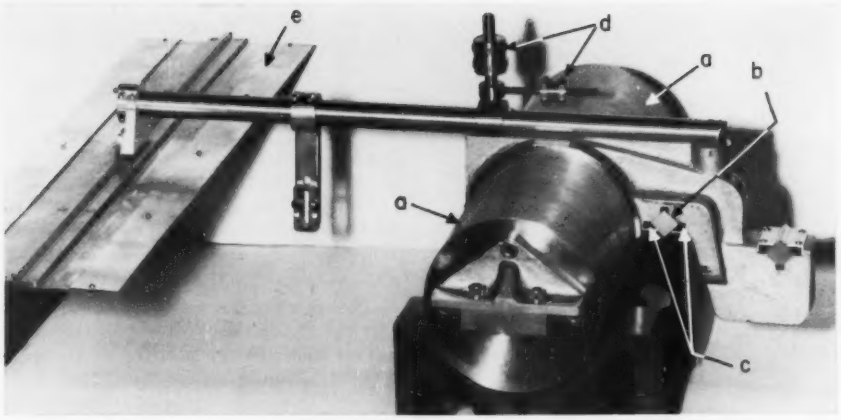

FIGURE 2. *Weighbeam assembly.*

The principal, rigidly designed, arrestment arm (fig. 3) is cam operated and pivoted about a horizontal shaft fixed to the massive aluminum bed plate. This shaft is located 15½ in. from the terminal knife. The arrestment arm carries three vertically upward pointing fingers (inverted cup, V groove, and a plane) which engage three points fixed to the upper plate of the hangdown (figs. 3a and 4a). The pan arrestment mechanism (see below) serves to raise the pan end of the balance gently until two upward-pointing fingers (fig. 3b) rigidly fixed to the bed plate engage a downward-pointing slot and cup (fig. 3c) on the ends of the counterweight. The principal beam arrestment arm then slightly raises the hangdown so that the beam pivots about the two points on the counterweight, disengaging the center knife from its flat. The satisfactory operation of this arrestment depends on adequate parallelism of the line joining the fixed points with the center knive. The cup and slot therefore have a floating adjustment carried out by the manufacturer to ± 0.0001 in. to minimize the arrestment error. Instability of temperature dependence of this adjustment has not been detected.

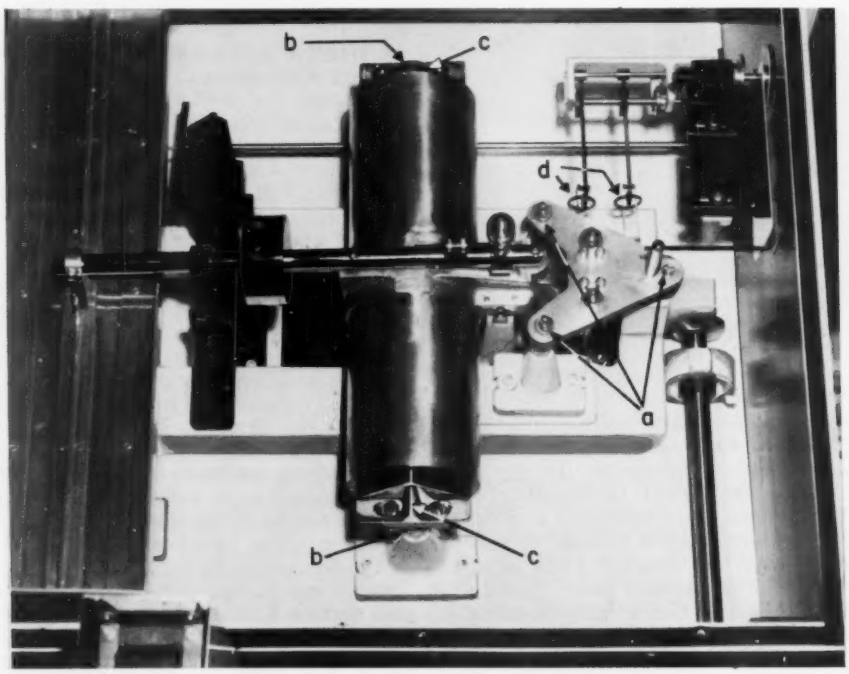

FIGURE 3. *Bedplate assembly with arrestment, beam, optical system, suspension, and calibration mechanism.*

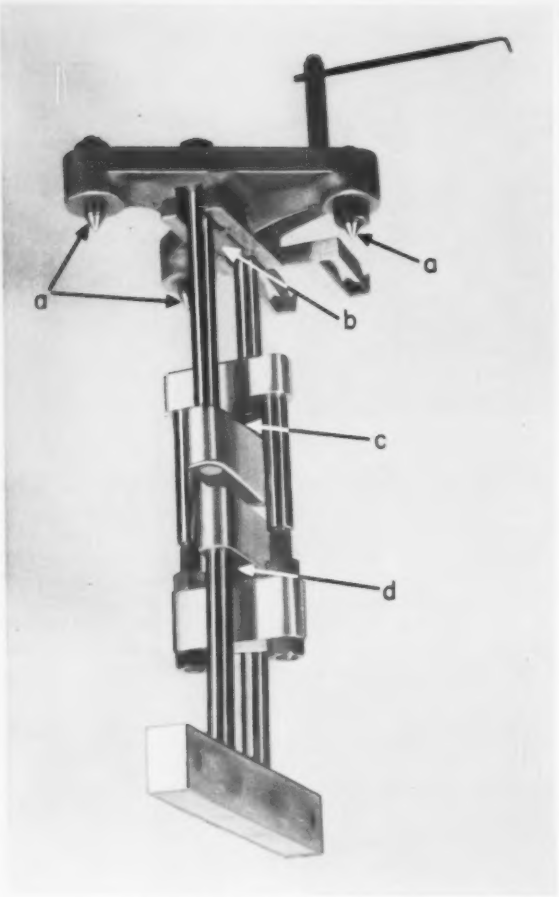

FIGURE 4. *Hangdown assembly.*

4.4. The Hangdown and Pan Arrest

The hangdown and pan are shown in figures 4 and 5a. The weight-bearing plane is 25 in. below the terminal flat (fig. 4b). The aluminum support rods (¾×1 in. section) are symmetrically placed on either side of the vertical center line under the terminal knife and in a plane perpendicular to the beam plane.

As discussed in section 3.3, compensation for misplacement of the weight on the pan perpendicular to the knife plane is required. Ideally, the compensating knife edge should be coplanar with the terminal knife edge. In practice, a vertical displacement can be tolerated if it is small compared with the distance from the terminal knife edge to the center of gravity of the loaded pan. The additional knife edge (fig. 4c) in this balance is actually 3 in. below the load-bearing knife.

Although the terminal knife does not leave its bearing on arrestment, a mechanism for ensuring that the center of gravity of the hangdown with load is vertically below the terminal knife edge and for damping out pan swing is a critical design feature. On final release no horizontal force component must be allowed to be exerted upon the pan. These requirements are achieved by a (3/16 in. diam) button (fig. 6a) of stainless steel acting on the underside of the pan; the area of contact is polished. The button is fixed to a horizontal arm (fig. 6b) pivoting on horizontal knife edges 9¼ in. from the button. At the opposite end of the frame are

(1) an adjustment counterweight to determine the force applied by the button, and

(2) a hydraulic dashpot that controls the upward vertical movement of the button.

The pan arrest operates in the following manner:

(1) In the arrested position the counterweight presses the pan-arrest button against the bottom of the pan with a force just sufficient to permit the pan to damp to zero velocity in a position very near to gravitational alinement of the pan assembly.

(2) When the beam is released, the pan-arrest button follows the vertical motion of the pan, but still provides sufficient force to dampen out the horizontal motion of the pan.

(3) The pan-arrest button is pulled away from the pan by a cam-operated finger.

During the above three steps the hydraulic dashpot is, for practical purposes, not part of the system.

The first step in arresting is to permit the button slowly to contact the bottom of the pan. Provided the beam is nearly balanced, the force of the pan-arrest button will push the pan vertically at a rate controlled by the dashpot. The beam will tilt back to its limiting position with the cup and slot on the counterweight in position against the fixed fingers on the bed plate. With this device there is no tendency to jar the bearings during arrestment.

An additional device is included to eliminate the possibility of motion of the terminal knife relative to its flat. It has been found that even relatively small disturbances to the load pan, particularly if in the form of a torque around a vertical axis running through the center of the knife, can introduce variability in readings. For this reason, the pan hanger is supported on a pivot (fig. 4d) with freedom to rotate around a vertical axis. In order to prevent rotation of the hanger about a vertical axis during loading and unloading of the pan, locating pins operated by the arrestment mechanism are inserted beneath the hanger. This device will be discussed below (in sec. 4.6) in connection with a procedure for centering the load on the hanger pan.

The load hanger is designed to offer a minimum surface to the movement of air within the weighing chamber. The load pan consists of a slotted plate in the form of a fork open towards the rear of the balance case. Below and at the two sides of the pan there is a rack on which counterweights can be placed manually in a symmetric array. Adjustable counterweights on the hanger permit it to be leveled with respect to the load-transposing mechanism described below (sec. 4.6).

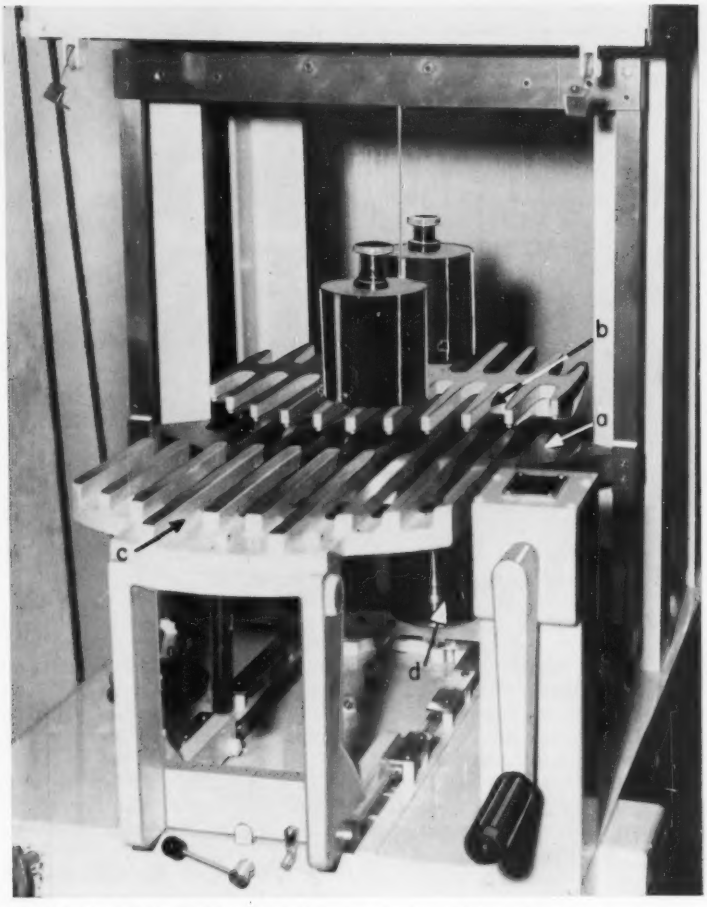

FIGURE 5. *Weight loading and transposing mechanism with truck, slotted pan, and elevating turntable.*

4.5. The Read-Out

A graticule mounted on the end of the beam is graduated with 140 (+70 to −70) radial lines (9 in. radius) equally spaced at 1½ angular minutes per line. It is fixed in the beam plane 9 in. from the center knife. A conventional projection system brings the image of the graticule to a screen at the front of the case. A cam-operated microvernier[7] permits ready estimation of the graduated scale to within 1/100 of a division from wide vernier marks representing 1/20 of a scale division. This is 10 times that required in the original specification, but the performance of the balance is such that the additional readability could be useful for potential uses of the balance.

In the design of the optical system, all heat-producing elements are placed outside and above the top of the case to minimize thermal effects. The residual heat flow into the balance helps to establish the positive gradient discussed in section 3.2. In addition the entire beam, arrestment and optical systems are mounted on the heavy bed plate which provides a thermal sink and reduces vertical movement of the air within the weighing chamber.

Two ring weights (fig. 3d) that have a mass corresponding to 50 scale divisions are supplied. The rings are so operated by a dial (figs. 1d and 3d) that with this dial at "zero," one of the rings is on the hanger. With exactly 50 pounds on the pan and the ring in place, the beam should balance with the scale indication at zero. When the control knob is set to "plus," the second ring is added to the hanger. It causes the balance to indicate +50 divisions provided it is properly adjusted. When the control knob is set to "minus," both rings are removed and the indication should be −50 divisions. If the balance is not properly calibrated (or if the ring weights need to be cleaned), the indication will be incorrect.

[7] This readout was incorporated as a result of the performance test (see sec. 5).

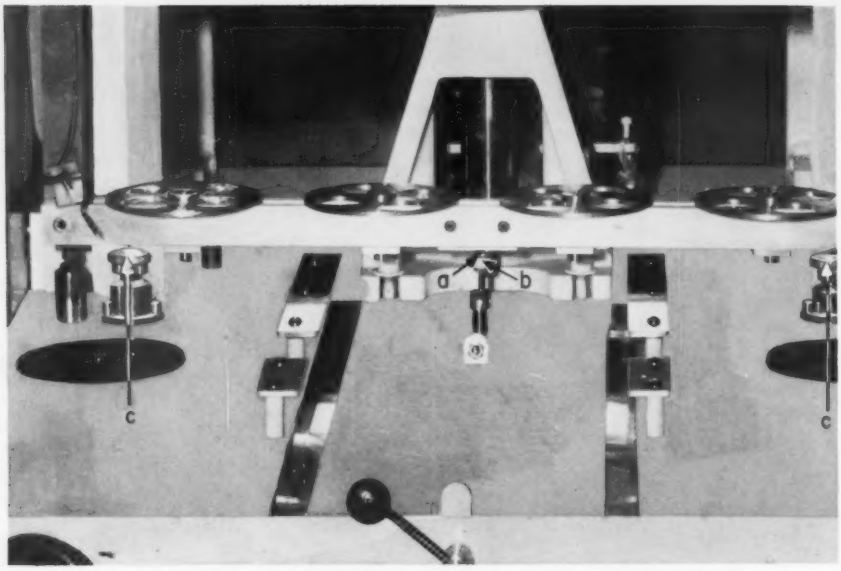

FIGURE 6. *Pan arrestment and load centering mechanism.*

A small nut on the beam can be adjusted vertically to bring the beam to the proper sensitivity.

A wide-range zero adjustment is also provided. For this adjustment the image of the projection scale can be moved by rotation of a flat mirror in the optical path. The balance can thereby be set to the accepted mass correction when weighing a standard weight. When weighing an unknown weight, no further arithmetic correction for the balance indication is necessary [3].

4.6. Weights and Weight Loading

The standard weight and unknown weight (or group of weights which constitute the unknown) are stored on a two-position turntable (fig. 5b) which can be rotated through 180°. The turntable is made in the form of a slotted plate which interlaces the pan of the balance and is located behind the pan and within the weighing chamber. It has vertical motion so that its weight-bearing plane can be raised to clear the top of the balance pan or lowered to a position below the weight-bearing plane of the pan. In the raised position, the turntable can be rotated to present either of two weights to the pan and is provided with two controls, one for elevation and one for rotation. Stops are incorporated for accurate positioning. Since the elevating mechanism is required to support a load of 100 lb consisting of a 50-lb test weight and a 50-lb standard, it has been decided that a multiple-turn handle is needed. This system can be operated without undue exertion.

Because of the difficulty of handling, the weights are introduced into the weighing chamber by means of a truck (figs. 1e and 5c) normally located outside the balance cabinet and capable of overriding the pan. Markings are provided on the truck to center the weights. However, since it is difficult to center the weights exactly, the following procedure is used [8] for the centering of the weights on the pan.

1. The turntable is lowered to a position just below the top of the truck. This position is indicated on a slide-rule dial connected to the operating handle.

2. The truck (fig. 1e) is moved into position just above the pan. The turntable is elevated until the weight is lifted off the truck, which is then removed.

3. The turntable is lowered transferring the weight to the pan. Until this time, two locating pins (fig. 6c) have been engaged in the bottom of the pan frame to prevent movement. These pins are automatically retracted just before the weight is transferred to the pan. After the weight is transferred to the pan, the pan swings, controlled by the pan-arrest button, into a position in which the center of gravity of the assembly is below the knife system.

4. The turntable is raised again until the weight is just lifted off the pan. The locating pins do not re-enter the pan frame so it is free to swing back to its normal vertical position.

5. The weight is so raised from and lowered onto the pan several times. At each successive stage the hanger assembly is brought nearer to gravitational alinement. After approximately three cycles there is no longer discernible movement of the pan during the transfer. The slide-rule dial indicates the correct position of the turntable so that it is not necessary actually to observe the transfer of the weight,

[8] The procedure includes changes in weight arrestment suggested as a result of preliminary tests (see sec. 5).

and the operation can be accomplished with the cabinet door closed. The weights can then be stored on the turntable without disturbing this adjustment.

Once the weight has been centered the turntable can be lowered completely out of the way. Continued rotation of the arrestment lever releases the beam as the elevator reaches its lowest position. The only further operation required to make a weighing is to operate the pan-release mechanism. In particular it is not necessary again to open the balance case doors, since the centering of the weights on the turntable remains undisturbed on careful rotation.

All the weight-transfer mechanisms are fastened to a heavy aluminum plate which is welded to an aluminum frame for rigid support. The plate also helps to provide thermal stability.

Since the 50-lb balance is intended to calibrate weights of a limited number of nominal mass values, individual tare weights are supplied to bring the balance to its full capacity of 50 lb. The cylindrically symmetric tare weights are made of stainless steel and shaped so that they can be stacked symmetrically on either side of the hanger pan (fig. 5d). The weights are arranged so that any value from zero to 50 lb in 5-lb steps can be calibrated. For ease of handling, no weight is greater than 10 lb. For symmetry, the smallest weight must be 2.5 lb.

4.7. The Balance Case

So that thermal effects will be minimized, the 42 in.×25 in.×26 in. cabinet has been designed to have both good insulating characteristics and low heat capacity. The cabinet panels are of double-wall construction with thin aluminum plates over a skeleton plywood support of ½ in. thickness. The space between the plates is such that the air trapped between them does not tend to circulate. The outer surfaces of the panels are painted a glossy white to reflect radiant heat. The inside is painted dull black to approximate to blackbody conditions. The panels are bolted to the heavy supporting members of the balance, and the counterbalanced front panel can be raised and lowered on slides. A small viewing window is provided.

5. Performance Test

Results of the tests on the 50-lb one-pan, two knife, substitution balance given below demonstrate that a high-precision balance can be designed and built according to the foregoing principles and specifications.

Because this balance is of untried design, some preliminary tests and weighings were made to help the authors to become familiar with the balance before proceeding with the evaluation tests. During this preliminary work, the need for some means of centering the load on the pan became apparent. This requirement was met by changing the arrestment cycle so that the load was transferred from the turntable to the pan before the load on the suspension was transferred from the arrestment mechanism to the terminal knife of the balance beam. This change made it possible to center the load on the pan by repeatedly putting the load on the pan and removing the load from the pan before the balance was released. When this change of the arrestment cycle had been made and the balance carefully adjusted, the performance test was made. The performance of the balance during this test exceeded the requirements specified in the development contract.

Because balances of this type will not always be used under the best attainable conditions, the tests were made under both good and poor weighing conditions. The balance was first tested under the conditions normally existing in the mass laboratory of the National Bureau of Standards. The second part of the test was made under simulated adverse conditions. The unfavorable conditions were created by heating the base of the balance radiantly and directing a current of hot air toward the balance. The performance test consisted of several series of weighings; each weighing measured the difference in the mass value of two weights having the same nominal value. The same two weights were used throughout a given series. The agreement of the results of the weighings in a given series was a measure of the performance of the balance. This measure was expressed as the standard deviation of a single weighing.

During the first part of the test the precision of weighing as measured by the standard deviation of a single weighing was 3 to 5×10^{-6} lb, or about 1 part in 10 million. The standard deviation of a single weighing during the second part of the test was about 15×10^{-6} lb, or about 3 parts in 10 million. On the basis of this test, the maximum weighing error that can be expected under adverse conditions is about one part in a million.

During the performance test, it was found that a large part of the imprecision of the balance could be ascribed to arrestment errors. A number of tests were made to determine if any single part of the balance mechanism was responsible for a significantly large part of these errors, but the results of these tests were inconclusive.

The tests demonstrated not only the balance's capabilities, but also the desirability of greater resolution in the read-out than the 1×10^{-5} lb of the original reading device and the need for a pan large enough to accommodate groups of weights with a total nominal value equal to the capacity of the balance. Therefore, two further modifications were made: The reading device was replaced by one readable to 1×10^{-6} lb; and the pan, turntable, and loading truck were replaced by similar parts large enough to accommodate groups of weights having a total mass value equal to the capacity of the balance.

After these modifications had been made the balance was placed in service as a calibration balance in the Bureau's mass laboratory. In this service, the precision of the balance as measured by the standard deviation of a single weighing is about 1 part in 10 million.

It is a pleasure and a privilege to acknowledge most gratefully the collaboration and advice from many experts at the National Bureau of Standards, at other research institutes, and balance manufacturing firms. It is difficult to choose just a few individuals for special mention, but Miss E. M. Clinton has carried out independent confirmatory investigations freely communicated to the authors. Professor A. H. Corwin by personal interest and as member of the Advisory Panel at the NBS Metrology Division, has often discussed this work most helpfully with the authors. Mrs. M. W. Jones is hereby thanked most cordially for her technical and experienced support of this and other researches in the Mass and Volume Section of the Bureau. Last but not least the authors express their appreciation for the kind background help always available from the NBS Editorial Section.

(Paper 68C3–159)

6. References

[1] F. A. Gould, Proc. Phys. Soc. B**62**, 817 (1949).
[2] A. H. Corwin, Weighing techniques of organic chemistry, Vol. I, Physical Methods of Organic Chem., 3d edition, pt. I, Ch. III, Interscience Publishers, New York (1949).
[3] H. S. Peiser, State mass standards, Rept. 45 Nat. Conf. on Weights & Measures, 45 (1960).
[4] H. E. Almer, J. Research NBS, **64**C, 281 (1960).
[5] L. B. Macurdy, J. Research NBS, **68**C, 135–40 (1964).
[6] H. E. Almer, L. B. Macurdy, H. S. Peiser, and E. A. Week, J. Research NBS, **66**C, 33 (1962).
[7] H. A. Bowman and L. B. Macurdy, J. Research NBS, **63**C, 91 (1959).
[8] NPL Staff; Balances, weights, and precise laboratory weighing; NPL Notes on Applied Science No. 7, Her Majesty's Stationery Office (1954).
[9] G. Guglielmo, Concerning two methods of determining the radius of curvature of the surface of the knife edges of balances and pendulums, Atti reale accad. lincei, Series 5, 11, 2d half-year (1902).
[10] H. A. Bowman and H. E. Almer, J. Research NBS **67**C, 227 (1963).
[11] G. F. Hodsman and F. A. Chappel, J. Sci. Instr. **29**, 10 Oct (1952).
[12] M. Thiesen, Trav. et mem. bureau international des poids et meas., **5**, pt 2 (1886).

JOURNAL OF RESEARCH of the National Bureau of Standards—C. Engineering and Instrumentation
Vol. 68C, No. 3, July–September 1964

Wave Front Shearing Prism Interferometer

J. B. Saunders

(April 9, 1964)

A small prism interferometer is described that is a modification of the Bates' wave front shearing interferometer. The prism is small, rugged, and versatile. The shape of any converging wave front from any optical element or compound instrument may be measured with this instrument.

Several variations of the prism are described that have characteristic properties. Special features are introduced for eliminating spherical aberration effects, for producing fringes of different characteristics, and for testing all wave fronts up to and exceeding that of an F.1 cone of rays.

Details for making and adjusting the prisms are given. Examples are given for interpreting the interferograms.

1. Introduction

The principles of the wave front shearing interferometer (WSI) have been described by Professor J. W. Bates [1]. This interferometer is particularly well suited for measuring the shapes of converging wave fronts. The difficulty of making the Bates instrument and others that have subsequently been described has limited the applications. This paper describes a simple form of WSI that is easily constructed, easily adjusted, and is practical. It is very small and can be mounted in an eyepiece cell for testing astronomical telescopes or as a convenient mount for other applications.

The WSI described by Bates consists of two beam dividers, two front-face mirrors, and two compensator plates. The angle of shear could be varied at will in the Bates model. Later models of the WSI by Drew [2] and Brown [3] are more compact. The Brown version is a relatively compact instrument of fixed shear. The instrument described here is more compact than any of the previous models, is quite easy to adjust, and is relatively free from vibration effects.

The WSI is quite suitable for testing lenses, mirrors, and combinations of these. It is also quite practical for studying atmospheric effects on light. Professor Bates described a method for analyzing the results from a WSI when the converging wave front is axially symmetrical. D. S. Brown [4] described another method of interpretation of sheared interferograms. The author of this paper has given a rigorous mathematical operation [5] for interpretation of sheared interferograms that does not depend upon symmetry of wave form. The solution is unique for any chosen "family" of reference points.

The elements forming this wave front shearing interferometer have been combined into a small compound prism that may be made into a variety of forms. Each form may be constructed with or without a built-in wedge that either permits or prevents rotation of the fringes. The two components of the prism are cemented together for stabilization of those adjustments that should remain fixed, without limiting the adjustments that are essential to its operation. The unit is small, rugged, compact, easily constructed, easily adjusted, and simple to use.

2. Basic Optical Principles

The wave front shearing interferometer (WSI) is a modification of that developed by Mach and Zehnder [6]. It differs from the MZ-interferometer in that convergent light is used instead of collimated light, the reflecting and beam-dividing surfaces are not parallel, the component beams emerge nonparallel, and the fringes are nonlocalized. The angle between the emerging components of any ray represents the angle of shear. To get observable interference between these two beams a source that is small [1] in the direction of shear is necessary.

The differential deviation of the component beams is accomplished in the Bates WSI by tilting one of the beam dividers, whereas in the Drew WSI it is effected by rotating one of the front-face mirrors. The vertex, or point of convergence, of one of the component wave fronts (images of the source) is always located near the optical element that is used to effect the differential deviation (angle of shear). The lateral separation of the two images of the source determines the width of the fringes (as in the Fresnel's mirrors [7] arrangement.)

In figure 1A, the lens, L, forms two images of the light source, S, at S_1 and S_2. The two component beams (represented by the two components of the principal ray and designated as 1 and 2) suffer total internal reflection at points P_1 and P_2. Each of these beams again divides at plane B into two components—the transmitted beam, 1, dividing into beams 1′ and 1″ and the reflected beams, 2, dividing into beams 2′ and 2″. An observer's eye located close to the prism so as to receive either pair of rays 1′ and 2″ or 1″ and 2′ will be able to see two images of L (L_1 and L_2, figure 1B).

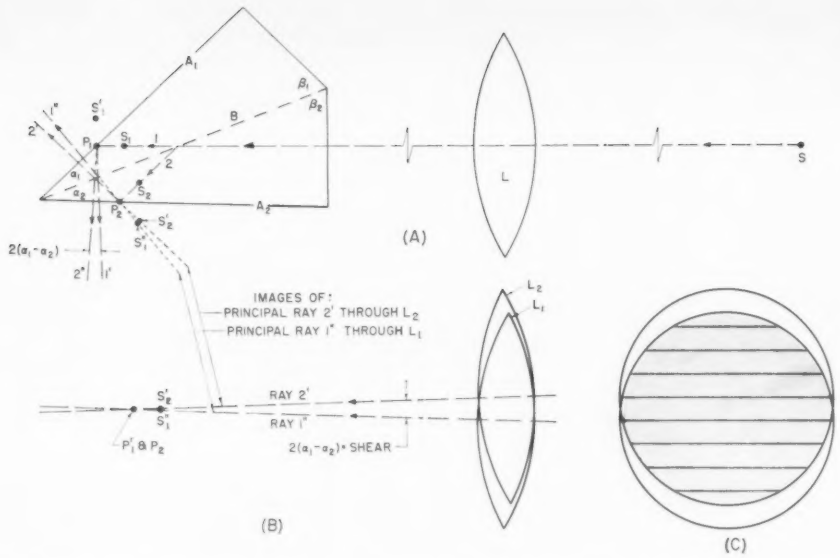

FIGURE 1A. *Optical arrangement for testing a lens, L. The two elements of the prism, A_1B and A_2B, are cemented together, with a semireflecting coat of aluminum on one of the cemented surfaces. Refraction at the two exit faces is assumed to be negligible.*

B. *L_1 and L_2 are images of L, as seen through prisms A_1B and A_2B, respectively, by an observer's eye located behind the prism and receiving rays 1'' and 2'. The image P_1' of P_1 appears to coincide with P_2.*

C. *Fringes of interference that appear to be localized in the overlapping areas of the two images, L_1 and L_2.*

The two component prisms, shown in figure 1A, have angles α_1 and α_2 that differ by a chosen amount. Prism A_1B is assumed to have been moved parallel to the plane of figure 1 and relative to prism A_2B so that the image of $P_1[P_2]$, with respect to the semireflecting plane B, coincides with $P_2[P_1]$. This places P_1 and P_2 equal distances from both the source and the observer. The two emerging beams, $1'$ and $2''$, appear to intersect at P_1 and the other pair of beams, $1''$ and $2'$, appears to intersect at P_2. Images of S_1 and S_2 appear to be located at S_1'' and S_2', respectively. This adjustment of the prisms makes the two paths of light through the center of the lens equal so that when white light is used the zero order of interference is observed to pass midway between the centers of the two images of the lens. This fringe is almost colorless with a relatively pure colored fringe on each side of it. All other fringes are colored with varying tints due to overlapping of colors.

If the points P_1 and P_2 are further from L than S_1 and S_2, images of S are formed between the lens and these points. If, however, the points P_1 and P_2 are nearer the lens than S_1 and S_2, the images of S are beyond the points P_1 and P_2. By moving either the prism, the lens, or the source along the axis of the lens, the emerging components of the principal rays remain fixed relative to the prism and the two component images of the source, S_1'' and S_2' (see figure 1B), appear to move along the two components of the principal ray. If the two images are made to coincide with P_1' and P_2 they will also coincide with each other and the two components, $1''$ and $2'$ (or $1'$ and $2''$), of the principal ray intersect at P_2 (or P_1'). Consequently the lateral separation of the two coherent images, S_1'' and S_2', (figure 2A) may be varied at will by a simple linear translation of the prism along the axis of the lens.

Since the two images, S_1 and S_2, are coherent, of equal intensity, and equally distant from both the observer and the source, S, the two emerging cones of light will combine to produce low-order interference. The two coherent images act exactly as the two coherent sources in the Fresnel's mirrors [7] arrangement. The fringes of interference are nonlocalized. If either of the two pairs of beams, $1'$ and $2''$ or $1''$ and $2'$, is projected onto a photographic emulsion (on film or paper) a photograph of the fringes is obtained. Also using a camera to receive either pair of beams, the fringes may be photographed in good contrast. The focusing of the camera does not vary the contrast, but if the lens, L, is imperfect the nature of the interferogram (fringe pattern) will vary with changes in the focus of the camera because the shape of the wave front changes as it is propagated from one position to another.

Interference fringes appear only in the overlapping areas (fig. 1C) of the two component beams. These fringes will be straight if the lens, L, is free from axial aberrations. Figure 2A shows several sets of fringes that illustrate the effect of moving the prism along the axis of the lens. As in the Fresnel's mirrors arrangement, the fringes are always perpendic-

ular to the direction of the straight line joining S_2' and S_1'' and their width (or separation) is inversely proportional to the lateral distance between the two images S_2' and S_1''.

Since the two rays, $1''$ and $2'$, intersect (lying in a common plane) and since the two images, S_2' and S_1'', are equally distant from the point of intersection, the relative direction of the two images does not change. Consequently, the fringes do not rotate with movement of the prism along the principal ray.

If the compound prism (fig. 1A) is moved perpendicular to the axis of the lens and in the plane of figure 1A, the distance from the two images, S_2' and S_1'' (fig. 2B), to the observer becomes unequal and the zero order of interference moves away from the center of the field. The movements of the fringes, due to prism movements along the axis, will be similar to those in figure 2A and the zero order of interference will be displaced from the center of the field. The zero-order fringe is indicated in figure 2 by representing it with lines that are heavier than for other orders.

The analysis of wave fronts by the method described in reference [5] requires that a "family of reference points" (appendix A) be chosen along a line parallel to the direction of shear.

If prisms A_1B and A_2B (fig. 3) are each rotated a few degrees about an axis normal to B and through points P_1 and P_2, rays 1 and 2 will be deflected out of the plane of figure 3A. If the rotation is equal for the two prism components but in opposite directions the two component rays will be deflected by equal amounts. This results in a shearing of the wave front. The direction of shear is perpendicular to the plane of figure 3A, whereas the shear indicated by figure 1B was in the plane of figure 1A. The two emerging rays $1'$ and $2''$ (or $1''$ and $2'$) lie in a plane that is normal to that of figure 3A. Figure 3B shows the observed images of the lens as seen by beams $1''$ and $2'$, in a plane normal to that of figure 3A. The plane of figure 3B is also normal to that of figure 1B.

The two prisms shown in figures 1 and 3 shear the wave front in directions that are perpendicular and parallel, respectively, to the vertices of the prism angles. The spacing of the fringes in both prisms varies when the prism is moved along the principal ray. The fringes in both prisms move laterally, without change of spacing, when the prism is moved in the direction of shear and do not change for small movements of the prism perpendicular both to the principal ray and to the direction of shear.

If the prisms in figures 1 and 3 have been adjusted to place the images of P_1 and P_2 coincident, the two sources will always be equally distant from the intersection of the components of the principal rays. Consequently, the direction of the line joining the two image sources will not change and the interference fringes will not rotate. If the fringes are to be rotatable the components of the principal ray must not intersect each other.

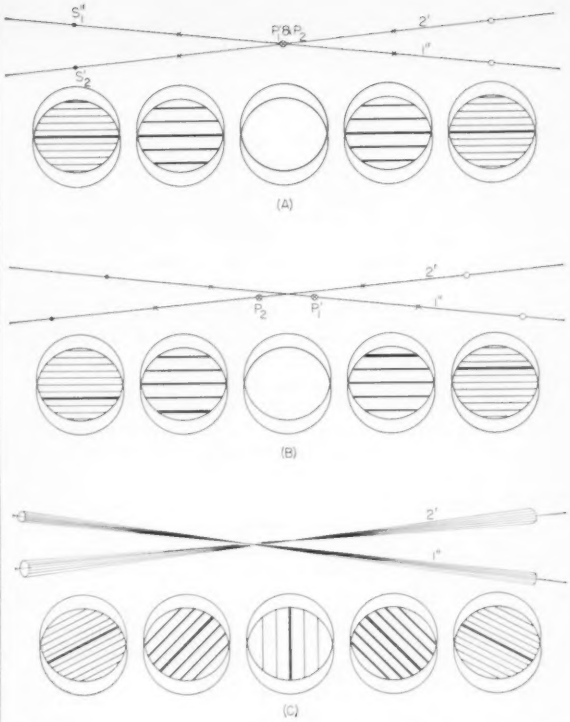

FIGURE 2A. *The components of the principal ray ($1''$ and $2'$ of fig. 1 B) intersect at coincident points P_1' and P_2. The fringe spacing varies with separation of images S_2' and S_1'' but do not rotate.*

B. *Components of principal ray intersect, but not at P_1' or P_2. P_1' and P_2 are equally distant from the point of intersection. The zero-order fringe is displaced from the center of the pattern.*

C. *The two component rays, $1''$ and $2'$ do not intersect. The horizontal component of the fringe width is invariant and the vertical component varies as in the above figures, A and B. This results in a rotation of the fringes. The fringe width is a maximum when the separation of the two images of the source are closest together.*

It is desirable, in many cases, to use white light sources for testing lenses—particularly for testing astronomical telescopes with light from celestial stars. When white light is used for the source the number of usable fringes is limited. In this case it is desirable that the fringes be as nearly parallel to the line of reference points as possible and with the zero-order fringe (the fringe of best visibility) located on or among the reference points. The prism described above and illustrated in figure 1 does not permit this adjustment without making the fringes too broad for accurate readings, unless the wave front has considerable distortion.

The WSI prism may be designed to permit rotation of the fringes. In the preferred design for rotatable fringes, the shearing of the component beams is accomplished by using two identical prism compo-

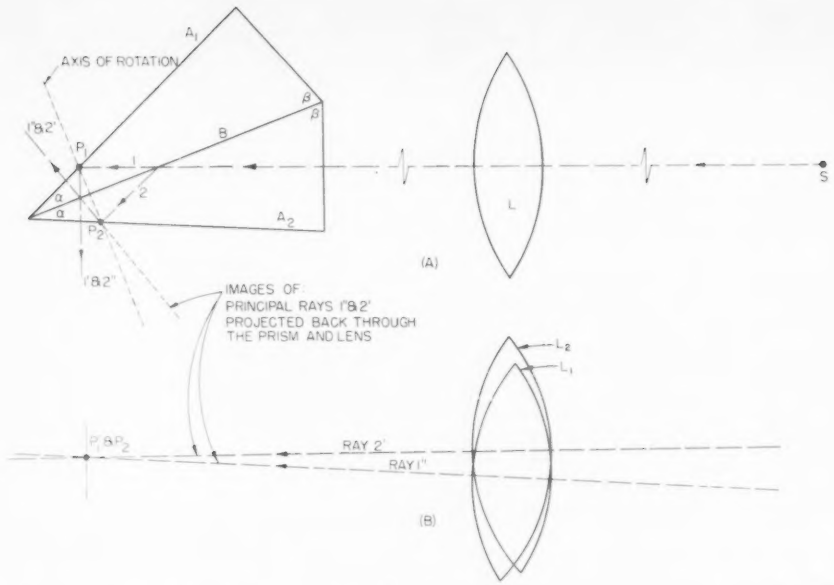

FIGURE 3A. *The two components of the prism are identical, with the aluminum coat on one prism only. Shear is obtained by rotating the two components about an axis normal to B, but in opposite directions.*

B. *The planes of figures A and B are normal to each other.*

nents with a relative rotation of these components about an axis that is normal to the dividing plane, B. If the angles of the two component prisms are equal and no shear is introduced, the two component rays 1′ and 2″ or 1″ and 2′ (figure 3) will coincide. The two images of L (shown in fig. 3B as L_1 and L_2) will coincide. The optical path difference between rays 1 and 2, and all other rays in the beam, will be zero. No fringes will be observed because the phase difference is constant over the entire beam.

To obtain rotation of the fringes the two component rays 1″ and 2′ (and also 1′ and 2″) are shifted, relative to each other, in the direction normal to the plane of figure 3B. Figure 4 shows the ray trace through a prism that has been adjusted to perform this shift. Dividing planes B_1 and B_2 are parallel to each other and separated by a distance, t, that is proportional to the resultant lateral separation, d, of the two component emerging beams.

The prism of figure 4 is adjusted to produce zero optical path difference for the two component principal rays. Shear is obtained by a relative rotation of the prisms, exactly as described for the prism of figure 3.

The two components, 1 and 2, of the principal ray will emerge in planes that are perpendicular to the plane of figure 4 and separated by the distance d. The component rays will make equal angles, but of opposite sign, with the plane of figure 4. When the prism is moved along the axis of the lens the two images of the source move along the two rays 1 and 2, remaining equally distant from both the source and the observer. The zero-order fringe remains at the center of the field. The separation and relative direction of the two images of the source change with this movement of prism. Consequently, the fringes rotate and change width during this movement.

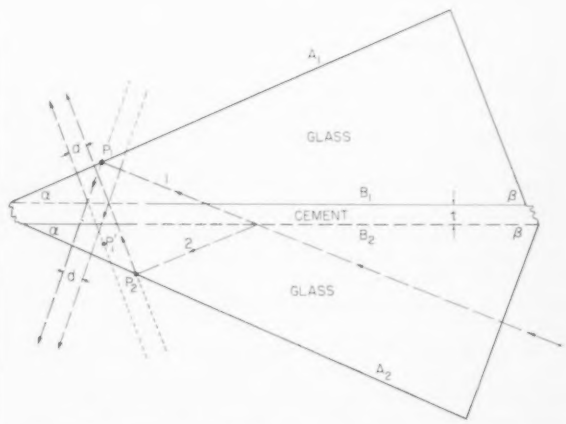

FIGURE 4. *The two components of the prism are identical.*

The reflecting film on P_2 extends from the vertex of β to the normal projection of P_2 onto P. The reflecting film on P_1 extends from the vertex of α to the normal projection of P_2 on P_1.

The uncoated parts of B_1 and B_2 virtually disappear if the index of the glass equals that of the cement.

Figure 2C indicates the two pencils of rays about the component rays 1 and 2. The direction and width of fringes for several positions of the prism, relative to the lens, are shown.

When the fringes are alined in the direction of shear they are of maximum width. Since the reference points must be on a line parallel to the direction of shear, the zero-order fringe can be alined with the line of reference points (assuming a good lens is being tested) and the zero-order fringe can be shifted laterally for most favorable reading of orders.

3. Symbolic Designation of Prism Types

The original prism interferometer was found to be a special case of a large variety of forms. Also, each form may be constructed and adjusted to provide a variety of properties, angles of shear, and other special adaptations. A description of one or two of these prisms would not adequately cover the development.

There are two geometrical forms, a quadrilateral and a hexagonal prism (see fig. 5). The usable angles of each of these two forms cover a considerable but finite range. Either form of prism with any combination of usable angles may be adjusted to have any angle of shear over a considerable range. There are two distinctive ways of producing shears which are normal to each other relative to the prism. Each of these types of shear is associated with adjustments of the interference fringes that have advantages and disadvantages for various types of measurements.

In order to describe these prisms adequately we will describe their common properties, method of adjustment, construction, etc., as a group. To do this an abbreviation will be used for designation of groups, and the abbreviations are so chosen that for future use definite specifications may be indicated for all types and forms. The chosen abbreviation is a compound letter-number symbol that indicates several of the prism's significant characteristics. The generalized symbol is *NEWS* (N=Number, E=Entrance face, W=Width of fringes, and S=Shear).

The first symbol, N, represents the number of sides or faces of the compound prism. When the numerical value of N is significant its value will appear as a subscript (N_4 for quadrilateral and N_6 for hexagonal prisms); otherwise N appears without the subscript.

The second symbol, E, indicates the form of the entrance face of the prism. When E appears without a subscript, the shape of the entrance face is not significant to the statement in which it appears. When the shape is significant it will be indicated by subscripts (E_p for plane and E_s for spherical entrance face).

The third symbol, W, represents the maximum width fringes that can be obtained, with a perfect wave front, by moving the prism along the lens axis. The value of W is finite if the direction of shear is parallel to the refracting edges of the prism (fig. 3) and the beam-dividing area is divided between the two component prisms (fig. 4). The value of W is infinite if the direction of shear is perpendicular to the refracting edges of the prism, regardless of whether the beam-dividing areas are confined to one prism or divided between the components.

The lateral separation of the components of the principal ray, obtained by separating the planes of the two beam-dividing areas, corresponds to the introduction of a fixed wedge between the two component wave fronts. Similarily, the wedge between the wave fronts that is caused by a separation of the two coherent images of the source in the direction of shear may be called the variable wedge. When the directions of these wedges are the same they cannot be distinguished and the fringes act exactly as they do in a prism without a fixed wedge, When the direction of the fixed wedge is perpendicular to that of the variable wedge, the widths of the fringes in these two directions are proportional to the magnitude of the two wedges, respectively. The width in one direction (horizontally in fig. 2) is invariant and the width in the other direction (vertically in fig. 2) varies with the position of the prism relative to the lens (or point of convergence).

A prism with a built-in wedge that is perpendicular to the direction of shear will be designated by W_s (s stands for German *senkrecht*, meaning "perpendicular"). If the numerical value of W is to be indicated also it will appear as a subscript of W and expressed in units of milliradians. Thus a prism with a built-in wedge of 2.1 mrad will be indicated by $NEW_{2.1s}S$.

A prism with a built-in wedge that is parallel to the direction of shear will be designated by W_p (p for "parallel"). Similarily, a prism with no built-in wedge (aluminum on one surface only) will be designated by W_∞ because the magnitude of W is given by this subscript.

It will be noted that the numerical value of W in a NEW_pS-type prism is also infinity. However, it is desirable to discriminate between the three types and these symbols seem to be most appropriate.

The fourth symbol indicates the magnitude and direction of the shear. If the value and direction are insignificant to a statement in which it appears, the symbol S will suffice. If shear is produced by a relative rotation of the prism component, to be described later, its direction will be parallel to the refracting edges of the prism and the corresponding symbol is S_p. If shear is produced by using prisms of different angles, the direction of shear will be perpendicular to the refracting edges of the prism and the corresponding symbol is S_s. When the numerical value of the shear is to be indicated it will appear in units of milliradians as a part of the subscript of S. Thus a shear of 2.1 mrad in a prism having components of different angles will be indicated by $S_{2.1s}$. Similarily, a prism having a shear of 2.1 mrad that is introduced by a relative rotation of similar prism components will be designated by $S_{2.1p}$.

4. Geometry of the Prism Interferometer

The angles and size of the prisms for the shearing interferometer are not critical. The choice of size and angles of prisms that can be used to produce a workable instrument is so diverse that only optimum forms will be considered. These forms are chosen because they fulfill significant favorable operational performances that are unique for the different forms.

4.1. Size of the Prism

An optimum size prism (length of face B in fig. 1) has a dividing plane of 1.5 in. A 1.0 in. or a 1.7 in. dividing plane would be almost equally satisfactory. Larger prisms require better glass and introduce larger aberrations because of thickness, unless a spherical entrance face is used. Small prisms are more difficult to polish and adjust than larger ones.

4.2. Surfaces

All reflecting surfaces of the prism interferometer are planes. The flatness of the beam-dividing plane is critical. The outer reflecting surfaces are less critical because the cones of light have small cross sections (being near the vertex of the cone) at the points of reflection. The entrance and exit faces may be planes if the angle of the cone of light does not exceed 1/8 rad (as when testing an $f/8$ lens with one conjugate relatively large). When larger cones are used, the spherical aberration of the prism introduces appreciable deformation of the wave front and consequently error into the results of measurement. This error is introduced at the entrance face because of the difference in refraction of any two rays that are combined to produce interference. Deformation of the wave front by the entrance face is practically eliminated if a planoconvex lens (figs. 5E and 5J) having the center of curvature of its spherical surface located near the point of internal reflection, P_1, is cemented to the entrance face.

Since any two rays that are combined to produce interference emerge parallel and nearly coincident, the shape of the exit face has little effect on the order of interference observed at any point in the aperture of the lens.

Distortion by a plane exit face does not contribute error to the measurements if they are made visually or photographically, provided reference points are established in the aperature of the objective being tested. If photography is used without previously established reference points (reference points inserted in the photograph), the distortion by the exit face will be appreciable for large cones of light but negligible for small cones.

4.3. Angles of the Prism

The angles of the prism are not critical. Since the magnitude of the angles does not affect the difficulty of construction, but does affect the performance, the choice of angles will be based on certain optimum constraints or requirements of performance. Thus, the angles will be so chosen that when the principal ray of light from a circular lens (circular cone of rays) enters the plane entrance face normally and at the center of this face (thus permitting a maximum size cone of rays to be accepted) the components of this principal ray will emerge from one exit face of the prism with minimum refraction. This condition provides minimum refraction for the entire cone of light and, consequently, minimum error in the results of measurement caused by aberration in the prism.

The prisms shown in figure 5 represent the several forms that are recommended. Other forms are possible but these are adequate and sufficient for all possible applications. For purposes of discussion the characteristic angles of the several prisms are represented as follows: the N_6EWS_p-type prisms by α', β', and ω' (fig. 5A); the N_4EWS_p-type prisms by α' and β' (fig. 5F); the N_6EWS_s-type prisms by α_1, α_2, β, and ω (fig. 5B, the angles β and ω may or may not be equal for the two component prisms); the N_4EWS_s-type prisms by α_1, α_2, and β (fig. 5G). The angles shown here for all $NEWS_p$-type prisms represent the components of the prism angles in the plane of this drawing. Since the elements of these prisms are rotated (about an axis lying in this plane) to produce shear the refracting edges are no longer perpendicular to the figure. If the angle of rotation of any two prism components are $+\Omega$ and $-\Omega$, respectively, all refracting edges are at angles of $(90°\pm\Omega)$ to the plane of figure 5. The angles of the prisms shown here are α, β, and ω. The corresponding components of the prism angles in the plane of figure 5 are α', β', and ω'. The relationship between any prism angle (unprimed) and its component in the plane of this drawing (primed) is

$$\text{Tan } X=\cos\,\Omega \tan X',\ (X=\alpha,\ \beta,\ \text{or}\ \omega). \qquad (1)$$

The deviation of the components of the principal ray out of the plane of figure 3, at the points of internal reflection, P_1 and P_2, depends upon the angles α and Ω. Since the deviations are equal and of opposite signs, and since the angle between the two emerging components from either exit face is the angle of shear, ϕ, the approximate relationship between ϕ, Ω, and α is given by

$$\tan 1/2\ \phi=n \sin\,\Omega \tan\,\alpha, \qquad (2)$$

where n is the refractive index of the glass.

The angle of shear in the $NEWS_s$ prism is, approximately,

$$\phi=2n(\alpha_1-\alpha_2). \qquad (3)$$

When the angle α, of the N_6EWS_p prism is small and the components are rotated π radians the prism becomes a N_6EWS_s type. Such a prism, shown in

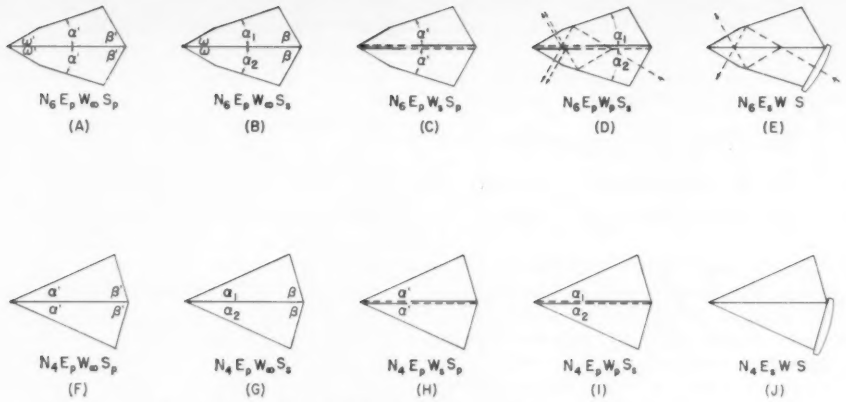

FIGURE 5. *Several different types of prism interferometers.*
The letter-number abbreviations, described in section 3, describe these prisms.

figure 6A can be made with adequate shear and to accept an $f/1$ cone of light. However, for testing such small f-value systems, spherical faces (fig. 6B) should be used on the prism to avoid spherical aberrations. When the angle of rotation, Ω, equals π radians, the angle, α, of one prism is reversed and the shear, ϕ, equals $4n\alpha$. Consequently, the angle, α, is usually small for such prisms.

Minimum refraction is obtained in plane face prisms when the principal ray of the entrance cone is normal to the plane entrance face and the two components of this principal ray, that emerge from each of the exit faces, make equal angles, but of opposite sign, with the exit face. If the prism is of the $NEWS_p$ type, the angles of emergence of the two pairs of beams are equal. However, the angles of emergence for the $NEWS_s$-type prisms, because $\alpha_1 \neq \alpha_2$, cannot be a minimum for both pairs simultaneously. Consequently the pair of beams that emerges from face A_2 (fig. 1) will be ignored when considering the constraints of angles. When rays, $1''$ and $2'$, (fig. 1A), that emerge from face A_1 suffer minimum refraction, their angles of emergence are $+(1/2)\phi$ and $-(1/2)\phi$, respectively, and the rays $1'$ and $2''$, that emerge from face A_2 will be $0°$ and ϕ, respectively. The reason for minimizing refraction of the beams that emerge from face A_1, instead of those from face A_2, is due to their greater equality

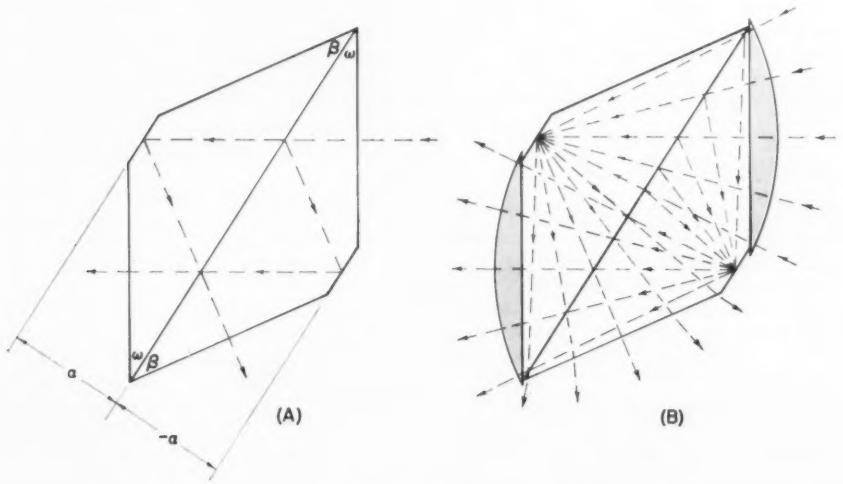

FIGURE 6A. *Prism interferometer for testing very large cones of light.*
B. *Spherical entrance and exit faces eliminate error due to refraction of the prism surfaces.*

of intensity and, consequently, better visibility of fringes. This pair of beams will usually be used for making measurements.

It can be shown by simple triangulation that minimum refraction is obtained in plane face prisms if

$$\left.\begin{aligned} \beta &= 3\alpha' && \text{for all } N_4E_pWS_p\text{-type prisms,} \\ \beta &= 2\alpha' + \omega' && \text{for all } N_6E_pWS_p\text{-type prisms,} \\ \beta &= 2\alpha_1 + \alpha_2 && \text{for all } NE_pWS_s\text{-type prisms.} \end{aligned}\right\} \quad (4)$$

We will, therefore, impose these constraints on the design of all prisms described here. Since the face of prism A_1B (fig. 1), that corresponds to the entrance face of prism A_2B, is not used it may be left unpolished. If, however, one wishes to be able to use either prism for receiving the light this surface should be polished and the angle β_1 should be equal to β_2.

The angles may have a variety of values consistent with eq (4). The range of these values depends upon factors such as the magnitude of the angle of shear (defined by ϕ), the form of prism to be used, the refractive index of the glass, the maximum size cone of light that is to be used, and whether or not the outer reflecting surfaces are to be coated for increased reflection.

The range of usable values for α' in the N_6EWS_p prism is from 0° to ω'. Obviously, as α' approaches ω' the N_6EWS_p prism becomes N_4EWS_p in form. The upper limit for α' in the N_4EWS_p prism is $\pi/7$ rad (=25.7°, approximately). Figure 7 illustrates the limitations of α' for this type of prism. If α' ($=\omega'$) is greater than $\pi/7$ rad (assuming the principal ray enters the center of the entrance face and normal to it), the beam will not suffer two divisions at the beam dividing plane, as is shown in figure 7A.

The lower limit of $\omega'(=\alpha')$ for the N_4EWS_p prism depends upon whether the outer reflecting faces are coated to prevent transmission of light or, if not coated, on the refractive index of the glass. As shown in figure 7H, the internal angle of incidence, ψ, increases with decreasing values of α'. Also the angle ψ is different for different rays of the cone. When ψ exceeds the critical angle of internal reflection, some of the light is transmitted at the internal reflecting surfaces and becomes lost. Consequently, if the principal ray is incident at the critical angle, then one-half of the observed image of the lens will appear poorly illuminated. If the reflecting areas of the prism do not appear in the emerging beam, these areas can be optically coated for increased reflection (as shown in fig. 8). The above discussion also applies to hexagonal prisms (fig. 8B). In this case, the entire areas of the reflecting surfaces may be coated.

A N_4EWS_p prism having a value of 24° for α' will provide total internal reflection to a 15° cone of light (corresponding to an $f/3.8$ cone) if it is made of borosilicate crown glass ($n=1.517$). The same shape prism, if made from a dense flint glass ($n=1.72$), will provide total internal reflection to a 25° cone, which corresponds to an $f/2.3$ beam.

We have described in section 2 above how to obtain and control the angle of shear by rotating one prism relative to the other (all $NEWS_p$ prisms), We have also described how shear may be obtained by using component prisms with different angles. Shear may also be obtained by purposely introducing (by grinding and polishing) pyramidal error into the prisms. Obviously this has the same effect on deviating the beams out of the plane of figure 1A that a relative rotation of the components has when the two components are cut from a single original prism.

In general, when two surfaces are cemented together, as described above, they will not be parallel. Also the vertex of the wedge between them may have any direction. Consequently, neither component of this wedge, perpendicular or parallel to the edges of either prism component, will be zero.

If the dividing plane is confined to one surface, the cement effectively becomes a part of the component

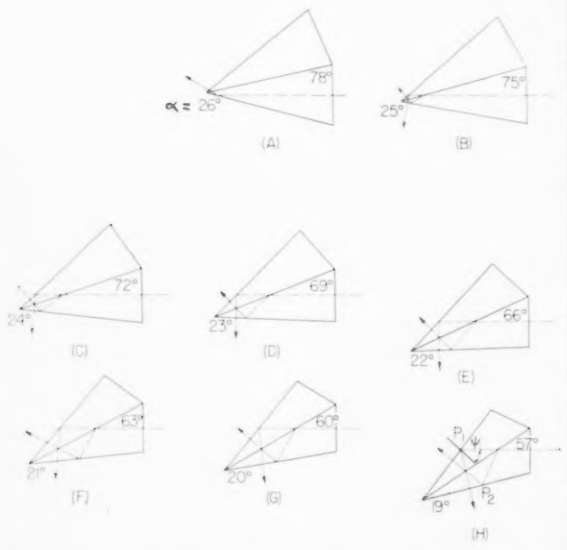

FIGURE 7. *Several prism interferometers showing the effect on the rays, from above the upper limit of α (=26°) to the lower practical limit (=19°).*

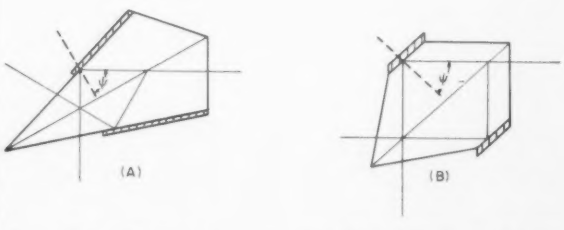

FIGURE 8. *Prism interferometers with opaque reflecting surfaces to prevent transmission of light when the angle of incidence, ψ, is larger than the critical angle.*

prism that is uncoated and we have dissimilar prism components even though the original components were identical. In general, two of the angles are different and one prism has pyramidal error.

5. Construction of the Prism Interferometer

Only prisms of optimum form will be described. All prisms are assumed to be free from pyramidal error, i.e., all refracting edges of a prism component are assumed to be parallel.

5.1. $N_6E_pW_\infty S_p$-Type Prisms

Using the symbolic designation described in section 3, the original *WSI* prism illustrated in figure 5A, was a hexagonal prism (N_6), with a plane entrance face (E_p). The two beam-dividing areas were produced by evaporating a semireflecting layer of aluminum on one of the inner surfaces of the prism (W_∞, dividing planes coplanar), and shear was introduced by a relative rotation of the two prism components.

Figure 9 illustrates how this prism was constructed from a single original prism (figure 9A) having angles β, γ, and ω. None of these angles is critical but their values may be advantageously chosen, as described above. The angle γ is removed by grinding and polishing a fourth face, A, that makes an angle, α, between it and the opposite face, B, as shown in figure 9B. The prism AB is then cut into two equal prisms, A_1B_1 and A_2B_2, by sawing it parallel to the plane of figure 9 This produces two quadrilateral prisms (figure 9C) that have identical angles, each of these component prisms being one-half as high as the original (minus the thickness of the saw cut).

A semireflecting coat of aluminum is put on surface B_2, and the two component prisms are cemented, together as shown in figure 9D. The thickness and variations of thickness of the cement are not critical. Optimum conditions, however, favor a thin parallel film of cement that has optical properties approximating those of the glass prisms. The reflectivity of surface B_1 is negligible and the cement effectively becomes a part of prism A_1B_1.

5.2. $N_6E_pW_\infty S_s$-Type Prisms

This prism is formed from two dissimilar prisms that have a difference in the two angles α_1 and α_2 (fig. 5B) that equals approximately one-half of the angle of shear divided by the index of refraction of the glass.

A practical procedure is to make two prisms, as described in section 5.1. above, with different values for α. After sawing the prisms into equal parts the pairs are crossed by cementing one component of an original prism to a component of the other. Thus, two prisms of this type are obtained.

The reason for making prisms long enough to be sawed into two components is because two small surfaces are more difficult to polish than one larger surface.

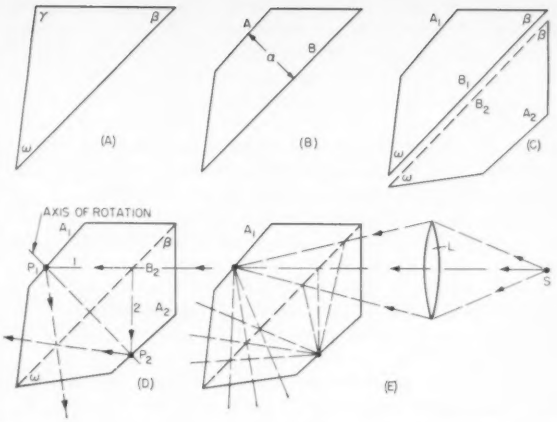

FIGURE 9. *Several forms of a prism interferometer during stages of its construction and adjustment.*

Figure 9 E shows how the prism acts upon a converging beam of light to produce two coherent images of the source.

5.3. $N_6E_pW_sS_p$ and $N_6E_pW_pS_s$-Type Prisms

These prisms differ from the $N_6E_pW_\infty S$ (either $N_6E_pW_\infty S_p$ or $N_6E_pW_\infty S_s$), described above, by having semireflecting dividing planes on each of the two surfaces B_1 and B_2 of figure 9C. The dividing plane of first incidence, B_2, extends from the vertex β of prism A_2B_2 to a vertical line in this plane that passes through the normal projection of P_2 onto it. The dividing plane of second incidence, B_1, extends from the vertex ω of prism A_1B_1 to a vertical line in this plane that passes through the normal projection of P_1 onto it.

5.4. NE_sWS-Type Prisms

The only difference between this prism and the NE_pWS described above is that a planoconvex lens is cemented to the entrance face. Best results are obtained if the lens and prisms are made of similar glass. The center of curvature of the convex surface should coincide approximately with the point P_1, where the principal ray suffers reflection from face A_1 of the prism.

5.5. N_4EWS-Type Prisms

The only difference between the N_4EWS prisms and the corresponding N_6EWS types described above is that the angle α is equal to ω. This changes the component prisms from quadrilateral to triangular in form. They are easier to construct, easier to adjust, and in some respects, have significant advantages over the N_6EWS types.

6. The Beam-Dividing Plane

The recommended optical coating for reflection and transmission of the beam-dividing plane is aluminum. Dielectric coatings that have been tried produced unfavorable polarization effects.

The ratio of reflection to transmission is more critical in this prism interferometer than in many other types of interferometers. If we assume R_1 and T_1 to be the reflection and transmission, respectively, of the beam divider at the first incidence and R_2 and T_2 the same at the second incidence, then the relative intensities of the several component beams may be designated by these quantities before and after each incidence on the beam divider. If we assume unit intensity for the beam before its first incidence, then the transmitted and reflected components are T_1 and R_1, respectively (see fig. 10). The T_1-beam is again divided at the second incidence into a T_1 T_2-beam and a T_1 R_2-beam. The R_1-beam is divided into a R_1 T_1-beam and a R_1 R_2-beam.

If the beam divider is coated with a uniform film, the difference between R_1 and R_2 (or T_1 and T_2) is due only to the difference in angle of incidence. The difference in angle of incidence varies from one type prism to another with variation in the prism angles, and also from one ray to another in the converging beam.

If the first division of the beam occurs at the inner surface of one prism (see fig. 4) and the second division at the inner surface of the other prism, then the difference between R_1 and R_2 (or T_1 and T_2) may be decreased by placing one prism closer to the source during the aluminizing process.

The contrast in the fringe pattern depends upon the ratio of the intensities of the two beams that combine to produce interference. Since the difference between R_1 and R_2 (or T_1 and T_2) is usually much smaller than the difference (T_1-R_1 or T_2-R_2), the pair of beams R_1 T_2 and T_1 R_2 are nearer equal than the pair R_1 R_2 and T_1 T_2. Consequently, the former pair will produce the best contrast and are, therefore, the beams usually used for making observations. When the fringes are to be photographed the R_1 R_2-T_1 T_2 beams will be used for visual adjustments for and during exposure.

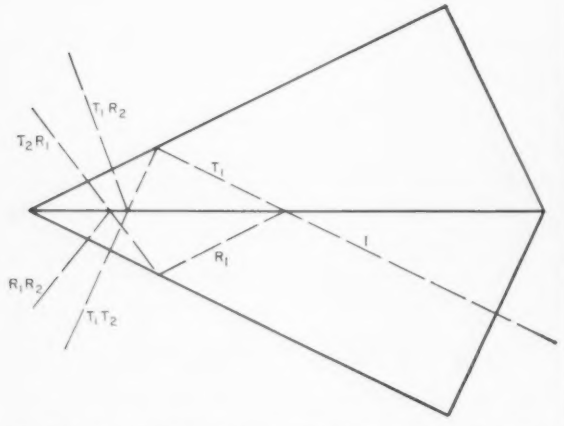

FIGURE 10. *Ray trace showing relative intensities of the four emerging beams*

An adequate test for the ratio of reflection to transmission of the beam divider is to observe visually the two images of a small source by means of the R_1 R_2-T_1 T_2 beams. If the images appear to differ in intensity by no more than a factor of about 2, the contrast and intensity of fringes produced by the R_1 T_2-T_1 R_2 beams will be adequate.

7. Optical Cement

Any optical cement that can be worked as a liquid, becoming hard at ambient temperatures, can be used in these prisms. Canada balsam has been used quite successfully. Its hardness is adjusted, by distillation of volatile constituents, to a consistency considered proper by an experienced optician for cementing lenses.

The advantages of Canada balsam over other cements is that its viscosity may be varied at will with temperature, and almost unlimited time is available for making the adjustments. This cement should be cooked until it is quite hard at ambient temperatures. Other cements are more stable than Canada balsam, do not require elevated temperatures, and do not permit unwanted changes in the adjustments after the prism is put to use.

8. Prisms Support and Adjusting Screws

The adjustment of the *WSI* prism is quite similar to that for the Kösters prism described in reference [8]. The two type prisms, N_6EWS and N_4EWS, require different blocks for adjusting the prisms.

A photograph of the block used for adjusting N_6EWS-type prisms is shown in figure 11. It consists of a compartment that approximates the shape and is slightly larger than the prism. Four vertical adjustable screws contact the bottom surface with

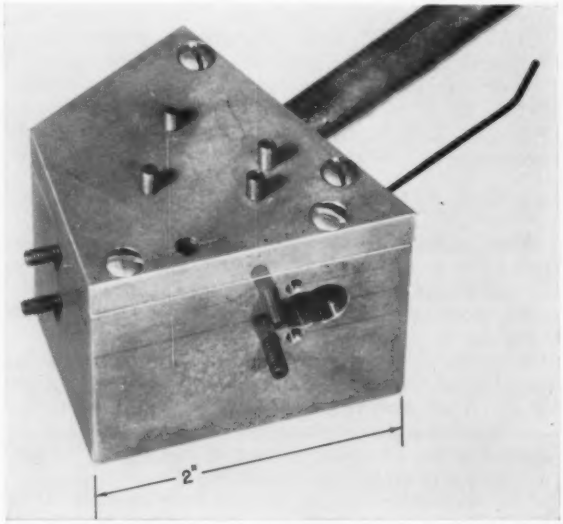

FIGURE 11. *Photograph of adjustable block for adjusting N_6EWS-type prisms.*

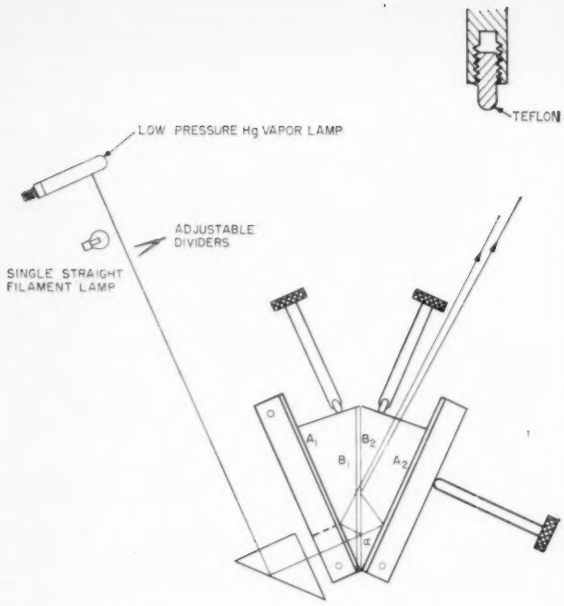

FIGURE 12. *Schematic diagram of V-block for adjusting N_4EWS-type prisms.*

The inset shows how the contacting ends of the screws are modified to avoid injuries to the glass surfaces. The adjustable dividers serve to measure the angle of shear.

two screws supporting each component prism. The top of the block has four vertical screws placed directly above those in the base of the block.

Two horizontal screws contact the entrance face of the prism and two others contact the exit face of the same component prism. Also, four similarly placed screws contact the corresponding faces of the other component prism. An entrance aperture, not shown in the photograph, and an exit aperture permit the light to pass through the prism to the observer. A supporting rod is shown for holding the block steady during the adjustment. This block may be heated on a simple hotplate.

The *V*-block for adjusting the N_4EWS prisms illustrated in figure 12 is very similar to that used for the Kösters prism. Additional detail that applies to this adjustment appears in reference [8], which should be consulted.

9. Illumination for Adjusting the Prism

Monochromatic fringes of interference are obtained from a low-pressure mercury vapor lamp. This lamp is cylindrical in form, is approximately 3 cm in diameter, and 16 cm long. White light fringes are obtained from a galvanometer lamp that has a spherical globe 2.5 cm in diameter and a single straight filament. A right-angle prism is used to reflect the light into the prism.

The mercury lamp is located, as shown in figure 12, approximately 120 cm from the prism. The galvanometer lamp is in line with the prism and mercury lamp and approximately 10 cm closer to the prism. This permits simultaneous use of both sources. The light passes through the prism in the reverse direction of that for normal use. This reversal of direction may be applied to almost any interferometer.

A low power telescope that permits a broad range of focusing is quite helpful for viewing and counting the interference fringes that are formed in the prism. These fringes are localized as in the conventional Mach-Zehnder interferometer.

10. Adjustment of the Prism Interferometer

The adjustment of quadrilateral prisms (N_4EWS) is no different from that of hexagonal prisms (N_6EWS). Consequently, a description of one type is sufficient. Since the former type is simpler in structure and easier to adjust because of differences in the mechanism for performing the adjustments, the N_4EWS type will be used for this description.

If the entrance face is to be spherical (NE_sWS), a plane entrance face prism is constructed and adjusted before the planoconvex lens is cemented to the plane entrance face.

A description of the adjustments of all types of prisms is provided by describing those for the four types shown in figure 13. Figures 13A and 13B show prisms with dissimilar components ($\alpha_1 \neq \alpha_2$). Figures 13C and 13D show prisms with similar components. The two beam divisions occur at a common dividing plane in figures 13A and 13C and at different planes in figures 13B and 13D.

There are four adjustments to be performed on a prism. Some of these are important and some are relatively unimportant to the performance of the prism. These adjustments are as follows: (1) to adjust the optical path of the two components of the

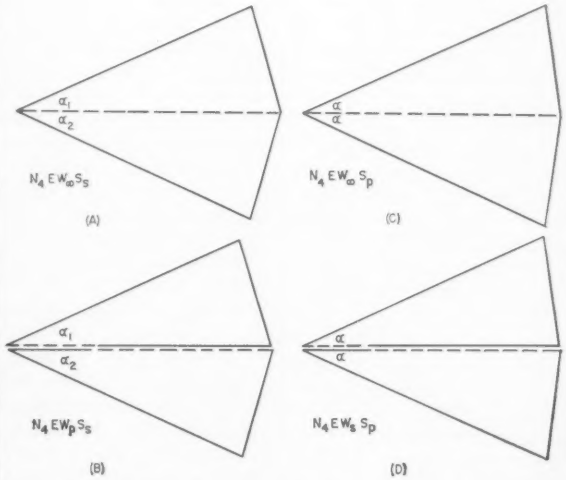

FIGURE 13. *Four types of prism interferometers.*

principal ray 1 and 2 (fig. 9D) to equality so that the zero order of interference is centered in the fringe pattern; (2) to adjust the thickness, t, of the cement; (3) to parallel the film of cement so that surfaces B_1 and B_2 (fig. 9C) are approximately parallel to each other; and (4) to adjust the magnitude of the angle of shear, ϕ.

There is no definite order for making these four adjustments except that number (4) should be fourth and last. The other three can be performed in any order. However, by first making adjustment number (1), and maintaining it, fringes of good contrast are available for making the other adjustments.

10.1. Interferometric Fringes for Observing Prism Adjustments

There are two types of interference fringes that are used for making prism adjustments. One of these sets of fringes is nonlocalized and the other is localized with a high degree of variability in the position of the plane of localization. The nonlocalized fringes are produced by two images of a small source. A lens or mirror must be used to produce an image of the source and the prism forms two images of it by amplitude division of the beam. The arrangement shown in figures 1 and 9 with a suitable source will fulfill the requirements. The direction and angular width of the nonlocalized fringes, mentioned in section 2 above, depend, respectively, upon the direction of the line joining the two coherent images of the source and on the angle subtended by this line at the point where the fringes are observed. This source must be small [1] in the direction of shear. The nonlocalized set of fringes is unnecessary for making adjustments except when a large angle of shear is used. When ϕ is large the localized fringes cannot be seen without the use of a long-focus microscope because they are so closely spaced.

The localized fringes may be used for making all necessary adjustments if the value of ϕ is not too large (approximately 0.02 rad). These fringes are, in all respects, similar to the fringes produced by a Mach-Zehnder [6] interferometer. They may be localized anywhere from $+\infty$ to $-\infty$. The plane of localization shifts so much during initial adjustments that a low-power telescope with a large focusing range is quite useful. These fringes may also be seen with the unaided eye. An extended source may be used when the fringes have moderate spacing and the order is small, but a source that is narrow in the direction of shear improves the contrast and is necessary when the fringes are very closely spaced.

When the dividing plane is confined to one plane as in the $NEW_{\infty}S$-type prisms (figs. 13A and 13C) and an extended or narrow source is used without a lens, as shown in figure 12, only one set of fringes is seen. When the dividing planes are divided between the two prism components (figs. 13B and 13D), three sets of fringes are seen. Figure 14 illustrates how the paths of the light rays differ for the three sets.

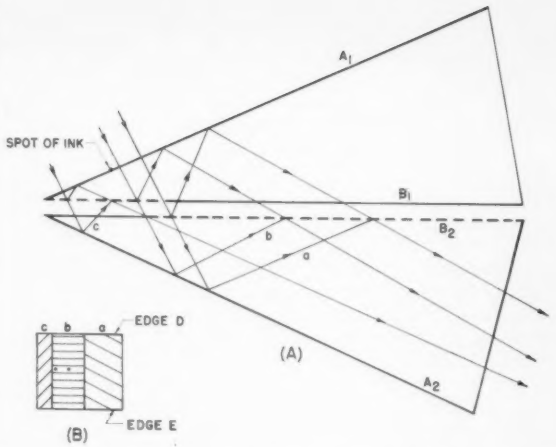

FIGURE 14A. *Ray trace showing how three sets of interference fringes are obtained when the dividing planes are on the two surfaces B_1 and B_2.*

B. *Appearance of fringes when illuminated as illustrated in figure 12. The edges, D and E, are the intersections of face A_2 with the base and top surfaces of the prism.*

10.2. Preparation of Prism for Adjustments

The prism components are cemented together initially in much the same manner as described for the Kösters [8] prism. The cement is assumed to be Canada balsam. The faces of the prism are cleaned. A small spot of ink is then placed on the exit face, A (which becomes the entrance face during the adjustment), approximately 2 mm from the vertex of angle α and midway between the edges D and E (fig. 14B) of the prism. The compound prism is placed in the adjustable V-block (fig. 12) and the assembly in an oven. See reference [8] for oven characteristics. Using the mercury lamp, illustrated in figure 12, and observing the spot of ink one sees three spots. One is a direct image of the inkspot and the other two are images in silhouette produced by light reflected from faces A_1 and A_2. The images of this spot aid the observer in finding fringes and in placement of the zero-order fringe when adjustments are complete.

10.3. Adjustment Procedure

The separation of the two images of the spot of ink, described above, is a coarse (or rough) measure of the prism adjustment. A low-power telescope or a long-focus microscope is convenient for observing both the spot and the interference fringes. A lateral separation (in the direction perpendicular to edges D and E, fig. 14B) of the images indicates either a relative rotation of the prism components or a lateral wedge in the cement. A separation in the direction perpendicular to the vertex of α indicates a difference in the two light paths. In general, if one prism is moved relative to the other in this latter direction, the two images change their relative separation in this direction and, consequently, can

be made to approach coincidence. When they're close together, fringes of interference can usually be seen in the section (a, b, or c of fig. 14B) in which the images are seen.

If the prism is of the NEW_pS_s or NEW_sS_p type, the original inkspot should be located at a distance from the vertex, α, such that the two images of it appear in the central section, b, of figure 14B, because this section transmits the light when the prism is used later for making measurements. The relative movement of the images of the inkspot is performed by sliding one prism on the other with the cement as a fluid lubricant. Heating the cement permits the viscosity to be altered at will.

After interference fringes are obtained with the mercury lamp their visibility can usually be improved by reducing the order of interference. When the order approaches zero, white light fringes may be seen with the tungsten lamp. Both lamps may be in use simultaneously. The order of interference is altered by a relative movement of the prisms perpendicular to their refracting edges (vertices of the angles).

When the direction of the wedge is known the adjustable V-block and its screws can be adjusted to correct the cement wedge. Reducing the angle of the block and applying pressure to the tops of the prisms causes the cement wedge to become thinner at the top. Conversely, by opening the V-block wedge until it is larger than the sum of the prism angles, 2α or $(\alpha_1+\alpha_2)$, the cement wedge becomes thinner at the bottom. These adjustments are described in reference [8] and apply equally well to this prism. A zero wedge in the cement is desirable for all prism types $NEWS_p$.

The wedge in the cement of prism types NEW_pS_s (fig. 13B) is unimportant. This prism is relatively easy to adjust if the angle $(\alpha_2-\alpha_1)$ is not large. The fringes are rotated parallel to the refracting edges of the prism and the zero order is adjusted to center (on the inkspot shown in fig. 14A). Best compensation is obtained for white light use if the thickness of the cement is small. The effect of cement thickness on the nature of the interference fringes is insignificant in prism types $NEWS_s$ (fig. 13B) but is important in prism types NEW_sS_p (fig. 13D).

The localized fringes in prism types $N_4E\ W_\infty S_s$ (fig. 13A) will always be relatively narrow, since the angle between the two emerging wave fronts approximates the angle of shear and is usually too large to yield broad fringes. The wedge in the cement adds to this angle and is difficult to distinguish from the component due to the prism angles. However, the cement wedge can always be reduced to insignificance by heating it to produce low viscosity and applying a little pressure on the prisms. Even if a wedge remains in the cement of this prism, it can be counteracted or compensated for by rotating one prism relative to the other until the fringes are parallel to the vertices of the prism angles. Thus, a residual wedge in this prism does little harm.

The localized fringes in the $N_4EW_\infty S_p$-type prism (fig. 13C) will be very broad if there is no wedge in the cement and no relative rotation of the component prisms. If the fringes become parallel to the prism's refracting edges when one prism is rotated about an axis normal to the dividing plane, the vertex of the cement wedge is parallel to that of the prism. The maximum fringe width, during this rotation of prism components, is then a measure of the magnitude of the wedge. The direction can be determined by the usual test for increasing orders. If the reflecting film is on surface B_2 (fig. 12) and the cement is thicker at the top than at the bottom, the fringes will move away from the vertex of angles α when prism A_2B_2 is moved downward. Also, they will move toward the vertex of α when prism A_1B_1 is moved downward or prism A_2B_2 is moved upward.

The light that passes from a source, arranged as indicated in figure 12, through a NEW_sS_p-type prism produces three sets of interference fringes. These are indicated in figure 14B and labeled a, b, and c. One of the two interfering beams in each set is reflected from A_1. The second beam in each set travels the following paths: beam a is reflected from B_2 to A_2 and finally from B_2 again; beam b is reflected from B_2 to A_2 and finally from B_1; beam c is reflected from B_1 to A_2 and finally from B_1 again. The set a is identical to the fringes seen in prism type $NEWS_p$ (fig. 13C). Set c is the same as would be seen in this prism should it be rotated 180° in the adjustable V-block. The fringes in set b are independent of the wedge in the cement (assuming plane surfaces and homogeneous media). Consequently, these fringes will always be normal to the refracting edges of the prism. A relative rotation of the prisms will cause these fringes to become very broad. This occurs when Ω (defined above) becomes equal to 0. When this condition exists the fringes in set a are parallel to the vertex of the wedge formed by the two surfaces B_1 and B_2. Also, the width of these fringes is a measure of the magnitude of this wedge. The direction of increasing thickness of the cement wedge is the same as the direction of movement of the fringes (in set a) when prism A_2B_2 (fig. 12) is moved downward. When the direction and magnitude of the cement wedge are known, corrective measures may be taken to reduce it. When the surfaces B_2 and B_1 become parallel, all three sets of fringes will remain equally wide as Ω is varied for introducing shear. The angle of relative rotation of the prisms, Ω, may be held to a value that produces fringes of a convenient width for counting. By adjusting the zero-order fringe in set b to a reference point on the boundary between b and c the difference in order between sets b and c can be counted while component prism A_1B_1 is moved upward relative to component A_2B_2. This difference in order multiplied by the wavelength of the light is equal to $2t\sqrt{n_2^2-n_1^2\sin^2 3\alpha}$, where t is the thickness of the cement at the bottom of the prism (fig. 12), n_2 and n_1 are the refractive indices of the cement and glass, respectively. Thus the thickness of the cement wedge may be measured.

A similar count of the difference in order between sets a and b will also give a value for t. The change

730-853—64——3

of zero order in set b to zero order in set a is obtained by moving component prism A_2B_2 downward relative to component A_1B_1. This difference in order multiplied by the wavelength equals $2t\sqrt{n_2^2-n_1^2sin^2\alpha}$. Since this latter quantity is larger than that for sets b and c by a factor of 2 or 3, and since this count is not critical, the smaller value will usually be used for obtaining t.

If t becomes too small it can only be increased by recementing the prisms. Spacers in the form of paper strips placed along the margins (edges D and E, fig. 14B) will serve to control the thickness of the cement. If t is found to be too large, it can be readily reduced by prolonged pressure on the prisms which causes the cement to be forced from between the prism components. Usually a value of t that is within 50 percent of the optimum value will be satisfactory.

When the required value of t is obtained the prism components are rotated to produce the desired shear, the zero-order fringe is adjusted to the center of the prism aperture, and the temperature is reduced sufficiently slowly (approximately 25° per hour or less) to avoid excessive gradients during cooling.

11. Angular Deviation by the Prism

The mean deviation of a pair of interfering beams is the angle between the entrance beam and the bisector of the angle between any two emerging beams that combine to produce interference.

The range of deviation of interfering beams that may be obtained with this prism interferometer is considerable. There may be occasions when it is desirable to have a mean deviation of a pair of interfering beams equal to 0°, 90°, or both. The N_4EWS prism cannot be made to produce zero deviation. A 90° mean deviation, however, is obtained with the N_4EWS_p prism by making $\alpha=22.5°$. The N_6EWS_p prism will produce a 90° mean deviation of two interfering beams if $(\omega+\alpha)=(\beta-\alpha)=45°$. The N_6EWS_s prism will produce a mean deviation of 0° for one pair of beams and 90° for the other pair of interfering beams if $\alpha_1=-\alpha_2$ and $\beta=\omega=45+2\alpha_1$.

12. Summary

Many types of prisms have been constructed and tested. They are found to be quite useful for measuring the shapes of wave fronts and changes in wave fronts with time. Prisms with large shear angles yield higher accuracy when testing high-quality (telescopic) optical systems, and prisms with small shear angles yield relatively high accuracy when testing systems that have large aberrations (large OPD variations).

Important advantages of the several prism types are: N_6EWS prisms can be most economically made by grinding and polishing one surface, A, (fig. 9B) on right-angle reflecting prisms, which are readily available commercially. N_4EWS prisms are easier to make from unworked glass because only three faces have to be polished, instead of the four required for the N_6EWS prisms. The range of deviations for the N_6EWS prisms is different from that of the N_4EWS type, and this is sometimes important. The vertex of the cone of light, received by an N_4EWS prism (image S, fig. 1), can be much closer to the exit face than for the N_6EWS prism, which is important for observation of large cones of light from high-power optics, because the size of the pupil is limited. The NEW_sS prism permits rotation of the fringes whereas the NEW_pS prisms do not. The N_6EWS prism can be made to accept a larger cone of light than that for the N_4EWS type. The N_4EWS prisms requires a simpler fixture for making adjustments (fig. 12) than does the N_6EWS type (fig. 11). These and other differences permit the choice of a best type for any given application.

All prisms used in this development were made by Mr. John V. McDermott.

13. Appendix A

Reference Points

The analysis of data taken with the WSI requires that the reference points be chosen in a manner that permits the application of the operations described in reference [5]. The reference points should be equally spaced on a straight line (usually a diameter of the lens or mirror being tested) that is parallel to the direction of shear. The angular spacing of the points is equal to the angle of shear. Such a set of points is defined as a "family" of reference points.

If the reference points are labeled (see fig. 15A) P_0, P_1, P_2 . . . P_N, where $(N+1)$ is the number of points in the family, the corresponding images will be labeled (fig. 15B) P_0' and P_0'', P_1' and P_1'', P_2' and P_2'', . . . P_N' and P_N''. One image of each point will coincide with images of the adjacent points. One image of P_2 (i.e. P_2') will coincide with image P_1'' and the other image of P_2 (i.e. P_2'') will coincide with image P_3''. If one point (such as P_2 in fig. 15C) is displaced from its family position the images of it will not concide with those of the neighboring points (fig. 15D). If the line of reference points (fig. 15E) is not parallel to the direction of shear the images will not coincide in pairs.

The number of points in a family depends upon the angle of shear and the angular aperture of the lens or mirror being tested. The ratio of aperture angle to shear angle is equal to the number of spaces between the points plus the excess spaces between the border and end points. The excess fraction of spaces allows for a possible change of one in the number of members of a family. For instance, if there are 3½ spaces and one point is chosen at the center, then only 3 points can be included in the family. However, if one point is chosen near the margin, there will be 4 points in the family.

The position of the family of points on the line is not critical. When one point is chosen, however, the positions of all members of the family are known.

The chosen point may be at the center, at the margin, at any chosen distance from the margin or center, and on any line parallel to the direction of shear. The chosen line is usually a diameter of the circular aperture (if it is circular) but may be any chord of this circle that is parallel to the direction of shear and of sufficient length.

It sometimes happens that the number of points in a family is too small and, consequently, the spacings are too large for sufficient data. For example, if an $f/11$ (5.2° aperture angle) telescope objective is to be tested with a prism whose angle of shear equals one degree (see fig. 16), the largest number of reference points that may be included in a family is six. This is obtained by choosing one point (whose images, P_0' and P_0'', appear as dots in the figure) near the margin. If one point (whose images P_5' and P_5'' appear as small circles in fig. 16) is chosen at the center of the lens, it will be found that the family consists of only five points; and since the number of reference points in the fringe pattern is one less than the number in the family, there will only be four points for reading data. Five or six points may not provide data at sufficiently close intervals along the line of reference points—especially if the optics that are being tested have zonal errors.

The number of usable points along the line of reference points may be increased by using two or more families. Thus, two families of points (labeled family No. 1 and family No. 2, in fig. 16) may be combined to decrease the angular spacing to 0.5°. A third family may be added to provide additional points. Any integral number of families may be added to obtain data at as many points as desired.

Reference [5] describes how to compute for one family of points. We will show here how to apply more than one family. When two or more families of points are combined, it is desirable to use a different unit for r and to choose equal spacings for the points. This permits the use of integers for subscripts with no added complications. When two families are to be used, the separations of the points equal one-half the shear. When three families are used, the spacing is one-third the shear, etc.

We will use the fringe pattern of reference [5] (shown in fig. 17A) to show how to apply two families of points. The second family is added (fig. 17B) as small circles located midway between adjacent points of the original family of points. The orders of interference, for all points in the fringe pattern, are listed in column 2 of table 1.

The equations of observation (No. 5, ref. [5]) for family No. 1 are

$$\left.\begin{aligned}
\delta_2&=\delta_0+2.74+r-2\epsilon\\
\delta_4&=\delta_2+2.10+r-4\epsilon\\
\delta_6&=\delta_4+1.70+r-6\epsilon\\
\delta_8&=\delta_6+1.45+r-8\epsilon\\
\delta_{10}&=\delta_8+1.30+r-10\epsilon\\
\delta_{12}&=\delta_{10}+1.00+r-12\epsilon\\
\delta_{14}&=\delta_{12}+0.30+r-14\epsilon
\end{aligned}\right\} \qquad (10)$$

and the set for family No. 2 are

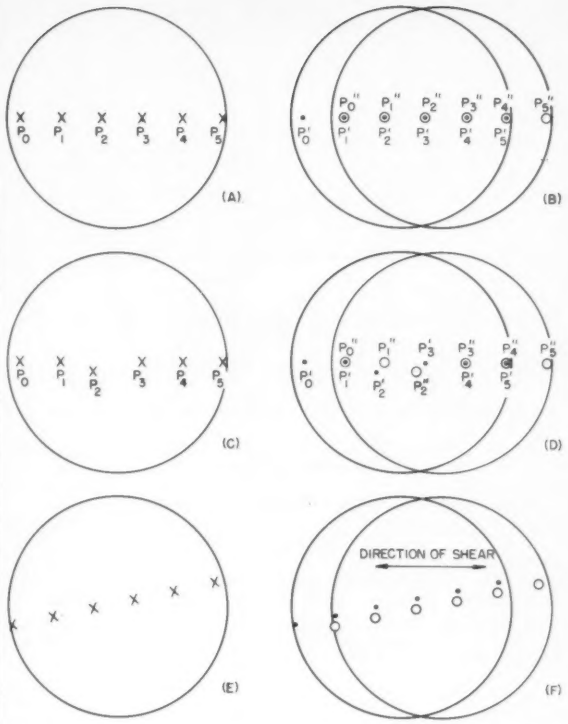

FIGURE 15. *Illustration of the characteristics of a family of reference points.*

$$\left.\begin{aligned}
\delta_3&=\delta_1+2.40+r-3\epsilon\\
\delta_5&=\delta_3+1.88+r-5\epsilon\\
\delta_7&=\delta_5+1.56+r-7\epsilon\\
\delta_9&=\delta_7+1.37+r-9\epsilon\\
\delta_{11}&=\delta_9+1.18+r-11\epsilon\\
\delta_{13}&=\delta_{11}+0.71+r-13\epsilon
\end{aligned}\right\} \qquad (11)$$

When using two or more families of reference points, the methods of solution described in reference [5] are impractical. The deviations (δ's) of one family will not, in general, fall on the same curve (which represents the shape of the wave front) that passes through the other family of deviations. The two families may be required to fall on one and the same wave front shaped curve by applying Newton's interpolation formula [9] and requiring that it be a polynomial of degree $(N-1)$. This is obtained by requiring that,

$$\delta_0+(1-N)\delta_1+\frac{(1-N)(2-N)\delta_2}{2!}+\frac{(1-N)(2-N)(3-N)\delta_3}{3!}+\cdots+\frac{(1-N)(2-N)\ldots(-1)\delta_{(N-1)}}{(N-1)!}=0 \qquad (12)$$

where N is the total number of points in the two families.

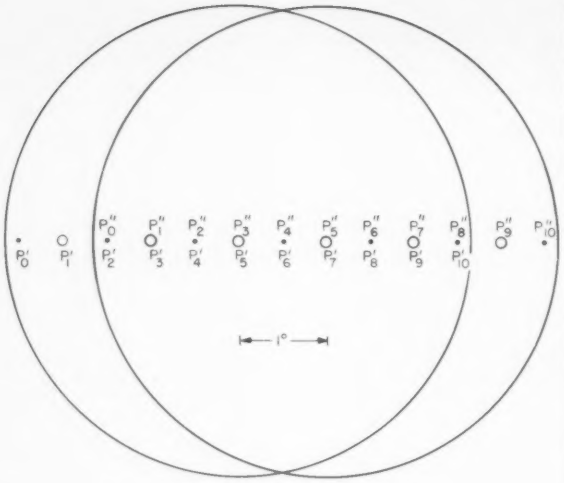

FIGURE 16. *Illustration of how two families of points may be combined to increase detail in the computed wavefront.*

The dots, labeled P_0, P_2, P_4, P_6, P_8 and P_{10} form a family of points that are defined as family No. 1. The circles, labeled P_1, P_3, P_5, P_7, and P_9 form another family of points that are defined as family No. 2.

The two families of deviations are referred to a common reference sphere by requiring that

$$\left.\begin{aligned}\delta_0+\delta_1+\delta_2+\delta_3+\delta_4&=0\\ \delta_5+\delta_6+\delta_7+\delta_8+\delta_9&=0\\ \delta_{10}+\delta_{11}+\delta_{12}+\delta_{13}+\delta_{14}&=0\end{aligned}\right\} \tag{13}$$

and the deviations are required to fit the same wave front curve by requiring ($N=15$ in equation (12)) that

$$\delta_0-14\delta_1+91\delta_2-\ldots\delta_{14}=0 \tag{14}$$

On combining eqs (10), (11), (13), and (14) and solving them as a set of simultaneous equations, we obtain the deviations shown in table 1, column 3.

Equation (14) may be replaced by the equivalent simpler equation,

$$\begin{aligned}15(\delta_1+\delta_{13})-90(\delta_2+\delta_{12})+365(\delta_3+\delta_{11})\\ -1000(\delta_4+\delta_{10})+2003(\delta_5+\delta_9)\\ +3002(\delta_6+\delta_8)-3432\delta_7=0,\end{aligned}$$

which is obtained by subtracting $\sum_{\nu=\alpha}^{14}\delta_2$ (which from 13, equals 0) from 14.

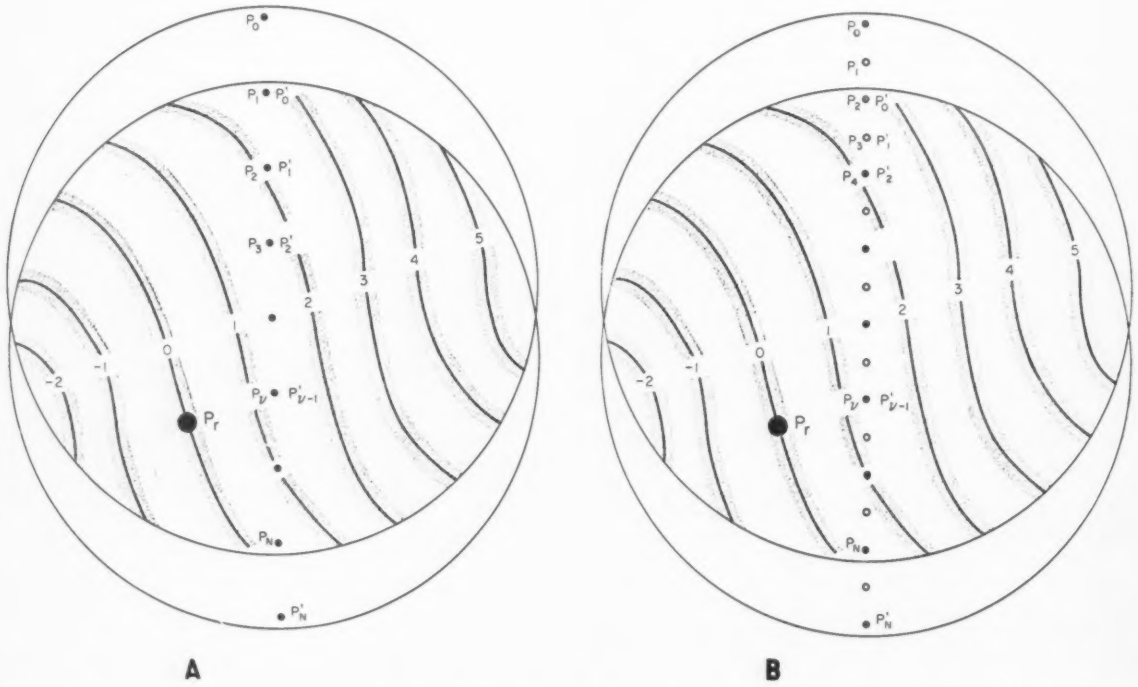

FIGURE 17A. *A fringe pattern with one family of points.*

B. *A fringe pattern with two families of points.*

TABLE 1. *Observed orders of interference, q_ν, and computed deviations, δ_ν, from figure 17*

ν	q_ν	δ_ν
0	----	−0.28
1	----	−.05
2	2.74	.09
3	2.40	.13
4	2.10	.11
5	1.88	.07
6	1.70	.02
7	1.56	−.02
8	1.45	−.04
9	1.37	−.02
10	1.30	.04
11	1.18	.09
12	1.00	.11
13	0.71	.01
14	.30	−.24

(Paper 68C3–160)

14. References

[1] Bates, W. J., Proc. Phys. Soc. (London), **59,** 940 (1947).
[2] Drew, R. L., Proc. Phys. Soc. (London), B, **64,** 1005 (1951).
[3] Brown, D., Proc. Phys. Soc. (London), B, **67,** 232 (1954).
[4] Brown, D. S., J. Sci. Instr., **32,** 137 (April 1955).
[5] Saunders, J. B., J. Res. NBS **65B** (Mathematics and Mathematical Physics), No. 4 (Oct–Dec 1961).

Errata-Reference [5]

Change the term $\sum_{\sigma=0}^{\nu-1}\sigma$ in each equation, (8) and (11), to read $\sum_{\sigma=1}^{\nu}\sigma$. Change the third member of eq (12) to read $\delta_1+3\delta_2+6\delta_3+10\delta_4+15\delta_5+21\delta_6+28\delta_7=0$. Change the second member of eq (16) to read $14\delta_0+11\delta_1+9\delta_2+8\delta_3=0$.

[6] Candler, C., Modern Interferometers, p. 487, Hilger & Watts Ltd. (1951).
[7] Jenkins, F. A., and White, H. E. Fundamentals of Optics, p. 241, McGraw-Hill Book Co., Inc. (1957).
[8] Saunders, J. B., Construction of a Koesters double-image prism, J. Res. NBS **58,** 21 (1957) RP2729.
[9] Milne-Thompson, L. M., The Calculus of Finite Differences, p. 2, Macmillan and Co., Ltd., St. Martin's Street, London (1951).

JOURNAL OF RESEARCH of the National Bureau of Standards—C. Engineering and Instrumentation
Vol. 68C, No. 3, July–September 1964

A New High Resolution Small-Angle X-Ray Camera

H. Brumberger[1] and R. Deslattes

(March 9, 1964)

A novel small-angle x-ray camera, utilizing the Borrmann effect in the 220 Laue reflection from germanium to form the incident beam, has been designed and tested. A test pattern of amorphous carbon showed angular resolution of 0.8 milliradian. In principle, an improvement of resolution by an order of magnitude is possible.

Introduction

A thin single crystal diffracting in the Laue position astigmatically images the source at a distance from the crystal equal to that of the source from the crystal. [2]

The focusing is not dependent on the spectral purity of the source to a first approximation. If the source is made small (i.e., a microfocus tube) and the optical path length made large, conditions obtain which are of interest for small-angle scattering; the scatterer is placed close to the crystal between it and the detector and a beam stop employed at the focus. Since crudely monochromatized radiation suffices in most small-angle scattering work, the lack of wavelength discrimination in the above arrangement may be exploited to gain intensity.

Realization of such a scattering camera is, of course, crucially dependent on the perfection of the crystal. The problems of preparing a suitably thin ($\mu t < 1$) crystal and subsequently mounting it in some strain-free fashion appear somewhat formidable. The requirement that the crystal be thin may be avoided by employing a crystal of sufficiently high perfection that it exhibits a strong Borrmann effect. Such crystals have recently become readily available and have been used in the device described below. The intensity loss in the crystal used ($\mu t \approx 40$) is, however, quite appreciable compared to the thin crystal case so that, when intensity requirements are severe, efforts toward realization of the thin crystal case should be considered.

Description of Apparatus

The collimating crystal used was of germanium [3] approximately 20 × 5 mm in aspect and 1 mm thick. It was cut according to figure 1 for Laue diffraction from the 220 planes.

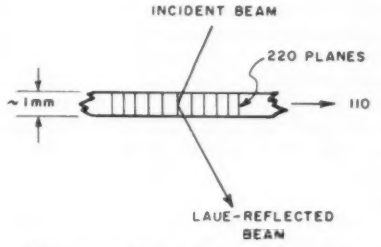

FIGURE 1. *Orientation of* Ge *crystal.*

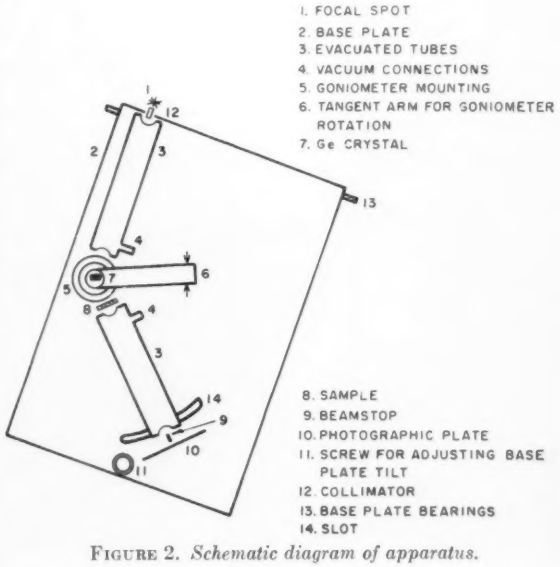

FIGURE 2. *Schematic diagram of apparatus.*

The camera is shown schematically in figure 2. After it left the focal spot (1), the beam was collimated by a lead tube (12) whose aperture was just sufficient to permit illumination of the entire crystal at a distance of 50 cm from the focal spot. The beam entered an evacuated tube (3) whose ends were fitted with Mylar windows (1.9 × 1.3 cm). The germanium crystal (7) was cemented to a brass

[1] Department of Chemistry, Syracuse University, Syracuse, N.Y., 13210.
[2] A. Guinier and J. Tennevin, Acta Cryst. **2**, 133 (1949).
[3] The crystal was furnished by H. Cole of International Business Machines, Thomas J. Watson Research Center, Yorktown Heights, N.Y. The authors are most grateful to Dr. Cole for his assistance.

plate which had an aperture of 1.5 × 0.5 cm. The latter was provided with a pin by which it was held in a goniometer head of the type used in single crystal diffractometry. The goniometer head was supported by a closely fitted dry bearing (5) whose angular position could be sensitively adjusted by means of a tangent arm (6). The sample (8) was held in an apertured brass plate with Mylar films on both sides between which the sample was contained. The sample holder was supported by a second evacuated tube (3) at the exit window of which was placed the primary beam stop (9). The beam stop was a piece of clock-spring mounted edgewise to the beam. Its dimensions were 0.05 × 0.6 cm. It was mounted in a fashion which permitted fine rotation about the beam axis and micrometer driven translation in the plane of dispersion of the instrument. The photographic plate (10) was placed close to the beam stop in the orientation shown.

The components were all supported by adjustable riders mounted on commercial optical bench sections, with the exception of the collimator and goniometer head. The entire apparatus rested on ¾-in. aluminum jigplate which could be pivoted about a horizontal bearing (13) on the x-ray unit by the screw (11) in order to adjust the camera to a 6° takeoff angle.

The front section of the optical bench, and the goniometer bearing, were rigidly bolted to the base plate after alinement with the x-ray beam. The back section of the optical bench, which could be pivoted around the goniometer bearing, rode in a slot (14) allowing adjustment of the angle made with the front section within a 10-deg range about 135°.

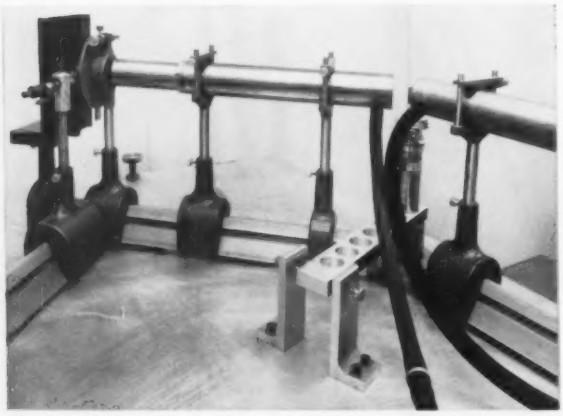

FIGURE 3. *Photograph of camera.*

Figures 3 and 4 show photographs of the camera and goniometer head mounting respectively.

A Jarrell-Ash Microfocus x-ray unit with the electron gun furnishing a nominal 100 μ spot focus was used as the source of CuKα radiation.

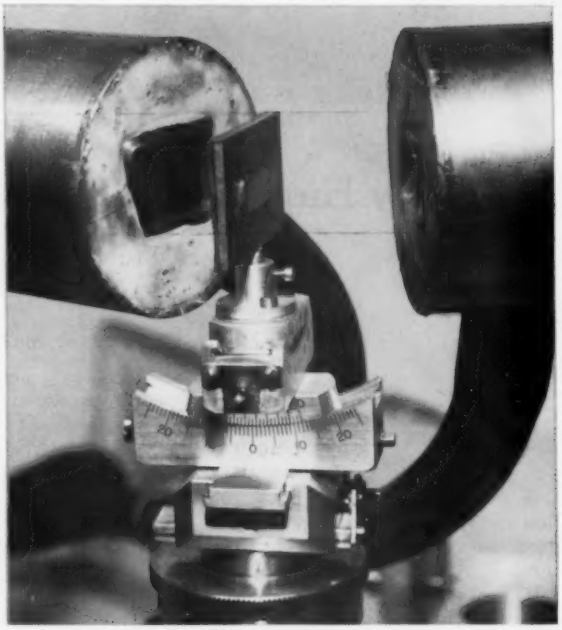

FIGURE 4. *Photograph of goniometer head mounting.*

Adjustment and Operation of the Camera

All components were alined with a proportional counter in place of the photographic plate. Once the 220 reflection was found, a series of 1-min exposures (Ilford G film) were made with the crystal at slightly different angles to allow reflection by its different parts. No significant differences were observed. A photometer trace of one of these exposures is shown in figure 5.

A photographic plate placed close behind the crystal was exposed. The components of the α doublet were well resolved and, as expected from dispersion considerations, separated by approximately 0.6 mm. With this pattern roughly centered in the crystal aperture, the β components and remote continuum effects were automatically excluded. Should a situation arise in which the α_1, α_2 wavelength difference were troublesome, α_2 could easily be rejected by further restricting the horizontal aperture.

The beam stop was inserted and adjusted to give the minimum reading with proportional counter and rate meter. Final adjustment was made with the aid of photographs.

Sample Run

A sample of "lamp black", amorphous carbon, was used because of its known scattering ability at small angles. The sample was exposed under the following conditions:

Exposure time—6 hr at 50 kV, 1.4 mA
Sample to film distance—450 mm
Sample thickness—0.4 mm.

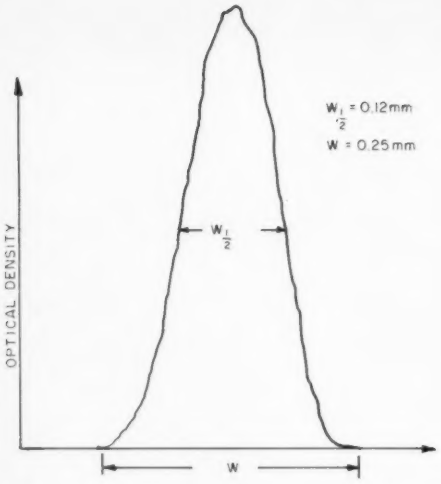

FIGURE 5. *Photometer trace of 220 reflection.*

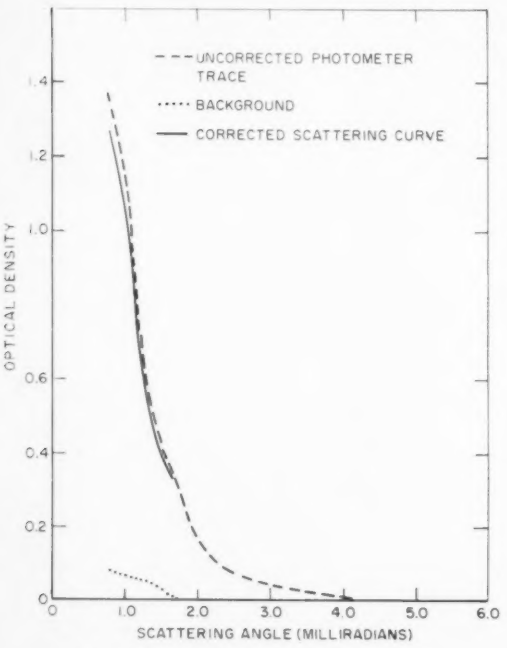

FIGURE 6. *Scattering curve of carbon sample (6 hr exposure).*

A background exposure was made on the same film under the same conditions. Some spillover can be observed but is at most 6 percent of the scattered intensity at the smallest angles. This is partly air scattering, partly fluorescence from the beam stop (which can be eliminated by plating the latter). There is practically no slit scattering, since the only limitation on the beam is in its height, due to the windows of the evacuated tube. The background scattering obtained from a photometer curve and corrected for sample absorption, is shown in figure 6, together with the corrected and uncorrected scattering curves for the carbon sample.

A resolution of about 1900Å was achieved in this experiment, corresponding to a scattering angle of $\sim 8\times10^{-4}$ radians.

Discussion

Considering the simplicity of the apparatus, its performance is excellent. The low cost—about $1,500—also adds to its attractiveness.

By increasing the source-crystal and crystal-detector distances (which would not entail the entire loss of intensity normally associated with increased distance), and/or decreasing the size of the focal spot, increased resolution is possible. Certainly 1-m distances are easily achieved, and a nominal 40 μ focus is available for the Jarrell-Ash unit; the combined effects would give an increase in resolution by a factor of 5, i.e., to 10,000 Å, or better if some of the beam stop spillover can be eliminated.

The beam formed by Borrmann effect is highly polarized. This may offer difficulties in the interpretation of some scattering measurements. On the other hand, there may be circumstances in which such a polarized source may be exploited.

Finally, the large spatial separation of the Kα doublet at the exit face of the crystal while introducing a severe requirement of specimen homogeneity in scattering experiments, suggests the possible utility of the device as a "Laue Monochromator" for diffraction studies. In such an application the entire device could be vastly scaled down with a corresponding gain in intensity. In particular with a 50 μ focal spot, an equal aperture at the crystal and 5 cm distance between the two, CuKα_1 would be satisfactorily isolated.

One of us (HB) wishes to thank the National Bureau of Standards, in particular Dr. Harry C. Allen, Jr., and Mr. H. Steffen Peiser for the hospitality shown him during his stay. The authors are grateful to all coworkers for their advice and interest.

(Paper 68C3–161)

JOURNAL OF RESEARCH of the National Bureau of Standards—C. Engineering and Instrumentation
Vol. 68C, No. 3, July–September 1964

Experimental Determination of Air Drag on a Textile Yarn Struck Transversley by a High-Velocity Projectile

Jack C. Smith, Carl A. Fenstermaker, and Paul J. Shouse

(March 8, 1964)

In recent research, rifle bullets having velocities in the range 100 m/s to 500 m/s have been shot at textile yarns, and flash photographs of the resulting configurations used as data for calculating stress-strain behavior. McCrackin [J. Research NBS **66C**, 317 (1962)] has shown how air drag may affect these data and calculations. McCrackin's theory is tested here on a 93.3 tex nylon yarn and on 26.1 tex and 124.3 tex polyester yarns. The effect of yarn tex on air drag was found to agree with the theory. Curvature in the yarns resulting from air drag also agreed with theoretical predictions. Although curvature was noticeable in all tests, the effect of air drag on yarn tensile stress was negligible except for the 26.1 tex polyester yarn, in which case a small correction was necessary for accurate stress-strain calculations.

When a yarn or other filamentous material is struck transversely by a high-speed projectile, strain waves and waves of transverse motion are caused to propagate along the yarn away from the point of impact. In recent years, flash photographs of these yarn configurations have been obtained, and analyzed to provide stress-strain data [1–5].[1] In the analysis, it is desirable to estimate the effects of air drag on the yarn, and McCrackin [6] has recently shown how this may be done. In this paper McCrackin's theory is tested by applying it to some experimental data. The theory is then used to estimate the errors which would be incurred by neglecting the effect of air drag.

1. Behavior of the Filament Without Air Drag

Consider first the predicted behavior of the filament when air drag is neglected. Let the filament be struck transversely by a projectile moving with velocity V. The impact causes two waves of variable strain to propagate outward along the filament in each direction away from the point of impact. In the strained region between the two wave fronts, material of the filament is set into motion longitudinally toward the point of impact with velocity W_0 given by

$$W_0=\frac{1}{\sqrt{m}}\int_0^{e_0}\sqrt{\frac{dT}{de}}\,de \tag{1}$$

where m is the mass per unit length of the unstrained filament, e_0 the maximum strain resulting from the impact, and T the tension required to produce a strain e.

The inward flowing material forms itself into a wave shaped like a straight-sided wedge with the impacting projectile at the vertex. Material in this wave moves transversely with velocity V. The front of the transverse wave propagates along the filament with velocity λ_0 given by

$$\lambda_0=\sqrt{\frac{T_0}{m\,(1+e_0)}} \tag{2}$$

where T_0 is the tension in the filament resulting from the impact. The velocity λ_0 is expressed elative to the unstrained filament, i.e., with respect to a Lagrangian coordinate system.

The velocity actually observed, i.e., expressed relative to a coordinate system fixed to the laboratory, is U_0 given by

$$U_0=\lambda_0(1+e_0)-W_0. \tag{3}$$

The angle φ_0 between the original direction of the filament and the sloping side of the transverse wave is given by the relation

$$\text{Cos}\ \varphi_0=\frac{U_0}{\lambda_0}. \tag{4}$$

The theory is completed by an additional relation between the quantities just defined

$$V^2=2W_0(1+e_0)\lambda_0-W_0^2. \tag{5}$$

If the effects of air drag are neglected, the above equations can be used to calculate T_0 as a function of e_0 from U_0 versus V data obtained experimentally.

2. Effect of Air Drag

The force on the filament between the projectile and the transverse wave front due to air drag can be resolved into two components, one parallel and the other perpendicular to the filament. According to McCrackin, the effect of the parallel component is small and may be neglected. McCrackin also shows

[1] Figures in brackets indicate the literature references at the end of this paper.

theoretically that the perpendicular component causes the filament to bend into the shape of a circular arc having a radius of curvature given by

$$R=\frac{T}{F} \tag{6}$$

where T is the tensile force in the filament and F is the normal force per unit length on the filament due to air drag. In addition the perpendicular component causes the strain and tension in the filament to increase from e_0 and T_0, respectively, by small amounts dependent upon the time elapsed after impact. The increases in strain and tension cause the transverse wave front to travel at increasing velocities slightly greater than U_0. Thus in actuality the strain, tension, and transverse wave front velocity are slightly greater than they would be if air drag were not present:

McCrackin shows that the strain e in the filament when air drag is present is given approximately by

$$e=e_0+a_2t^2+\mathrm{O}(t^4) \tag{7}$$

and the tensile force by

$$T=T_0+Ka_2t^2+\mathrm{O}(t^4) \tag{8}$$

where t is the time elapsed after impact, K is the slope of the tension-strain curve of the filament at strain e_0, and $\mathrm{O}(t^4)$ refers to terms of the order of t^4. The value of the coefficient a_2 as given by McCrackin is

$$a_2=\frac{F^2}{4T_0^2}\cdot\frac{(1+e_0)^4\lambda_0^4}{(4\lambda_0+2\sqrt{K/m}+kW_0)(1+e_0)+W_0(1-2\sqrt{K/m}/\lambda_0)} \tag{9}$$

where k is an abbreviation for K/T_0. To the same approximation, the velocity at which the transverse wave front travels is given by

$$U=U_0+[\lambda_0k(1+e_0)+\lambda_0-2\sqrt{K/m}]a_2t^2/2+\mathrm{O}(t^4). \tag{10}$$

Equations (9) and (10) can be simplified slightly by use of some substitutions. The velocity, in Lagrangian coordinates, at which the strain e_0 propagates along the filament is given by

$$C_0=\sqrt{\frac{1}{m}\left(\frac{dT}{de}\right)_{e=e_0}}=\sqrt{\frac{K}{m}}. \tag{11}$$

Equations (2) and (11) together with the definition $k=K/T_0$ give the relationship

$$k(1+e_0)=\frac{C_0^2}{\lambda_0^2}. \tag{12}$$

By use of eqs (6), (11), and (12), eqs (9) and (10) can be expressed as follows:

$$a_2=\frac{1}{16R^2}\cdot\frac{(1+e_0)^3\lambda_0^2}{1+\frac{C_0}{2\lambda_0}+\frac{W_0}{4(1+e_0)\lambda_0}\left(\frac{C_0}{\lambda_0}-1\right)^2} \tag{13}$$

$$U=U_0+\frac{a_2\lambda_0}{2}\left(\frac{C_0}{\lambda_0}-1\right)^2t^2+\mathrm{O}(t^4). \tag{14}$$

3. Experimental Tests

In order to test McCrackin's theory on the effects of air drag, high velocity transverse impact tests were performed on three samples of textile yarns: a high-tenacity polyester (polyethylene terephthalate) yarn, 26.1 tex,[2] 50 filament; a high-tenacity polyester (polyethylene terephthalate) yarn, 124.3 tex, 250 filament; and a high-tenacity nylon (polyhexamethylene adipamide) yarn, 93.3 tex, 140 filament, ½ Z turns/in. manufacturer's twist.[3]

The yarns were suspended vertically under a light load of approximately 1 g/tex. The polyester yarns were given an additional twist of 2 Z turns/in. to prevent spreading of the filaments after impact. In the tests on nylon yarns some of the samples were twisted ½ Z and the others 1½ Z turns/in. The yarns were struck with rifle bullets at various velocities, and the resulting configurations during a series of short time intervals after impact were recorded by multimicroflash photography. A detailed description of the apparatus and technique has been given elsewhere [5].

The distance from the point of impact to either the top clamp or to the load affixed to the bottom of the yarn was 1 m. Thus the front of the strain wave resulting from an impact traveled 100 cm to an end and returned approximately 80 cm before an interaction occurred between the reflected strain wave and the oncoming transverse wave. During the time required for the strain wave front to travel this distance, the velocity and the configuration of the transverse wave could be examined to determine the effects of air drag. For the polyester yarns this time was approximately 500 μs, and for the nylon yarn approximately 600 μs.

Figure 1 shows a specimen of the polyester yarn, 26.1 tex, impacted at 308 m/s. Fifteen successive flash pictures taken at 33.3 μs time intervals have been recorded as a multiple exposure. Only the left-hand side of the transverse wave is shown. The wave front in this case travels with a velocity U of 450 m/s. Curvature due to air drag is quite apparent when a straight edge is laid alongside the wave for comparison.

4. Results and Discussion

Curvature due to air drag was observed in the polyester and nylon yarns at all of the transverse impact velocities. However, the wave front veloc-

[2] Yarn fineness or linear density is expressed in tex units. The tex value of a yarn is equal to the weight in grams of a 1000 m length of the yarn.

[3] A yarn has "Z" twist if, when held in a vertical position, the spirals or helices formed by the filaments incline in the same direction as the central portion of the letter "Z".

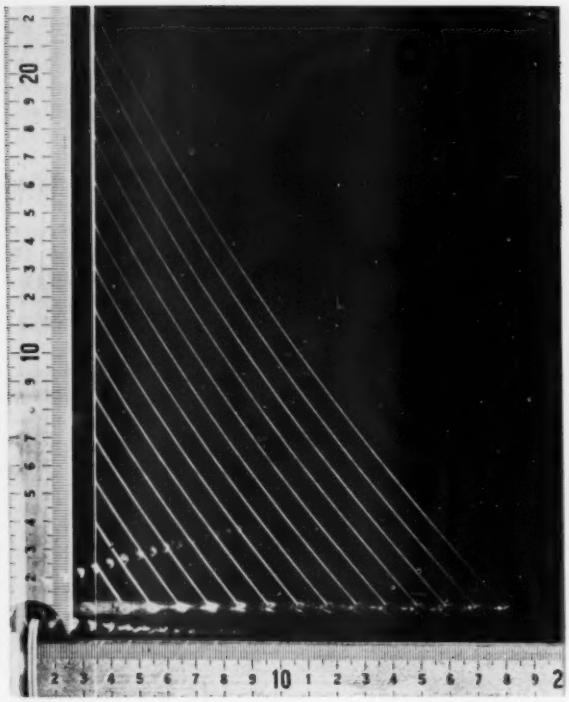

FIGURE 1. *Effect of air drag on 26.1 tex polyester yarn.*

Transverse impact velocity was 308 m/s, and velocity of resulting transverse wave 450 m/s. Time between flashes was 33.3 μ s. Radius of curvature due to air drag is 85 cm for the final yarn configuration shown.

ities U of the transverse waves resulting from impact were found in each case to be constant; i.e., the wave front velocities showed no measurable increase with time. Thus the effect of air drag predicted by eq (14) was negligible for these yarn samples at the transverse impact velocities employed in the tests.

In the photographic enlargements the yarn configuration for each flash exposure could be closely approximated by a circular arc. To obtain the radius of curvature, a chord of length 2a was drawn between two points on the yarn and the perpendicular distance b from the midpoint of the chord to the yarn measured. The radius of curvature is equal to $(a^2+b^2)/2b$.

In figure 2 the radius of curvature of the 26.1 tex polyester yarn is plotted as a function of the distance traveled (in laboratory coordinates) by the transverse wave front. For each transverse impact velocity, the radius of curvature is seen to increase toward a a plateau of constant values, as the transverse wave front advances along the yarn. This effect, which was not predicted by McCrackin's theory, may be due to the influence of different air drag forces at the impact and transverse wave front regions of the yarn. Air drag in the impact region is difficult to estimate, but air drag at the transverse wave front is small. Thus shortly after impact, when the length of yarn in the transverse wave is short, the air drag at the center of the transverse wave is greater than the air drag near the transverse wave front. The apparent radius of curvature calculated from measurements of the span $2a$ and sag b would be small under these conditions. As the length of yarn in the transverse wave increases, the air drag becomes more uniformly distributed in the central region and the influence of the drag forces at the impact point and transverse wave front ends diminishes. Thus the apparent radius of curvature increases approaching the value predicted by McCrackin's theory, which did not consider end effects.

The radii of curvature are also observed to decrease as the velocity of impact is increased; i.e., curvature is more pronounced at the higher impact velocities, in agreement with McCrackin's theory. Similar behavior to that shown in figure 2 was observed for the nylon and 124.3 tex polyester yarns.

Tables 1, 2, and 3 present data obtained for the yarn samples. The values of transverse impact velocity V and transverse wave front velocity U obtained from measurements on the multimicroflash photographs for each test are given in the first two columns. The quantity φ in the third column is the angle between the original position of the yarn and a straight line drawn from the wave front to the vertex of the transverse wave as determined from measurements on the photographs. R is the radius of curvature obtained from measurements described previously.

Since air drag did not cause the wave front velocity to increase with time, its effect could be assumed negligible, and the U, V data obtained from the tests could be used to calculate the tension strain behavior of the yarn for these impact conditions. The procedure, using theory neglecting the effects of air drag, has been described elsewhere [5]. The values of T given in column 5 of the tables were determined by these calculations.

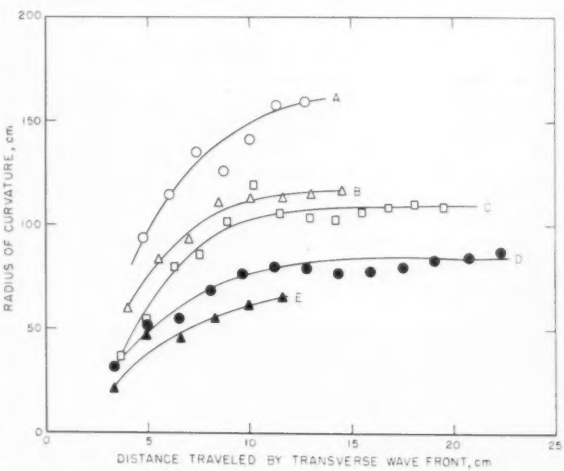

FIGURE 2. *Plot of radius of curvature of 26.1 tex polyester yarn as a function of distance traveled by transverse wave front.*

Impact velocities are: Curve A, 107 m/s; B, 138 m/s; C, 224 m/s; D, 324 m/s E, 381 m/s.

TABLE 1. *Data from impact tests on 26.1 tex high-tenacity polyester yarn*

V	U	Cos φ	R	T	F	$F/V^2\cos^2\varphi$
m/s	*m/s*		*cm*	10^6 *dyn*	10^3 *dyn/cm*	10^{-3} *g/cm²*
107	262	0.926	170	0.201	1.18	1.20
138	300	.910	117	.283	2.42	1.54
169	343	.897	120	.368	3.07	1.34
201	377	.883	110	.458	4.17	1.32
224	395	.868	110	.530	4.82	1.27
273	427	.842	93	.673	7.24	1.37
308	450	.822	85	.799	9.41	1.47
324	469	.820	85	.818	9.62	1.36
359	498	.806	72	.921	12.79	1.53
381	501	.786	70	.984	14.05	1.57

TABLE 2. *Data from impact tests on 124.3 tex high-tenacity polyester yarn*

V	U	Cos φ	R	T	F	$F/V^2\cos^2\varphi$
m/s	*m/s*		*cm*	10^6 *dyn*	10^3 dyn/cm	10^{-3} *g/cm²*
103	249	0.930	325	0.93	2.86	3.13
210	380	.875	250	2.26	9.04	2.68
300	434	.826	190	3.28	17.28	2.81
342	447	.807	180	3.79	21.05	2.76
389	473	.774	150	4.32	29.54	3.26
408	485	.770	150	4.72	31.4	3.18

TABLE 3.—*Data from impact tests on 93.3 tex high-tenacity nylon yarn*

V	U	Cos φ	R	T	F	$F/V^2\cos^2\varphi$
Additional twist ½ *Z* turns/in.						
m/s	*m/s*		*cm*	10^6 *dyn*	10^3 dyn/cm	10^{-3} *g/cm²*
184	323	0.867	150	1.28	8.50	3.33
189	323	.864	145	1.29	8.91	3.35
Additional twist 1½ *Z* turns/in.						
306	427	0.810	147	2.39	16.28	2.65
395	475	.772	137	3.42	24.92	2.68

The transverse force per unit length of yarn due to air drag was calculated from the values of R and T using eq (6). This quantity F was tabulated in column 6. The tabulated values of T and F give the forces to which a yarn is subjected in a transverse impact test, and in this way add to an intuitive understanding of the process. For instance, it is seen from table 1 that the 26.1 tex polyester yarn impacted at a velocity V of 381 m/s is subjected to a tensile force of 0.984×10^6 dyn (1.004 kg) and a transverse air drag of 14.05×10^3 dyn/cm (14.34 g/cm).

According to aerodynamical theory, the force per unit length F due to air drag is given by [6, 7, 8]

$$F=\tfrac{1}{2}\rho d C_D V^2 \cos^2\varphi \qquad (15)$$

where ρ is the density of the air, d the diameter of the yarn, and C_D a dimensionless drag coefficient which varies slowly with Reynolds number. For the yarn diameters and impact velocities encountered in these tests Reynolds number has values between 2×10^3 and 2×10^4, and over this range of values the dimensionless drag coefficient is almost constant. According to data tabulated by Morrison and Ingle [7], C_D for circular cross sections increases from 1.0 to 1.1 as Reynolds number increases from 1×10^4 to 2×10^4. McCrackin, using data given by Hoerner [8], chose a value for C_D of 0.99 as applicable to textile yarns impacted transversely at velocities between 100 m/s and 600 m/s.

From the discussion above it is seen that the quantity $\frac{1}{2}\rho d C_D = F/V^2\cos^2\varphi$ should be a constant for a yarn of given diameter. This quantity is tabulated in column 8 of the tables and is reasonably constant over the range of impact velocities used in the tests. Thus the values of F determined using eq (6) are proportional to $V^2\cos^2\varphi$ as predicted by eq (15). It is interesting to note that the values of $F/V^2\cos^2\varphi$ given in table 3 for nylon yarn are lower for the samples having a 1½ *Z* turns/in. twist than those for samples having only a ½ *Z* twist. Evidently the more highly twisted samples have a smaller effective diameter, and hence a smaller value of $\frac{1}{2}\rho d C_D$.

If C_D is taken as 0.99 and ρ as 1.20×10^{-3} g/cm³ (density of air at 20 °C) the quantity $F/V^2\cos^2\varphi$ becomes equal to 5.94×10^{-4} d. The average value of $F/V^2\cos^2\varphi$ for the 26.1 tex polyester yarn is 1.40×10^{-5} g/cm² so that the "effective" diameter of the yarn becomes $1.40\times10^{-5}/5.94\times10^{-4}=0.024$ cm. If, however, the yarn is assumed to be a solid cylinder of polyethylene terephthalate of density 1.38 g/cm³ [9], its diameter would be 0.015 cm. Since there is some looseness to the packing of the yarn filaments, the two values of diameter just computed are in good agreement. Similarly, the average value of $F/V^2\cos^2\varphi$ for the 124.3 tex polyester yarn is 2.97×10^{-5} g/cm², from which a yarn diameter of 0.050 cm is derived. The diameter calculated from the density is 0.034 cm, which is in good agreement. Average values of $F/V^2\cos^2\varphi$ for the nylon yarn are 3.34×10^{-5} g/cm² for the sample twisted ½ *Z* turns/in. and 2.66×10^{-5} g/cm² for the sample twisted 1½ *Z* turns/in. giving diameters of 0.056 cm and 0.045 cm, respectively. The diameter calculated using a density for polyhexamethylene adipamide of 1.14 [9] is 0.033 cm, which gives reasonable agreement.

The increase ΔU in transverse wave front velocity caused by air drag can be found from the expression

$$\Delta U=\frac{1}{32R^2}\,\frac{(1+e_0)^3\lambda_0^3\left(\frac{C_0}{\lambda_0}-1\right)^2 t^2}{1+\frac{C_0}{2\lambda_0}+\frac{W_0}{4(1+e_0)\lambda_0}\left(\frac{C_0}{\lambda}-1\right)^2} \qquad (16)$$

which is derived from eqs (13) and (14) given previously. Values of ΔU at times 200 μs and 500 μs after impact at velocities between 100 m/s and 500 m/s are given for the three yarn samples in table 4. In order to compute these values of ΔU, the experimentally obtained U versus V data uncorrected for air drag were used to calculate

the stress-strain curve, the associated velocities λ, W, and C, and the angle of inclination φ. Additional data on the nylon and 124.3 tex polyester yarns were available from other experiments [5]. Values of F were calculated from the average values of $F/V^2 \cos^2 \varphi$ given in tables 1, 2, and 3, and the values of R were calculated from F and T using eq (6).

The values of ΔU thus calculated are in most cases only a small percentage of the measured values of U, so that the effect of air drag may be neglected. However, in the case of the 26.1 tex polyester yarn, the values of ΔU after 500 μs are sufficiently large that some correction to the U, V data may be necessary. In estimating this correction it should be noted that the magnitude of ΔU is proportional to t^2, so that a plot of transverse wave front position as a function of time has a slight parabolic curvature. The velocity U_0, air drag neglected, is equal to the slope of the straight line tangent to this parabola at the origin. The value of U actually measured will probably exceed U_0, but not to the extent indicated by the calculated values of ΔU. The actual correction to be made is therefore a matter of judgment.

The two polyester yarns have similar stress-strain curves, but according to table 4, ΔU for the 124.3 tex yarn is approximately $\frac{1}{7}$ the value of ΔU for the 26.1 tex yarn. Thus impact tests on larger diameter yarns are less subject to air drag effects than are tests on smaller diameter yarns of the same material. This is in agreement with the theory, as the following argument shows.

TABLE 4. *Increase in transverse wave front velocity due to air drag*

Impact velocity V	Increase in transverse wave front velocity ΔU					
	200 μs after impact			500 μs after impact		
	Polyester 26.1 tex	Polyester 124.3 tex	Nylon 1½Z twist	Polyester 26.1 tex	Polyester 124.3 tex	Nylon 1½Z twist
m/s	*m/s*	*m/s*	*m/s*	*m/s*	*m/s*	*m/s*
100	0.2	0.0	0.0	0.9	0.2	0.2
200	.7	.1	.1	4.4	.6	.9
300	1.1	.2	.3	6.7	1.0	2.0
400	2.0	.3	.6	12.7	1.9	3.5
500	3.4	.5	1.2	21.1	3.1	7.5

According to eqs (1), (2), (3), and (4) the velocities U_0, λ_0, and W_0, and the angle ϕ_0 are specific quantities independent of the diameter of the yarn. However, according to eq (15), the force per unit length F due to air drag is proportional to d. Since the tension T in the yarn is proportional to d^2, it may be seen from eq (6) that the radius of curvature R is proportional to d. Thus from eq (16) ΔU is inversely proportional to d^2. The tex value of a yarn is proportional to d^2, so that ΔU is inversely proportional to the tex. For the two polyester yarns the tex ratio is 5 to 1.

5. Summary

McCrackin's theory on the effects of air drag has been tested by transverse impact experiments on two samples of high tenacity polyester yarn, 26.1 tex and 124.3 tex, and one sample of high tenacity nylon yarn, 93.3 tex. Impact velocities ranged between 100 m/s and 400 m/s. In all of the tests curvature due to air drag was observed in the yarn configuration

As the length of yarn in the transverse wave increased with increasing time after impact, the radius of curvature increased, approaching a constant value consistent with that predicted by McCrackin's theory. The radius of curvature also decreased as the impact velocity was increased, in agreement with the theory. Results gave approximate agreement with the theoretical prediction that the radius of curvature is proportional to yarn diameter.

For tests at 500 m/s impact velocity on the 26.1 tex polyester yarn, a small correction to the measured value of transverse wave front velocity was necessary in the calculation of an accurate stress-strain curve. For the other two yarns these corrections for the effect of air drag were negligible.

6. References

[1] D. R. Petterson, G. M. Stewart, F. A. Odell, and R. C. Maheux, Dynamic distribution of strain in textile materials under high-speed impact, Part I: Experimental methods and preliminary results on single yarns, Textile Research J. **30,** 411–421 (June 1960).

[2] D. R. Petterson and G. M. Stewart, Dynamic distribution of strain in textile materials under high-speed impact, Part II: Stress-strain curves from strain position distributions, Textile Research J. **30,** 422–431 (June 1960).

[3] M. N. Pilsworth, Tensile impact on rubber and nylon, Pioneering Research Division, Quartermaster Research and Engineering Center, Natick, Mass., Technical Report PR–3 (May 1962).

[4] J. C. Smith, C. A. Fenstermaker, and P. J. Shouse, The behavior of filamentous materials subjected to high-speed tensile impact, ASTM special technical publication No. 336, Symposium on the dynamic behavior of materials, 47–69 (1963).

[5] J. C. Smith, C. A. Fenstermaker, and P. J. Shouse, Stress-strain relationships in yarns subjected to rapid impact loading, Part X: Stress-strain curves obtained by impacts with rifle bullets, Textile Research J. **33,** 919–934 (Nov. 1963).

[6] F. L. McCrackin, Effect of air drag on the motion of a filament struck transversely by a high-speed projectile, J. Research NBS **66C** (Engr. and Instr.) No. 4, 317–322 (1962).

[7] R. B. Morrison and M. J. Ingle, Design data for aeronautics and astronautics (John Wiley & Sons, Inc., New York, N.Y., 1962).

[8] S. F. Hoerner, Fluid dynamic drag (1958) published by S. F. Hoerner.

[9] Textile World (330 West 42d St., New York 36, N.Y.), 1962 Man-made fiber chart.

(Paper 68C3–162)

JOURNAL OF RESEARCH of the National Bureau of Standards—C. Engineering and Instrumentation
Vol. 68C, No. 3, July–September 1964

Publications of the National Bureau of Standards*

Selected Abstracts

Compressibility of natural rubber at pressures below 500 kg/cm², L. A. Wood and G. M. Martin, *J. Res. NBS* 68A (*Phys. and Chem.*), *No. 3,* (*May–June 1964*), *70 cents.*
The specific volumes of unvulcanized natural rubber and of a peroxide-cured vulcanizate of natural rubber were measured at pressures of 1–500 kg/cm² at temperatures from 0 to 25 ° C. Observations on mercury-filled dilatometers were made through a window in the pressure system. No time effects or hysteresis phenomena were observed. The specific volume V in cm³/g over the range studied can be represented by

$$V = V_0, 25\{1 + A(t-25)\} \{1 + [\alpha_{25} + k_1(t-25)]\, P + [\beta_{25} + k_2(t-25)]P^2\}$$

where P is the pressure in kg/cm², and t the temperature in ° C. The constants for the unvulcanized and for the peroxide-cured samples are:

$V_0,25 = 1.0951$ and 1.1032 cm³/g;
$10^4 A = 6.54$ and 6.36 per degree;
$10^6\alpha_{25} = -50.5$ and -50.4 (kg/cm²)$^{-1}$;
$10^6 k_1 = -0.227$ and -0.203 per degree;
$10_0\beta_{25} = 10$ and 11.5 (kg/cm²)$^{-2}$;

and $10^9 k_2 = 0.048$ and 0.073 per degree, respectively. The compressibility of unvulcanized natural rubber at 25° and 1 kg/cm² is thus 50.5×10^{-6} (kg cm²)$^{-1}$ falling to 40.6×10^{-6} (kg/cm²)$^{-1}$ at a pressure of 500 kg/cm². It is concluded that a low degree of vulcanization produces no significant changes in the constants listed. The values are not far different from those obtained by extrapolating to zero sulfur content the observations of Scott on the rubber-sulfur system. Calculations of values of compressibility (and its reciprocal the bulk modulus), "internal pressure", bulk wave velocity difference between specific heats, and several other physical properties are in reasonable agreement with those obtained by direct observations by other workers. For the prediction of values at pressures above 500 kg/cm² the use of the Tait equation is recommended.

Determinations based on duplication of readings, J. A. Speckman, *J. Res. NBS* 68B (*Math. and Math. Phys.*), *No. 2,* (*Apr.–June 1964*), *75 cents.*
This paper is concerned with a statistical estimation procedure in which measurements of a quantity are taken until two identical readings are obtained; this duplicated value is then taken as the estimate of the magnitude of the quantity concerned. The properties of this estimation procedure have been investigated numerically, under the assumptions that the individual observations are rounded values of measurements which have a normal distribution, and this estimator is compared with the arithmetic mean of two observations. It is shown that an arithmetic mean of two observations from the rounded distribution is almost always superior to the estimator described above. The exception is where the rounding interval is so wide and the rounding lattice is so advantageously placed that the only real reason for taking repeat measurements would be as a protection against gross errors.

General application of Youden's rank sum test for outliers and tables of one-sided percentage points, T. A. Willke, *J. Res. NBS* 68B (*Math. and Math. Phys.*), *No. 2, 55–58* (*Apr.–June 1964*), *75 cents.*
The rank sum test for outliers advanced by W. J. Youden provides a method for detecting if the measurement distribution of any one of a group of objects has a mean significantly different from the rest. This paper discusses a more general application of the rank sum procedures which permits a similar test on other parameters, such as the variance, with the same tables. Tables of the critical values of the extreme rank sum and the corresponding significance levels for one-sided tests are given in this paper to supplement similar tables for two-sided tests already published.

Fitting $y = \beta x$ when the variance depends on x, J. Van Dyke, *J. Res. NBS* 68B, (*Math. and Math. Phys.*), *No. 2, 67–72* (*Apr.–June 1964*), *75 cents.*
This paper presents some results concerning the selection of a method for estimating the slope of a straight line through the origin. For fitting the line $y = \beta x$ when the variance of y is proportional to x^p, it is well known that the best estimate of β depends on p. In practice, however, only integer values of p would be convenient to work with. One of the estimators appropriate for $p = 0,1,2$ would probably be used if the value of p were in fact fractional, or if it were only approximately known. This paper provides some guides for choosing the best among these estimators in a particular situation.
Formulas for the best estimators of β and their variances are given. Estimators of β appropriate for integer values of p are compared in the case when p is not integral, but is known, and in the case when p is only approximately known. Estimation of the variances of estimators of β is considered. Finally, some results are given on the effect of the spacing of the x values on the comparison of the estimators.

Inequalities for solutions of mixed boundary value problems for elastic plates, J. H. Bramble and L. E. Payne, *J. Res. NBS* 68B (*Math. and Math. Phys.*), *No. 2, 75–92* (*Apr.–June 1964*), *75 cents.*
In this paper a number of explicit a priori inequalities for solutions of the plate equation are derived. These inequalities together with the Rayleigh-Ritz technique may be used to compute error bounds in various mixed boundary value problems for elastic plates.

Electrical properties of sea ice at 0.1 to 30 Mc/s, F. L. Wentworth and M. Cohn, *Radio Sci. J. Res. NBS/USNC-URSI* 68D, *No. 6, 681–692* (*June 1964*), *$1.00.*
This paper sets forth the details of an experimental program in which the resistivity and dielectric constant of Arctic sea ice were measured. Fourteen ice samples ranging in salinity from 0.067‰ (parts per thousand) to 23‰ by weight were studied. The values of dielectric constant and the computed values of loss tangent are given as a function of frequency (0.1–30 Mc/s) for temperatures from −5 to −40 °C. The relationship of dielectric constant and conductivity at 3 Mc/s are also given as a function of salinity for temperatures of −10, −20, and −30 °C.

Wave propagation in stratified random media, J. M. Chen, *Radio Sci. J. Res. NBS/USNC-URSI* 68D, *No. 6, 743–748* (*June 1964*), *$1.00.*
The problem of wave propagation in stratified media is reexamined from the stochastic point of view by introducing the concept of random media. For a small inhomogeneity, this problem is investigated by utilizing the effective refractive coefficient of Chen [1964]. For a large inhomogeneity, this problem is treated by subdividing the medium into many parallel homogeneous layers of random media and utilizing the derived reflection and transmission coefficients of Chen [1964]. In each case, it is found that the small randomness has no drastic and unexpected effects on the behaviour of the wave motion in the media considered. Hence, our reliance on the results obtained by a nonrandom approach is increased.

A spectrographic interferometer, R. H. Lee and J. W. Warwick, *Radio Sci J. Res. NBS/USNC-URSI* **68D**, *No. 7, 807–812 (July 1964), $1.00.*
The paper includes a description of the principal novelties of a swept-frequency interferometer operating between 7.6 and 41 Mc/s at the High Altitude Observatory in Boulder, Colorado since July 1959. Records of Jupiter's decametric radio emission, and of a solar harmonic type III burst are included, with a cursory description of the corner-reflector antenna system used to feed the receiver. The receiver employs unique "minimum detection" circuits to reduce the deleterious effects of telecommunciations stations on detection of the weak astronomical signals of interest to us. For interferometry, the receiver uses an inversion circuit to present both negative and positive fringes as darkening on the final record, and to sharpen fringe crossovers.

Shielding against gamma rays, neutrons, and electrons from nuclear weapons, A review and bibliography, J. H. Hubbell and L. V. Spencer, *NBS Mono. 69 (Feb. 24, 1964), 30 cents.*
The problem of predicting dose rates and of estimating the effectiveness of shielding from radiations resulting from nuclear explosions is discussed. A number of existing calculations and supporting experiments regarding the penetration and diffusion of gamma rays, neutrons, and electrons through air and bulk materials are summarized. Indications are given of gaps in such input information. A selection of 485 references from the unclassified literature is presented, of which 388 are cataloged as to source geometry and energy, absorber material and configuration, type of data presented, and method of calculation or experimental technique. These cataloged references include radiation field studies ranging from the point-source infinite-medium situation up through such complicated geometries as foxholes, shelters, and conventional structures. The other references are of a general or review nature or contain input spectral data.

Safe handling of radioactive materials, *NBS Handb. 92 (Mar. 9, 1964), 40 cents (supersedes Handb. 42).*
This handbook presents recommendations of the National Committee on Radiation Protection and Measurements. It is designed to help the user of radioactive materials to handle radionuclides without exposing himself or others to doses in excess of maximum permissible limits. It provides background material on the principles of radiation protection and then gives recommendations on personnel, physical safeguards, procedural safeguards, instrumentation, transportation of radioactive material and radioactive waste disposal.

Safety standard for non-medical x-ray and sealed gamma-ray sources, Part I. General, *NBS Handb. 93 (Jan. 3, 1964), 30 cents.*
This Handbook is intended to serve as a guide toward the safe use of x-ray and sealed gamma-ray sources for non-medical purposes and of equipment emitting x rays serving no useful purpose. Its main objectives are to reduce needless exposure of persons to radiation and to ensure that no one receives more than the maximum permissible dose. These objectives are achieved by the use of appropriate equipment, ample structural shielding and most important, safe operating procedures.

Inspection of processed photographic record films for aging blemishes, C. S. McCamy, *NBS Handb. 96 (Jan. 24, 1964), 25 cents.*
Inspections of microfilms have recently revealed blemishes which apparently developed 2 to 20 years after the films were processed. Most of the blemishes are small spots, usually reddish or yellowish in color, ranging from about 15 to 150 microns across. These blemishes have been classified on the basis of size, shape, color, and character. This publication describes and gives colored illustrations of the various types, describes the method of observing them, and recommends sampling procedures for microfilm inspectors. The cause, the exact mechanism of formation of the various types, and generally accepted preventive measures are not as yet known. This publication is intended to promote uniform terminology, inspection, and reporting.

Vitreous china plumbing fixtures, *CS20–63, 20 cents (supersedes CS20–56).*
This Commercial Standard covers material, grading, dimensions, certain features of construction, and the types and sizes of vitreous china plumbing fixtures currently in general use and demand. Also given are definitions, inspection methods, tests, and means for identifying fixtures that comply with the standard. Certain recommendations for installation of the fixtures are also given.

Hot-rolled rail steel bars (produced from tee-section rails), *CS150–63 (Dec. 15, 1963), 10 cents (supersedes CS150–48).*
This Commercial Standard covers the mechanical properties, and the dimensions, weights, and tolerances for 17 standard structural sections of hot-rolled rail steel bars. The standard also includes a provision for the labeling and identification of bars complying with the standard.

Polyethylene (PE) plastic pipe (SDR-PR), *CS255–63 (July 1, 1963), 10 cents.*
The PE pipe covered in this Commercial Standard is made in standard thermoplastic pipe dimension ratios and is pressure rated for water. Included are criteria for classifying PE plastic pipe materials and PE plastic pipe, a system of nomenclature for PE plastic pipe, and requirements and methods of test for materials, workmanship, dimensions, pressure rating, sustained pressure, burst pressure, and environmental stress cracking. Methods of marking and practices for indicating compliance with this standard are also given.

Polyvinyl chloride (PVC) plastic pipe (SDR-R and class T), *CS256–63 (July 1, 1963), 10 cents.*
The PVC pipe covered in this Commercial Standard is made in standard thermoplastic pipe dimension ratios and is pressure rated for water. Included are criteria for classifying PVC plastic pipe materials and PVC plastic pipe, a system of nomenclature for PVC plastic pipe, and requirements and methods of test for materials, workmanship, dimensions, pressure rating, sustained pressure, burst pressure, flattening, chemical resistance, and extrusion quality. Methods of marking and practices for indicating compliance with this standard are also given.

Gypsum board products, *SPR266–63, 10 cents.*
This standard lists six varieties of gypsum board and lath products and the various types and sizes of each in greatest demand. It further indicates the sizes for which demands are decreasing but which are not sufficiently low to warrant their deletion from the standard at this time. These are not recommended for regular stock, but may be obtained "on order", subject to possible delay in delivery.

Soviet research in field emission, 1960–1963; an annotated bibliography, T. W. Marton and R. Klein, *NBS Tech. Note 234 (Feb. 24, 1964), 30 cents.*
Soviet field emission research, including both the experimental and theoretical aspects of field electron and ion emission from metals and semiconductors, is the subject of this bibliography. Over 80 complete references to original publications and 50 meeting papers were selected after an extensive search of the Soviet and East European technical literature published from January 1960 through November 1963. Most of these papers are in Russian; a few are in Czech, English, Hungarian, Polish, and Ukrainian. Full references are given to English translations of the entries whenever available. A list of relevant scientific meetings, papers read at these meetings, bibliographic references, and a brief subject index are appended to the compilation. This bibliography represents the continuation of the survey published in October 1960 as U.S. NBS Technical Note 75.

Galvanic currents observed during outdoor exposure of an iron-nickel cell. A progress report (AES Research Project No. 19, F. Ogburn and R. L. Myklebust, *50th Annual Tech. Proc. American Electroplaters Society, pp. 24–28 (1963).*
An iron-nickel cell simulating a pit extending through a nickel

coating to the steel substrate was exposed outdoors for a year. Cell current, continuously recorded, was generally in the range of 0.025 to 0.5 ma/cm² with an anode about 0.2 mm in diameter. Corrosion was proportional to the time during which the cell was visibly wet.

Determination of propylene in ethylene-propylene copolymers by infrared spectroscopy, J. E. Brown, M. Tryon, and J. Mandel, *Anal. Chem.* **35,** *2172–2176 (Dec. 1963).*
Pyrolysis of ethylene-propylene copolymers produces derivatives that are rich in unsaturated carbon-carbon functional groups. This unsaturation exhibits strong absorption in the region of infrared light. It was found that the ratio of the absorption of the vinyl groups to that of the vinylidene groups varies with the mole fraction of propylene in ethylene-propylene copolymers. Making use of this ratio an analytical method has been developed for determining propylene in both raw and vulcanized ethylene-propylene copolymers.

A method for localized variation of the paths of two paraxial rays, L. E. Sutton, *Appl. Opt.* **2,** *No. 12, 1275–1280 (Dec. 1963).*
This paper treats lens systems which consist of spherical and plane refracting surfaces, and for which fixed values of the indices of refraction have already been assigned. Simple algebraic equations are derived which allow changes to be made in the curvatures of two consecutive surfaces, together with changes in two specified vertex separations, subject to the following invariance condition: the heights and slope angles of both the marginal and principal paraxial rays must be left unchanged at all surfaces of the system other than the two surfaces undergoing modification. These equations may be considered to constitute a generalized "bending," though no attempt is made to retain the Petzval contribution as an invariant. The use of a series of such "bendings," applied independently at separate elements of the system, for certain adjustments of the third order aberrations is immediately evident. Lagrange's invariant allows a surprisingly concise formulation of the final equations. If the first surface of an element is located at the primary focal point of the second surface, a separate solution is derived in which only two lens parameters are to be changed. These results are apparently new, though similar results for single paraxial rays are well known. Tentative suggestions as to additional applications are made.

Recalibration of NBS standards of spectral transmittance, H. J. Keegan, J. C. Schleter, and M. A. Belknap, *J. Opt. Soc. Am.* **54,** *No. 1, 69–74 (Jan. 1964).*
In 1934, Gibson, Walker, and Brown developed sets of four colored glass filters to serve as working standards of spectral transmittance for checking the reliability of spectrophotometers. Several sets of these glasses were measured carefully and reserved and designated as future reference standards. Duplicate standards evaluated by comparison with the reference standards are available by purchase to the public. The current set of reference standards was established in the years 1945 to 1947, and one of these reference standards (selenium-red) was recalibrated in 1952. This paper reports a recalibration, made in 1961 and 1962, of all four glasses (selenium-red, carbon-yellow, copper-green, cobalt-blue) on three spectrophotometers (Cary 14, Beckman DU, Köning-Martens). Except for the cobalt-blue standard, the values of spectral transmittance found differ from those previously assigned by amounts differing at some wavelengths by as much as or slightly more than the uncertainties estimated for the present values, though not by amounts exceeding the combined uncertanties of the present and previous determinations. The indicated changes for these three standards are fairly regular, however, and support the view that the selenium-red and carbon-yellow standards are changing chiefly by formation of a reflectance-reducing film on the surfaces. The indicated rate of upward drift is slow, and suggests that it takes about 10 years for the drift to exceed the assigned uncertainty.

Scheme for obtaining integral and fractional multiples of a given radiance, D. E. Erminy, *J. Opt. Soc. Am.* **53,** *1448–1449 (Dec. 1963).*
A scheme has been devised for obtaining to a high accuracy known integral and fractional multiples of a given radiance. To demonstrate this scheme, an example of a representative device and a technique of using it is presented.

Pitfalls in thermal emission studies, W. N. Harrison (*Symp. Measurement of Thermal Radiation Properties of Solids, Dayton, Ohio, Sept. 5–7, 1962*), *Natl. Aeron. and Space Admin. SP–31, Session 1, Paper 1, p. 3 (1963).*
Attention is called to several pitfalls that often beset investigators who make thermal emission studies. The pitfalls mentioned include the following: (1) conflicting meanings of several frequently used terms as found in the literature, each meaning having authoritative sponsorship; (2) incomplete and hence potentially misleading descriptions of specimens on which reported data are based; (3) reference to emissivity or emittance as a property of a surface rather than a volume property (influenced by the surface); (4) occasional omission of diffuse reflection from analyses of the optical properties of inhomogeneous bodies; (5) failure to observe the restrictions upon conditions that are required for validity of basic equations; (6) uncertainties as to the effective temperature, peculiar to specimens having low absorption indices; and (7) lack of suitable physical standards. Several suggestions are made for avoiding or minimizing the consequences of the pitfalls discussed.

Foundations of the Callaway theory of thermal conductivity, R. E. Nettleton, *Phys. Rev.* **132,** *No. 5, 2032–2038 (Dec. 1, 1963).*
The equation derived by Peierls for the occupation numbers N_q of phonon states with wave vector $\mathbf{q}$ and appropriate polarization is linearized to give a maser equation for the deviations $n_q \equiv N_q - N_q^0$ from equilibrium. This master equation, with transition probabilities calculated from first-order time-dependent perturbation theory, is then compared term by term with the linearized form of an approximate master equation proposed by Callaway. The latter assumes that the effects of normal and umklapp processes can be represented by two relaxation frequencies, τN^{-1} and τ_r^{-1}, respectively, which are both proportional to q^2. This assumption is contradicted by the present analysis, which shows that the condition that the solution of the Callaway equation should also satisfy the Peierls equation in the case of steady-state heat flow leads to τN^{-1} proportional to q in first approximation. Furthermore, the Callaway equation contains nonzero transition probabilities for a great many phonon processes which are absent from the Peierls equation. Thus, while Callaway's equation, with a modified τN, can indeed give a good approximation to the phonon occupation numbers in the steady state, it does not describe the approach to that state from an arbitrary initial distribution. These conclusions are found to remain true when boundary and point-defect scattering are included, in addition to three-phonon processes. A first approximation to the wave number and temperature dependence of the corresponding contribution to the Callaway relaxation times is given for each scattering mechanism.

Surface flammability measurements by the radiant-pane. method, A. F. Robertson, *Am. Soc. Testing Mat. Spec. Tech. Publ. 344, 33–46 (1962).*
It is suggested that the flammability of solids may be considered as a function of the ratio of heat release rate to critical ignition energy of the material being studied. Based on this concept, the radiant-panel flammability test method has shown its usefulness as a research tool. A review is included of previous studies made by use of this method.
Recently obtained experimental data are presented which illustrate the large changes in flammability which can occur with changes of the relative humidity of the ambient conditioning atmosphere. Data are presented which suggest that the subsurface heat-dissipation behavior of the material under test may have an important influence on flammability.
The paper concludes with the suggestion that, although the radiant panel flammability test method has achieved some recognition, it would be a mistake to assume that it, or any

other test method, would be ideal for prediction of the surface flammability hazard of all materials in all situations.

Stress-strain relationships in yarns subjected to rapid impact loading. Part X: Stress-strain curves obtained by impacts with rifle bullets, J. C. Smith, C. A. Fenstermaker, and P. J. Shouse, *Textile Res. J.* **33,** *919–934 (Nov. 1963).*
When a yarn is struck transversely, a V-shaped wave of transverse motion is caused to spread outwards at a velocity U depending upon the impact velocity V. In this research data on U vs V for impact velocities between 10 m/sec and 700 m/sec are analyzed to determine stress-strain behavior in high-tenacity nylon and polyester yarns. The data are obtained by shooting rifle bullets at a yarn and recording the resulting configurations by microflash photography. A strain-rate-independent theory for transverse impact behavior is used to calculate stress-strain data.
It was found that the time required to break a yarn depended upon the impact velocity. Nylon yarns broke 10 μsec after impact at 650 m/sec with a calculated breaking strain of 10.0% and tenacity of 77 g/tex. At 495 m/sec velocity the yarn broke within 100 μsec at 7.4% strain and 52 g/tex tenacity. The corresponding values in polyester yarn were, for a 10-μsec break, 620 m/sec, 10.5%, and 67 g/tex; for a 100-μsec break, 420 m/sec, 6.5%, and 40 g/tex.

Wavelength of Hg^{198} Zeeman filter relative to that of the 2537-Å absorption line of an atomic beam, W. G. Schweitzer, Jr., and K. G. Kessler, *J. Opt. Soc. Am.* **53,** *No. 12, 1382–1388 (Dec. 1963).*
We have made a precise comparison of the wavelength passed by a Hg^{198} Zeeman filter with that of the 2537-Å absorption line of an atomic beam. This was done by passing the light from the filter through the atomic beam and then comparing the amplitude of the two peaks in the resulting reversed lines. A calibration was obtained by measuring the ratio of peak amplitudes with the beam tilted at various angles to the optic axis so as to introduce known Doppler shifts. The wavelengths of the Zeeman filter and atomic beam are shown to be equal to about one part in 10^9.

Wavelength passed by Hg^{198} Zeeman-split absorption filter, W. G. Schweitzer, Jr., *J. Opt. Soc. Am.* **53,** *No. 11, 1250–1252 (Nov. 1963).*
We have measured the vacuum wavelength of the 2537-Å line of Hg^{198} as passed by a Zeeman-split absorption filter. The 6057-Å line of Kr^{86} was used as a standard. An evacuated Fabry-Periot interferometer was employed with spacers of 218-, 110-, and 21-mm length. The line width obtained by using the Zeeman filter is estimated to be about 5 mK. The measured wavelength, 2537.26874 ± .00003 Å is is in excellent agreement with the value obtained by Barger and Kessler for the wavelength emitted by an atomic beam of Hg^{198}.

Status of frequency and time control, W. D. George, *Frequency* **1,** *27–29 (Nov.–Dec. 1963).*
The current status and indicated improvement is given in high quality control oscillators and in standard frequency transmissions and time signals. A few of the problems in the field of frequency and time control and the importance of obtainlng solutions are discussed.

Effect of rate loading, time of trituration and test temperature on compressive strength value of dental amalgam, H. J. Caul, R. Longton, W. T. Sweeney, and G. C. Paffenbarger, *J. Am. Dental Assoc.* **67,** *670–678 (Nov. 1963).*
Factors affecting the compressive strength values of dental amalgams were investigated. Values for five amalgams increased with increase in rates of loading. When testing times were more than one minute, the machine applying a constant stress rate gave higher values than did that applying a constant strain rate. Differences between testing machine characteristics appeared to be the main cause that prevented close agreement on strength values obtained by four laboratories. Fast loading rates, causing fracture in less than one minute produced strength values less dependent on type of loading machine than did slower rates of either stress or strain application. An optimum trituration time defined as the minimum time necessary to produce maximum or near maximum strength was observed for each amalgam. As the testing temperature was increased from 23 to 60° C, compressive strength decreased about 50 percent.

The method for mechanical translation used by the National Bureau of Standards group and the structure of its machine glossary, I. Rhodes, *Am. Documentation Inst. 26th Annual Meeting, pp. 23–24 (Chicago, Ill., Oct. 1963).*
The method used by the Machine Translation Group at the National Bureau of Standards is known as "predictive analysis." It attempts to mechanize certain mental processes of speech comprehension. The method calls for a radically new type of machine glossary.

On the redefinition of the second and the velocity of light, G. E. Hudson and W. Atkinson, *IEEE Trans. Instr. Meas.* **IM–12,** *No. 1, 44–46 (June 1963).*
This summary article resulted from an informal discussion period held during the International Conference on Precision Electromagnetic Measurements, August 14–17, 1962. This session was presided over by Prof. Norman Ramsey of Harvard University. The Radio Standards Laboratory of the National Bureau of Standards in Boulder, Colorado, sponsored the meeting along with the IRE Professional Group on Instrumentation and the AIEE Instrumentation Division. Partial support for the conference came from a grant from the National Science Foundation.

Macro-pores in leather as determined with a mercury porosimeter, J. R. Kanagy, *J. Am. Leather Chemists Assoc.* **LVIII,** *No. 9, 524–550 (Sept. 1963).*
A study was made of the pore structure in leather and in other porous materials with a mercury porosimeter at absolute pressures ranging from 5 to 3000 psi. Pore radii corresponding to these pressures vary from 50 to 0.04 microns. This range is referred to as the macro-pore range. Leather and other natural collagenous materials were compared to microporous plastics and fritted-glass discs. The results indicate that a characteristic pore structure giving rise to many different-sized pores related to the fibrous structure exists in leather, whereas the pores in manufactured materials which are designed for a specific use are more uniform in size. A differential analysis of the integral volume-pressure curves indicates that a large part of the pore volume of collagenous materials in the form of hides occurs at radii of 5 to 0.5 microns. For rat tail tendons, a large fraction of the pore volume exists for pores in close proximity to this, 2.5 to 0.5 microns. The pores which constitute these volumes are believed to exist between the primitive fibers. The volume from pores smaller than 0.25 microns in radius very probably are within the fibril region.

An analysis of pressure and stress distribution under rigid Bridgman-type anvils, J. W. Jackson and M. Waxman, *Book, High-Pressure Measurement, pp. 39–58, ed. Giardini and Lloyd (Butterworth, London, England, 1963).*
Analytical expressions are derived for the pressure and stress distribution in a short cylinder compressed by Bridgman type anvils, assuming the anvils to be rigid plates. The short cylinder is considered to be composed of an inner cylinder bound by an outer shell. The deformation for each may be elastic or plastic.

Thermal radiation properties of solids at low temperatures, R. J. Corruccini (*Symp. Measurement of Thermal Radiation Properties of Solids, Dayton, Ohio, Sept. 5–7, 1962*), *Natl. Aeron. and Space Admin. SP–31, Session II, Paper 4, p. 33 (1963).*
This paper provides introductory remarks for a symposium session on thermal radiation properties of solids in the range 0°–200°K. A qualitative description is given of that part of the theory that is unique to low temperatures, after which experimental methods appropriate to low temperatures and present applications of low temperature data are mentioned.

Periodic heat flow in a hollow cylinder rotating in a furnace with a viewing port, B. A. Peavy and A. G. Eubanks (*Symp. Measurement of Thermal Radiation Properties of Solids,*

Dayton, Ohio, Sept. 5–7, 1962), Natl. Aeron. and Space Admin. SP–31, Session V, Paper 56, p. 553 (1963).
A rotating-specimen furnace has been designed and constructed for use in determining the thermal emittance, both spectral and total, of materials in the temperature range 1300° to 1800°K. In this apparatus, a hollow cylindrical specimen is rotated at constant speed in a concentric cylindrical furnace with heated walls, and the radiant flux from the specimen surface is measured as it passes a small viewing port.
An analytical method is given for estimating the surface temperature of the specimen as a function of rotation speed, thermal properties of the specimen material, and system geometry.
The apparatus is described, and data obtained with the specimen rotating at slow speeds are compared with values predicted by the analytical method.

A mechanism for the production of certain types of very-low-frequency emissions, S. F. Hansen, *J. Geophys. Res.* **68,** *No. 21, 5925–5935 (Nov. 1, 1963).*
It has been shown that some types of VLF emissions (hooks, risers, and falling tones) may be the result of cyclotron emission by energetic electrons trapped in the earth's magnetic field. Observational evidence suggests that a relatively intense electromagnetic whistler-mode wave may be necessary to trigger each such emission. An interaction mechanism is proposed by which certain electrons may couple with a wave already propagating along the same line of force. A gyroresonance is established which organizes the electrons so that cyclotron radiation can be coherent. A change in phase relationship occurs for those electrons that have a longitudinal velocity component such that the Doppler-shifted frequency of the whistler wave seen by the electron is equal or nearly equal to the electron gyrofrequency. This condition is met by electrons moving in a direction opposite to the whistler wave and is satisfied only over a certain fraction of the line of force. Observations also show instances of a sudden change in slope of the rising tail of a hook or other VLF emission at the crossing of the spectrums of the emission and a whistler. This change is interpreted as the effect of the encounter of a whistler with the electron stream that changes both energy and pitch angle of the emitting electrons.

Method for comparing two nearly equal potentials directly in parts per million, C. J. Saunders, *Rev. Sci. Instr.* **34,** *No. 12, 1452–1453 (Dec. 1963).*
T. M. Dauphinee has described a very useful technique for the comparison of potential differences present at different points in an electrical network. In its usual form, a capacitor is connected between the central poles of a *dpdt* chopper and is alternately connected across the two potential differences to be compared. Equal values may be indicated by nulling the galvanometer of the potentiometer which is in the circuit to one of the two potential differences, while differences may be measured by the insertion of a known emf in the circuit with the galvanometer.
The purpose of the present paper is to describe a major improvement in the above technique in which the potential difference is indicated directly in the calibration of an adjustable capacitor, without the necessity for indicating instruments in the circuit or for calculation.

Plasma resonances in the upper ionosphere, W. Calvert and G. B. Goe, *J. Geophys. Res.* **68,** *No. 22, 6113–6120 (Nov. 15, 1963).* Plasma resonances, detected in the upper atmosphere with the Alouette topside sounder satellite, have been examined. The resonant frequencies have been found to be f_N and $(f_N^2 + f_H^2)^{1/2}$, where f_N is the plasma frequency and f_H is the electron gyrofrequency. The two resonances are attributed to electron oscillations along and across the earth's magnetic field, respectively.

An operational information retrieval system in the field of cryogenics, N. A. Olien, *Proc. Am. Documentation Inst. pp. 157–158 (Chicago, Ill., Oct. 1963).*
A mechanized information retrieval system based on a coordinate index of two types of generically related terms has been developed and placed in operation. A thesaurus of these terms has been compiled along with a set of rules for its proper use. The coded information for documents is written on a magnetic tape which is later searched by means of a digital computer. The referencing information for documents is stored on punched paper tapes from which bibliographies on the low temperature properties of solids and fluids are prepared.

Thermocouple and radiation thermometry above 900 °K, H. J. Kostkowski and G. W. Burns (*Symp. Measurement of Thermal Radiation Properties of Solids, Dayton, Ohio, Sept. 5–7, 1963), Natl. Aeron. and Space Admin.* **SP-31,** *Session I, Paper 3, p. 13 (1963).*
This paper reviews the principles of thermocouple and radiation thermometry above 900 °K, the present day precision and accuracy and the commerical instruments currently available. The International Practical Temperature Scale and the Thermodynamic Kelvin Temperature Scale are briefly described. With regard to thermocouples, the presentation is confined to the more generally accepted base metal, noble and refractory metal types. Characteristics such as temperature range, stability and environmental limitations will be emphasized. The optical pyrometry section includes a discussion of emittance corrections, recommendations for using visual optical pyrometers and the status of photoelectric optical pyrometers. Finally, two color, three color and total radiation pyrometers are discussed; primarily to show that, in spite of the recent interest in these instruments, they are not generally as suitable for measuring temperature as optical (single color) pyrometers.

Coefficient of thermal expansion and Young's modulus for a one-dimensional model of a solid, J. Mazur and R. J. Rubin, *Am. J. Phys.* **34,** *No. 11, 835–836 (Nov. 1963).*
The classical statistical mechanical theory of one-dimensional systems of particles which interact only with their nearest neighbors is applied to a simple model of a solid. The relative distance between neighboring particles is limited to a finite range by the form of the assumed interaction potential. The virtue of the model is that simple exact expressions are obtained for the coefficient of thermal expansion and Young's modulus when the pressure on the system is zero.

Investigation of shallow reference cavities for high-temperature emittance measurements, D. G. Moore (*Symp. Measurement of Thermal Radiation Properties of Solids, Dayton, Ohio, Sept. 5–7, 1962), Natl. Aeron. and Space Admin.* **SP–31,** *Session V, Paper 52, p. 515 (1963).*
Total normal emittance measurements were made on small specimens with shallow reference holes of circular cross section. The ratio of the radiant flux density from the surface to the flux density from the hole was measured and this value then converted to emittance by a theoretical expression based on hole dimensions. The expression applies only to diffusely reflecting materials.
Measurements were made on four different diffusely reflecting materials. Specimens of oxidized nickel that had reference holes with depth-to-radius ratios of 1.7 to 3.7 gave corrected total normal emittance values at 1350° K in the range 0.85 to 0.87. The emittance of oxidized Inconel, when determined for a specimen with a reference hole having a depth-to-radius ratio of 1.7, was found to be in good agreement with values obtained by a heated strip method. The emittance measurements on four sintered alumina specimens varied from 0.43 to 0.47 when measured in air at 1375° K.
The determined emittance for a polished specimen of high-purity graphite with a shallow reference hole increased with temperature linearly from 0.59 at 1100° K to 0.74 at 2150° K. These values were in good agreement with those reported for polished graphite when measured by the rotating specimen method.

An approach to thermal emittance standards, J. C. Richmond, W. N. Harrison, and F. J. Shorten (*Symp. Measurement of Thermal Radiation Properties of Solids, Dayton, Ohio, Sept. 5–7, 1962), Natl. Aeron. and Space Admin.* **SP–31,** *Session IV, Paper 41, p. 403 (1963).*
A double-beam ratio-recording infrared spectrometer was modified to record directly the normal spectral emittance of strip specimens that are heated by passing a current through

them. A laboratory blackbody furnace and a hot specimen at the same temperature serve as sources for the respective beams. Temperature equalization is achieved by means of a differential thermocouple. Automatic data-processing equipment corrects for "zero-line" and "100%-line" errors on the basis of previously-recorded calibrations, and also computes from the spectral data, as the measurement progresses, total emittance or absorptance for radiant energy having any known spectral distribution of flux.

Electron monochromator utilizing the scattering resonance in helium, J. A. Simpson, C. E. Kuyatt, and S. R. Mielczarek, *Rev. Sci. Instr.* **34,** *1454–1455 (Dec. 1963).*
The 19 eV elastic scattering resonance in He is observed using the same resonance as an electron monochromator. The limits of the method are indicated.

Synchronization of two remote atomic time scales, J. A. Barnes and R. L. Fey, *Proc.* **IEEE 51,** *1665 (Nov. 1963).*
An improved method of keeping atomic time based on the United States Frequency Standard was put into operation. This involved relocating the time accumulation function from Beltsville, Maryland, to Boulder, Colorado, maintaining synchronization by means of a portable clock measurement.

Room temperature oxidation of iron at low pressure, J. Kruger and H. T. Yolken, *Corrosion* **20,** *No. 1, 29t–33t (Jan. 1964).*
The oxidation of high purity iron surfaces at 300° K prepared under ultrahigh-vacuum conditions was studied using ellipsometry to measure film thickness. By working at low oxygen pressures (between 10^{-7} to 10^{-4} Torr) it was found that the early stages of the oxidation process followed a linear growth law with rate being proportional to the pressure. This behavior is in agreement with a picture proposed by Cabrera. The sticking probability of oxygen in the pressure range studied was of the order of 5×10^{-3}. Traces of water vapor lowered the limiting thickness approached in the non-linear oxidation stage to 18 Å from the 26 Å found at all pressures for dry oxygen.

Choking two-phase flow of hydrogen: Some idealized solutions, R. V. Smith, *Proc. Nuclear Propulsion Conf., Aug. 15–17, 1962, Monterey, Calif., pp. 114–125 (1963).*
Solutions are presented for choking, two-phase flow using models intended to bracket the actual flow cases. Models used are for homogeneous and separated-flow patterns, assuming thermal equilibrium and metastable conditions. Mass-limiting flow is predicted at the point of choking and for Fanno and isentropic flow processes.
Final results are presented on charts to provide for a rapid determination of critical flow conditions for each model.

Two-crystal scintillation pair-spectrometer, B. Ziegler, J. M. Wyckoff, and H. W. Koch, *Nuclear Instr. Methods* **24,** *301–315 (Feb. 13, 1964).*
A total absorption X-ray spectrometer has been developed in which a coincidence requirement selects only those X-ray photons that have produced an electron-positron pair near the surface of a large sodium-iodide scintillation spectrometer. The X-ray energy resolution of the spectrometer that results is 2% and the detection efficiency is about 6% for 17.6 Mev Li^7 (p, γ) rays. Measurements and calculations of resolutions and efficiencies for 6 to 100 Mev photons are given as well as an illustration of the spectrometer application to the measurement of synchrotron bremsstrahlung spectra transmitted by long absorbers.

The use of an analog computer in side-on arc spectroscopy, J. B. Shumaker, Jr., and C. R. Yokley, *Appl. Opt.* **3,** *No. 1, 83–87 (1964).*
An analog computer which solves Abel's integral equation is described and its application to the side-on spectroscopic study of high current arcs is illustrated. By its use radially resolved spectra of cylindrically symmetric inhomogeneous sources are obtained with the same speed and simplicity as are spectra of homogeneous sources. Comparison of NI transition probability measurements using this computer with those using conventional numerical radial resolution techniques indicates that the computer errors are negligible.

Behavior of filamentous materials subjected to high-speed tensile impact, J. C. Smith, C. A. Fenstermaker, and P. J. Shouse, *Symp. Dynamic Behavior of Materials, ASTM Spec. Tech. Publ. 336, 47–69 (1962).*
When a filamentous material is subjected to an impact either transversely or longitudinally in tension, a strain wave is produced which propagates along the filament away from the point of impact. If this strain wave is sufficiently small the behavior of the material can be characterized by stress-strain and specific breaking energy data. A transverse-impact tester and a rotating disk longitudinal impact tester, both operating at impact speeds up to 70 m/sec, are used for this purpose.
When the magnitude of the strain wave is large, the material may be characterized by its stress-strain data and critical breaking velocity. These data are obtained by studying photographically the configurations and strain distributions in filaments struck transversely by rifle bullets at velocities up to 900 m/sec.
These methods are illustrated by data obtained on textile yarns, copper wires, and paper. The results are compared with theoretical predictions and the agreements and differences discussed.

Interlaboratory evaluation of procedures for tongue-tearing strength of woven fabrics, E. B. Randall, Jr., *Mater. Res. Std.* **4,** *No. 2, 53–61 (Feb. 1964).*
Procedures using either pendulum-type instruments or inertialess-type instruments for the measurement of the tongue tearing strength of woven fabric have been evaluated on an interlaboratory basis by use of the statistical technique of the linear model developed by Mandel and Lashof. The various sources of variability in the test procedures are examined. The results are interpreted in terms of this statistical model. The procedures using the inertialess-type instruments were found to be superior to those using the pendulum-type instruments. Two procedures used with the inertialess-type instruments, one using the five highest peaks from separate portions of the autographic record, and the other using the integrator reading, were found to have low within- and between-laboratory variability. Four pendulum-type instruments, a procedure in which the five highest peaks are averaged was found to be adequate for control use within one laboratory. Values of precision are reported for within- and between-laboratory comparisons of test results.

The standard potential of the silver-silver chloride electrode in water-mannitol solutions at 25°, M. Paabo and R. A. Robinson, *J. Phys. Chem.* **67,** *2801 (1963).*
The standard electrode potentials of the silver-silver chloride electrode at 25°C in 10 and 15 wt. % mannitol has been determined. They are found to be 0.21638 V and 0.21310 V respectively. The relation between the standard potential and the nature of the solvent is discussed.

Calibration of potentiometers by resistance bridge methods, D. Ramaley, *Instr. Control Systems* **37,** *106–108 (Jan. 1964).*
The use of the Universal Ratio Set is described in making up resistance bridge arrangements suitable for potentiometer circuit calibrations. A comprehensive list of references is given for the benefit of those desiring a more detailed explanation of procedures.

The melting (contraction) and recrystallization of fibrous proteins in non-aqueous media, L. Mandelkern, G. Canty, and A. F. Diorio, *J. Phys. Chem.* **67,** *No. 12, 2882–2884 (Dec. 1963).*
The melting (contraction) and recrystallization of the fibrous protein elastoidin in a non-aqueous medium has been demonstrated. A comparison of the thermodynamic stability, as indicated by the melting temperature of the polymer system, was made between the non-aqueous medium and water.
The ordered polymeric system was shown to have greater stability in the pure non-aqueous medium indicating that no inherent stability is endowed to the structure by water.

LiBr-ethylene glycol solutions were shown to be more effective than LiBr aqueous solutions in lowering the melting temperature. This result is consistent with the concept of having a greater number of effectively free ions to interact with the polymer chain.

Inductive voltage dividers with calculable relative corrections, T. L. Zapf, C. H. Chinburg, and H. K. Wolf, *IEEE Trans. Instr. Meas.* **IM-12,** *No. 2, 80–85 (Sept. 1963).*
A solution using network equations has been obtained for the corrections to the relative errors of inductive voltage dividers of specific design. Earlier theoretical considerations, confirmed by measurements of limited accuracy, indicated an S-shaped curve of ratio error versus nominal ratio and quadrature component versus nominal ratio. The results from recent calculations are in agreement with the earlier measurements and provide much better definition of the true shape of the S-curve. An algebraic equation has been derived for the limiting form of this S-shaped characteristic curve. A resistance analog of an inductive voltage divider was constructed to represent the lumped circuit parameters equivalent to the distributed shunt admittances and the winding impedances. Measurements of the gross errors in the analog have yielded experimental results in excellent agreement with those calculated from the network equations.

The meaning of "least" in least squares, C. Eisenhart, *J. Wash. Acad. Sci.* **54,** *No. 2, 24–33 (Feb. 1964).*
The Method of Least Squares was developed originally from three distinctly different points of view: (1) Least Sum of Squared Residuals (Legrendre, 1805), (2) Maximum probability of Zero Error of Estimation (Gauss, 1809), and (3) Least Mean Squared Error of Estimation (Gauss, 1821). These differ not only in their aims and in their initial assumptions, but also in the meanings that they attach to the numbers that all three yield as a common answer to any given problem. The evolution and implications of each of these three approaches to "Least Squares" are outlined.

Thermal expansion of silver iodide, A. Bienenstock and G. Burley, *J. Phys. Chem. Solids* **24,** *1271–1278 (Apr. 1963).*
The thermal expansion of silver iodide with the zincblende structure has been measured by X-ray diffraction techniques in the temperature range 4.2 to 300° K. Although dependent on sample preparation, it is negative to approximately 80° K, positive in the range 80° K to 110° K, and then attains a constant negative high temperature value. This expansion is explained in terms of a model which shows the dependence of thermal expansion on structure and bonding. It is shown that the primary role of covalency, in its contribution to the low-temperature contraction, is to reduce the interaction between next-nearest neighbors. The particular form of the interatomic interaction appears to contribute primarily to the balance between modes with positive and negative Gruneisen factors. In the case of AgI, it is the large n in the nearest neighbor repulsive interaction, r^{-n}, which accounts for the negative high temperature limit. The positive thermal expansion at intermediate temperatures is the result of transverse optical modes with lower frequencies than transverse acoustic modes.

Radiation-induced polymerization at high pressures, L. A. Wall and D. W. Brown, *J. Polymer Sci.: Pt. C, No. 4, 1151–1160 (1963).*
Several radiation-induced polymerization reactions were investigated at pressures between 5,000 and 17,000 atmospheres and temperatures between 20° C and 275° C. The most detailed studies have been with propylene and *n*-tetradecafluoroheptene-1. With both monomers the variation of rate of polymerization, R_p, with temperature and radiation intensity is consistent with a free radical mechanism. The maximum number of monomer units converted to polymer per 100 electron volts absorbed, G(M), is 108,000 and 7,600 in the polymerization of propylene and the heptene, respectively; thus the kinetic chains are long. However, the number-average degree of polymerization, DP_n, is low, the maximum values being about 75 in both polymerization. In the polymerization of propylene, transfer to monomer limits DP_n; the transfer constant becomes greater as temperature increases or pressure decreases. In the polymerization of the heptene, DP_n is determined by both transfer and termination. In the later polymerization both R_p and DP_n first increase and then decrease as the temperatures is raised at constant pressure because the depolymerization rate becomes appreciable at high temperature and reduces the observed R_p.

Use of photographic film for personnel dosimetry; basic physical considerations, M. Ehrlich, *Symp. Personnel Dosimetry Techniques for External Radiation, Apr. 1–5, 1963, Madrid, Spain, pp. 49–74 (Dec. 1963).*
The physical principles of the response of photographic film to high-energy ionizing radiation and of the use of photographic film for radiation dosimetry form the main topics of this paper. After some introductory remarks on the photographic emulsion and the photographic process, the interaction of high-energy radiation with the photographic emulsion is reviewed in general terms, with special emphasis on the dependence of grain developability on energy fluence and energy flux density. The processes involved in the interaction of photons, electrons, and neutrons with the photographic emulsion are then treated separately, under consideration of specific characteristics of the photographic effect of these particles. A comparison of the photographic sensitivity to photons, electrons, and neutrons concludes the first part of the paper.
The second part of the paper is devoted to a review of special problems encountered in photographic dosimetry. Errors in photographic dosimetry due to reciprocity failure, solarization, fading, and due to energy dependence of the photographic sensitivity are discussed and methods are outlined to reduce these errors. Current accuracy limits are given in conclusion.

Antireciprocity and memory in the statistical approach to irreversible thermodynamics, R. E. Nettleton, *J. Chem. Phys.* **40,** *No. 1, 112–116 (Jan. 1964).*
The macroscopic state of a large, closed system is specified by the ensemble averages α_j of a set of even dynamical variables A_j, together with the averages v_j of the quantities iLA_j, obtained by operating on the A_j with the self-adjoint Liouville operator L. Phenomenological equations for the time rates of change, $\dot{\alpha}_j$ and $\dot{v}_j$, are derived by a technique due to Zwanzig, in which one operates on Liouville's equation with a projection operator which projects out the part which is "relevant" to the phenomenological description employed. These phenomenological equations are shown to exhibit the Onsager-Casimir reciprocity relations, including antisymmetry relations whose derivation is found to require a slight modification of Zwanzig's mathematical assumptions. Since $v_j = \dot{\alpha}_j$, these equations also show that irreversible thermodynamics can be extended to the case where second-order time derivatives appear representing memory effects, as well as nonlinear terms in the α_j, provided the equations are still required to be linear in the v_j. Furthermore, Onsager's equations are obtained while allowing the phenomenological matrices to be functions of the variables α_j, and not merely of constants of the motion. This serves to generalize and extend Zwanzig's earlier treatment.

Some aspects of the mechanical properties of high polymers, H. Leaderman (*Proc. Conf. Mechanical Properties of Wood, Univ. Calif., Berkeley, Calif., Aug. 27–Sept. 1, 1962*), *Book, The Mechanical Behavior of Wood, pp. 43–83 (1963).*
Classical infinitesimal elasticity theory is introduced from the viewpoint of continuum mechanics. The constitutive equation is modified in two ways to introduce linear viscoelasticity from respectively the integral and differential operator formulations, phenomena associated with main-chain relaxation and secondary relaxation are considered, including the effects of temperature and relative humidity. Non-linear viscoelastic behavior is briefly discussed.

Impact noise in multifamily dwellings, R. D. Berendt, *Bldg. Res.* **1,** *No. 1, 40–42 (Jan.–Feb. 1964).*
An analysis of a large number of noise complaints indicates that the most prevalent problem in multifamily dwellings is one of impact noise control. The most common cause of

complaint is impact noise produced by foot traffic, dropping objects and sliding furniture. Plumbing noises ranked second in order of disturbance, followed by hallway noises, such as door slams, staircase traffic etc. Airborne noise primarily from sources such as radio, television and stereo sets, ranked fourth in importance. The noise control problem as found in multifamily dwellings is broad in scope, affecting not only the occupants but architects, builders, owners, investors and governmental agencies as well. Other factors which bear on the problem such as building techniques, apartment types, income brackets etc. are discussed.

Concentration-dependent diffusion coefficient of water in glass, W. Haller, *Phys. Chem. Glasses* **4**, *No. 6, 217–220 (Dec. 1963).*

The evaluation of diffusion coefficients by taking sorption measurements and concentration profiles is critically reviewed in the light of diffusion mathematics. Simple sorption measurements are insufficient to distinguish between various types of concentration-dependences of diffusion coefficients. While it is often assumed that the transport of water into silicate glasses is governed by a constant diffusion coefficient, theoretical considerations suggest a strongly concentration dependent coefficient. It is shown that the mechanism is further complicated by a pressure gradient which develops as a consequence of the diffusion process. The effect of the pressure gradient upon the diffusion process depends upon the ability of the system to release stress by flow relaxation and is therefore a function of the temperature. By applying a simplified schlieren-method to highly siliceous volcanic glass which had been exposed to atmospheric water vapor for 2000 years, its water concentration profile is reconstructed. The profile confirms that the diffusion coefficient is a function of water concentration.

Other NBS Publications

Journal of Research 68A (Phys. and Chem.), No. 3 (May–June 1964), 70 cents.

Compressibility of natural rubber at pressures below 500 kg/cm². L. A. Wood and G. M. Martin. (See above abstracts.)

A copolymer with lamellar morphology. R. K. Eby.

Variation of glass temperature with pressure in polypropylene. E. Passaglia and G. M. Martin.

Perfluorophenyl ether and related polymers. W. J. Pummer and L. A. Wall.

Cyclic polyhydroxy ketones II. *xylo*-Trihydroxycyclohexenediolic acid and keto-inositols. A. J. Fatiadi and H. S. Isbell.

Tritium-labeled compounds. XI. Mechanism for the oxidation of aldehydes and aldoses-*1-t* with sodium chlorite. H. S. Isbell and L. T. Sniegoski.

Medium effects on the dissociation of weak acids in methanol-water solvents at 25 °C. E. E. Sager, R. A. Robinson, and R. G. Bates.

Crystallization of anhydrous copper sulfate from sulfuric acid-ammonium sulfate mixtures. P. M. Gruzensky.

Detection of lattice deformation and recovery in epsilon phase silver-tin alloys. R. M. Waterstrat and G. E. Hicho.

Vapor pressures of ruthenium and osmium. N. J. Carrera, R. F. Walker, and E. R. Plante.

The 0–2 transition of CO in condensed oxygen, nitrogen, and argon. S. Abramowitz and H. P. Broida.

Journal of Research 68A (Phys. and Chem.), No. 4 (July–Aug. 1964), 70 cents.

Metallographic characterization of an NBS spectrometric low-alloy steel standard. R. E. Michaelis, H. Yakowitz, and G. A. Moore.

X-ray investigation of strain in cold-worked silver iodide. G. Burley.

Light scattering measurements on solutions of some quaternary ammonium salts. S. P. Wasik and W. D. Hubbard.

Thermodynamic properties of some methylphosphonyl dihalides from 15 to 335 °K. G. T. Furukawa, M. L. Reilly, J. H. Piccirelli, and M. Tenenbaum.

Calorimetric properties of some alkali pentaborate hydrates from 15 to 370 °K. G. T. Furukawa, M. L. Reilly, and J. H. Piccirelli.

Rates of adsorption and desorption of polystyrene on chrome surface. R. R. Stromberg, W. H. Grant, and E. Passaglia.

An iterative unfolding procedure. R. P. Uhlig.

Mass spectrometric study of photoionization. I. Apparatus and initial observations on acetylene, acetylene—d_2, benzene and benzene—d_6. V. H. Dibeler and R. M. Reese.

Journal of Research 68B (Math. and Math. Phys.), No. 2 (Apr.–June 1964), 75 cents.

Determinations based on duplication of readings. J. A. Speckman. (See above abstracts.)

General application of Youden's rank sum test for outliers and tables of one-sided percentage points. T. A. Willke. (See above abstracts.)

A generalization of Rennie's inequality. A. J. Goldman.

On the asymptotic joint normality of quantiles from a multivariate distribution. L. Weiss.

Fitting $y=\beta x$ when the variance depends on x. J. Van Dyke. (See above abstracts.)

Existence of k-edge connected ordinary graphs with prescribed degrees. J. Edmonds.

Inequalities for solutions of mixed boundary value problems for elastic plates. J. H. Bramble and L. E. Payne. (See above abstracts.)

Radio Sci. J. Res. NBS/USNC–URSI 68D, No. 5 (May 1964), $1.00.

URSI National Committee Report, XIV General Assembly, Tokyo, September 1963:

Commission 1. Radio measurement methods and standards.

Commission 2. Tropospheric radio propagation.

Commission 3. Ionospheric radio.

Commission 4. Magnetospheric radio.

Commission 5. Radio and radar astronomy.

Commission 7. Radio electronics.

Radio Sci. J. Res. NBS/USNC–URSI 68D, No. 6 (June 1964) $1.00.

Electrical properties of sea ice at 0.1 to 30 Mc/s. F. L. Wentworth and M. Cohn. (See above abstracts.)

ELF and VLF waves below an inhomogeneous anisotropic ionosphere. J. Galejs.

The effects of a small local change in phase velocity on the propagation of a VLF radio signal. D. D. Crombie.

Auroral-zone absorption effects on an HF arctic propagation path. R. D. Hunsucker.

Amplitude-probability distribution of atmospheric radio noise. P. Beckmann.

An approximate method for computing diffraction patterns caused by ionospheric irregularities. R. Gagnon.

Wave propagation in stratified random media. Y. M. Chen. (See above abstracts.)

Radar scattering from coated perfect conductors: application to the semi-infinite cone and use of exact eikonal. H. Überall.

Radio Sci. J. Res. NBS/USNC–USRI 68D, No. 7 (July 1964), $1.00.

Leader and junction processes in the lightning discharge as a source of VLF atmospherics. H. R. Arnold and E. T. Pierce.

The return stroke of the lightning flash to earth as a source of VLF atmospherics. A. S. Dennis and E. T. Pierce.

VLF propagation in a compressible ionosphere. R. B. Kieburtz.

A spectrographic interferometer. R. H. Lee and J. W. Warwick. (See above abstracts.)

Effect of lossy earth on antenna gain, part II. W. L. Curtis.

Calculation of groundwave attenuation in the far diffraction region. L. E. Vogler.

Some numerical results based on the theory of radio wave propagation over inhomogeneous earth. K. Furutsu, R. E. Wilkerson, and R. F. Hartmann.

A note on VHF reflection from a tropospheric layer. J. R. Wait.
Some remarks on the use of statistics in radar astronomy. I. Kay.
A meteorological parameter for radioclimatological purposes. P. Misme.

Radio Sci. J. Res. NBS/USNC–URSI 68D, No. 8 (August 1964), $1.00.
Extension of cosmic noise absorption measurements to lower frequencies, using polarized antennas. C. G. Little, G. M. Lerfald, and R. Parthasarathy.
Broadband radio-star scintillations, part I. Observations. D. G. Singleton.
F-region irregularities studied by scintillation of signals from satellites. K. C. Yeh and G. W. Swenson, Jr.
Angels, insects, and weather. A. H. LaGrone, A. P. Deam, and G. B. Walker.
Measurement of the attenuation of radio signals by jungles. J. W. Herbstreit and W. Q. Crichlow.
Influence of a circular ionospheric depression of VLF propagation. J. R. Wait.
An experimental study of mixed-path groundwave propagation. S. W. Maley and H. Ottesen.

Curves of input impedance change due to ground for dipole antennas, L. E. Vogler and J. L. Noble, NBS Mono. 72 (Jan. 31, 1964), 35 cents.
Report of the 48th National Conference on Weights and Measures 1963, NBS Misc. Publ. 254 (Dec. 30, 1963), 75 cents.
1963 Research highlights of the National Bureau of Standards, NBS Misc. Publ. 255 (Dec. 1963), $1.00.
Acrylonitrile-butadiene-styrene (ABS) plastic pipe (SDR–PR and Class T), CS254–63 (July 1, 1963), 10 cents.
Forms for two-way concrete joist floor and roof construction, SPR265–63, 5 cents.
Calculated diffraction effects at VLF from a localized ionospheric depression, J. R. Wait, NBS Tech. Note 208 (Jan. 16, 1964), 15 cents.
An atlas of solar flare effects observed on long VLF paths druing 1961, C. J. Chilton, F. K. Steele, and D. D. Crombie, NBS Tech. Note 210 (Mar. 13, 1964), 30 cents.
Sensitivity indices for Hall generators, S. Rubin and G. J. Rogers, NBS Tech. Note 233 (Feb. 6, 1964), 20 cents.
Knight shifts and line widths of the nuclear magnetic resonance of Pb^{207} in lead-indium alloys, R. J. Snodgrass and L. H. Bennett, Phys. Rev. **132,** 1465–1474 (Nov. 15, 1963).
Numercial solutions of the convolution-hypernetted chain integral equation for the pair correlation function of a fluid. II. The hard-sphere potential, M. Klein, J. Chem. Phys. **39,** No. 6, 1388–1397 (Sept. 15, 1963).
Comparison of the 3-out-of-7 ARQ with Bose-Chaudhuri-Hocquenghem coding systems, M. Nesenbergs, IEEE Trans. Commun. Systems **CS–11,** No. 2, 202–212 (June 1963).
Form and angular distribution of proton groups at about $Q=0$ Mev in the proton spectra of (d,p) reactions of heavy nuclei, J. Pfleger, U. Schmidt-Rohr, V. Spiegel, P. Turek, and W. Zuckschwerdt, Nuclear Physics **48,** No. 1, 22–32 (Sept. 1963).
Calculations of the potential and effective diffusion constant in a polyelectrolyte solution, S. R. Coriell and J. L. Jackson, J. Chem. Phys. **39,** 2418 (1963).
Syntactic integration carried out mechanically, I. Rhodes, Inform. Storage and Retrieval **1,** 215–219 (1963).
Numerical solutions of the convolution-hypernetted chain integral equation for the pair correlation function of a fluid. I. The Lennard-Jones (12,6) potential, M. Klein and M.S. Green, J. Chem. Phys. **39,** No. 6, 1367–1387 (Sept. 15, 1963).
Temperature measurements below 1000°K (Abstract), J. L. Riddle (Symp. Measurement of Thermal Radiation Properties of Solids, Dayton, Ohio, Sept. 5–7, 1962), Natl. Aeron. and Space Admin. **SP–31,** Session 1, Paper 2, p. 11 (1963).
ν_3 vibration of methane in condensed oxygen, nitrogen, and argon, S. Abramowitz and H. P. Broida, J. Chem. Phys. **39,** No. 9, 2383–2384 (Nov. 1, 1963).
The three-body scattering operator in nonequilibrium statistical mechanics, J. Weinstock, Phys. Rev. **132,** No. 1, 470–482 (Oct. 1, 1963).
Oluster formulation of the exact equation for the evolution of a classical many-body system, J. Weinstock, Phys. Rev. **132,** No. 1, 454–469 (Oct. 1, 1963).
Interaction energies and transport coefficients of Li+H and O+H gas mixtures at high temperatures, P. H. Krupenie, E. A. Mason, and J. T. Vanderslice, J. Chem. Phys. **39,** No. 10, 2399–2408 (Nov. 15, 1963).
Inertial effects in the phenomenological theory of thermal diffusion in liquids, R. E. Nettleton, Il Nuovo Cimento **28,** Serie X, 952–969 (Dec. 7, 1962).
Mass spectra and metastable transitions of H_2S, HDS, and D_2S, V. H. Dibeler and H. M. Rosenstock, J. Chem. Phys. **39,** No. 11, 3106–3111 (Dec. 1, 1963).
Computed transmission spectra for 2.7-micron H_2O band, D. M. Gates, R. F. Calfee, and D. W. Hansen, Appl. Opt. **2,** No. 11, 1117–1122 (Nov. 1963).
Spectrum of Nd^{3+} in $LaCl_3$, J. C. Eisenstein, J. Chem. Phys. **39,** No. 9, 2134–2140 (Nov. 1, 1963).
Two assumptions in the theory of attractive forces between long saturated chains, R. Zwanzig, J. Chem. Phys. **39,** No. 9, 2251–2258 (Nov. 1, 1963).
Recent advances in cryogenic engineering, Cryogenic Engineering Laboratory, NBS, Boulder, Chemistry **38,** 8–15 (Oct. 1963).
Binary mixtures of dilute bose gases with repulsive interactions at low temperatures, D. M. Larsen, Ann. Phys. **24,** 89–101 (Oct. 1963).
Highly ionized atoms: The configurations $s^2p^n(n=1, 2, 4, 5)$, F. Rohrlich and C. Pecker, Astrophys. J. **138,** No. 4, 1246–1261 (Nov. 15, 1963).
A plasma instability resulting in field-aligned irregularities in the ionosphere, D. T. Farley, Jr., J. Geophys. Res. **68,** 6083–6097 (Nov. 15, 1963).
Faraday effect in semiconductors, I. M. Boswarva, R. E. Howard, and A. B. Lidiard, Proc. Royal Soc. **A269,** 125–141 (1962).
Annual "Observatory Report" on research at NBS, C. E. Moore and L. M. Branscomb, Astron. J. **68,** No. 9, 658–659 Nov. 1963).
Statistics of irreversible termination in homogeneous anionic polymerization, B. D. Coleman, F. Gornick, and G. Weiss, J. Chem. Phys. **39,** No. 12, 3233–3239 (Dec. 15, 1963).
The structure of gaseous copper (II) nitrate as determined by electron diffraction, R. E. LaVille and S. H. Brauer, J. Am. Chem. Soc. **85,** 3597–3600 (Nov. 1963).
Spectrum of Er^{3+} in $LaCl_3$, J. C. Eisenstein, J. Chem. Phys. **39,** No. 9, 2128–2133 (Nov. 1, 1963).
Large-angle inelastic scattering of 500-keV electrons, J. W. Motz and R. C. Placious, Phys. Rev. **132,** No. 3, 1120–1122 (Nov. 1, 1963).
Zeros of polynomials and fractional order differences of their coefficients, G. T. Cargo and O. Shisha, J. Math. Anal. Appl. **7,** No. 2, 176–182 (Oct. 1963).
The nightglow, F. E. Roach, Book; Advances in Electronics and Electron Physics **18,** 1–44 (Academic Press Inc., New York, N.Y., 1963).
Broadening of the ν_3 lines of HCN due to argon, carbon dioxide, and hydrogen chloride, R. J. Thibault, A. G. Maki, and E. K. Plyler, J. Opt. Soc. Am. **53,** No. 11, 1255–1258 (Nov. 1963).
Vacuum ultraviolet photochemistry. VIII. Photolysis of *n*-butane, H. Okabe, and D. A. Becker, J. Chem. Phys. 39, No. 10. 2549–2555 (Nov. 15, 1963).
NBS activities for the American Rubber Industry, G. M. Kline, L'industria della gomma **VII,** No. 6, 29–33 (June 1963).
Annual "Observatory Report" on research at JILA, L. M. Branscomb, Astron. J. **68,** No. 9, 660–662 (Nov. 1963).
Synthesis and stability of bismutotantalite, stibiotantalite and chemically similar ABO_4 compounds, R. S. Roth and J. L. Waring, Am. Mineralogist **48,** 1348–1356 (Nov–Dec. 1963).

Review of mode theory of radio propagation in terrestrial waveguides, J. R. Wait, Rev. Geophys. **1,** No. 4, 481–505 (Nov. 1963).

Polymorphism of silver iodide, G. Burley, Am. Mineralogist **48,** 1266–1276 (Nov.–Dec. 1963).

Equilibrium pressures of oxygen over $Mn_2O_3 - Mn_3O_4$ at various temperatures, E. M. Otto, J. Electrochem. Soc. **111,** No. 1, 88–92 (Jan. 1964).

First-order perturbation corrections to the Hartree-Fock approximation for helium, A. W. Weiss and J. B. Martin, Phys. Rev. **132,** No. 5, 2118–2122 (Dec. 1, 1963).

The propagation time of a radio pulse, J. R. Johler, IEEE Trans. Ant. Prop. **AP–11,** No. 6, 661–668 (Nov. 1963).

Incoherent inelastic neutron scattering and self-diffusion, R. Zwanzig, Phys. Rev. **133,** No. 1A, A50–A51 (Jan. 6, 1964).

Radiometry, M. M. Reynolds, R. J. Corruccini, M. M. Fulk, and R. M. Burley, Am. Inst. Phys. Handb. 2d ed. 6–153—6–172 (McGraw-Hill Book Co. Inc., New York, N.Y., 1963).

On the relaxation of the hard-sphere Rayleigh and Lorentz gas, K. Andersen and K. E. Shuler, J. Chem. Phys. **40,** No. 3, 633–650 (Feb. 1, 1964).

The ionization constant of *m*-nitrophenol from 5 to 50°, R. A. Robinson and A. Peiperl, J. Phys. Chem. **67,** 2860 (1963).

Transition array for $d^3 \rightarrow d^2p$: vanadium III, H. Mendlowitz, Astrophys. J. **138,** No. 4, 1277–1296 (Nov. 15, 1963).

Calorimetry, G. T. Armstrong, Phys. Today **17,** No. 2, 50–54 (Feb. 10, 1964); Science **143,** No. 3602, 158–163 (Jan. 10, 1964).

Note on the 4-body system, T. Stovall and M. Danos, Physics Letters **7,** No. 4, 278–281 (Oct. 23, 1963).

Observation of optically forbidden transitions in the continuum of the rare gases by electron energy loss measurements, J. A. Simpson, S. R. Mielczarek, and J. Cooper, J. Opt. Soc. Am. **54,** No. 2, 269–270 (Feb. 1964).

On the nature of the crystal field approximation. II. Numerical results, R. T. Berger and C. M. Herzfeld, J. Chem. Phys. **39,** No. 4, 1122–1126 (Aug. 15, 1963).

Normal congruence subgroups of the modular group, M. Newman, Am. J. Math. **LXXXV,** No. 3, 419–427 (July 1963).

The direct determination of the crystal structure of $NaB(OH)_4 \cdot 2H_2O$, S. Block and A. Perloff, Acta Cryst. **16,** No. 12, 1233–1238 (Dec. 1963).

International symposium on the solar spectrum, Utrecht, 26–31, August 1963, C. E. Moore, Appl. Opt. **3,** No. 1, 12 (Jan. 1964).

Penetration of protons, alpha particles, and mesons, U. Fano, Ann. Rev. Nuclear Sci. **13,** 1–66 (Dec. 1963).

Empirical rules for predicting ground-state spins of light nuclei, T. Stovall, Phys. Rev. **132,** No. 2B, B268–B269 (Feb. 27, 1964).

Very-low-frequency radio waves and the ionosphere, D. D Crombie, Science **142,** No. 3591, 508–510 (Oct. 1963).

Mass spectrometric study of the recombination of bromine and chlorine atoms on Pyrex, J. T. Herron, J. Phys. Chem. **67,** 2864 (Dec. 1963).

Coulomb scattering without atomic excitation for 50–, 100–, 200–, and 400-keV electrons, J. W. Motz, R. C. Placious, and C. E. Dick, Phys. Rev. **132,** No. 6, 2558–2561 (Dec. 15, 1963).

Effect of additives on the ionic reaction mechanism in the radiolysis of methane, P. Ausloos, S. G. Lias, and R. Gorden, Jr., J. Chem. Phys. **39,** No. 12, 3341–3348 (Dec. 15, 1963).

Wave functions and oscillator strengths for the lithium isoelectronic sequency, A. W. Weiss, Astrophys. J. **138,** No. 4, 1262–1276 (Nov. 15, 1963).

Studies in scientific and engineering manpower. Part I. Patterns of utilization of scientific and engineering manpower in the United States and certain foreign countries. Part II. Trends in salaries of scientists and engineers, 1948–1962, M. S. Green, U.S. Department of Commerce, Office of the Assistant Secretary of Commerce for Science and Technology Staff Report: 63–1 (Oct. 1963), 40 cents.

Thermal conductivity, R. L. Powell, Am. Inst. Phys. Handb. 2d ed. 4–77—4–101 (McGraw-Hill Publ. Book Co., Inc., New York, N.Y., 1963).

Thermal stability of bis(8-hydroxy-5-quinolyl) methane co-ordination polymers, E. Horowitz and T. P. Perros, J. Inorg. Nucl. Chem. **26,** 139–159 (1964).

Salt effects and medium effects on indicator acid-base equilibria in a methanol-water solvent, D. Rosenthal, H. B. Hetzer, and R. G. Bates, J. Am. Chem. Soc. **86,** 549–554 (Feb. 20, 1964).

Pyrolysis of polytrifluoroethylene: influence of gamma radiation and alkali treatment, S. Straus and L. A. Wall, SPE Trans. **4,** No. 1, 61–65 (Jan. 1964).

Some properties of polystyrene networks formed from oriented chains, J. C. Halpin and L. Mandelkern, J. Polymer Sci.: Pt. B, **2,** 139–142 (1964).

Theory of irreversible processes in a plasma—derivation of a convergent kinetic equation from the generalized master equation, J. Weinstock, Phys. Rev. **133,** No. 3A, A673–A680 (Feb. 1964).

English translation of the Book, Vapor Pressure of the Chemical Elements, by A. N. Nesmeyanov, Editor, R. Gary, 462 pages (Elsevier Publ. Co., New York, N.Y., 1964).

Photolysis of cellulose in a vacuum with 2537 A light, J. H. Flynn and W. L. Morrow, J. Polymer Sci.: Pt. A, **2,** 81–89 (1964).

Pair correlations in closed-shell systems, M. Krauss and A. W. Weiss, J. Chem. Phys. **40,** No. 1, 80–85 (Jan. 1, 1964).

On an extreme rank sum test for outliers, W. A. Thompson, Jr., and T. A. Wilke, Biometrika **50,** No. 3–4, 375–383 (1963).

Microwave spectrum of lithium chloride, D. R. Lide, Jr., P. Cahill, and L. P. Gold, J. Chem. Phys. **40,** No. 1, 156–159 (Jan. 1, 1964).

Preparation and properties of difluoroborane, T. D. Coyle, J. J. Ritter, and T. C. Farrar, Proc. Chem. Soc. (London), p. 25 (Jan. 1964).

Theoretical studies on signal-to-noise characteristics of an FM system, H. Akima, IEEE Trans. Space Electron. Telemetry **SET–9,** No. 4, 101–108 (Dec. 1963).

Translational dispersion in gases, M. Greenspan, Estratto da Rendiconti della Scuola Internazionale di Fisica, E. Fermi **XXVII** Corso, 73–100 (1963).

Preparation of lantern slides, L. S. Taylor, Health Phys. J. **9,** No. 10, 1009–1011 (Oct. 1963).

A survey of ionospheric effects upon earth-space radio propagation, R. S. Lawrence, C. G. Little, and H. J. A. Chivers, Proc. IEEE **52,** No. 1, 4–27 (Jan. 1964).

Statistical thermodynamics of the lattice model of a polymer molecule, J. Mazur, J. Chem. Phys. **40,** No. 4, 1001–1007 (Feb. 15, 1964).

Standards, sources, and detectors in radiation measurements, R. Stair and W. E. Schneider, Symp. Thermal Radiation of Solids, Session III. Measurement Techniques (San Francisco, Calif., Mar. 4–6, 1964), Paper 3 (1964).

Problems in the application of norms of external radiation, L. S. Taylor, Symp. Personnel Dosimetry Techniques for External Radiation, Madrid, Spain, Apr. 15, 1963, pp. 35–47 (1963).

Pyrolysis of new fluoropolymers, S. Straus and L. A. Wall, SPE Trans. **4,** No. 1, 56–60 (Jan. 1964).

The surface composition of hydroxylapatite derived from solution behavior of aqueous suspensions, V. R. Deitz, H. M. Rootare, and F. G. Carpenter, J. Colloid Sci. **19,** No. 1, 87–101 (Jan. 1964).

The gas phase radiolysis of propane. Effect of pressure and added inert gases, P. Ausloos, S. G. Lias, and I. B. Sandoval, Discussions Faraday Soc. No. 36, pp. 66–74 (1963).

Infrared spectra of HCN from 2000 to 3600 cm^{-1}, A. G. Maki and L. R. Blaine, J. Mol. Spectry. **12,** No. 1, 45–68 (Jan. 1, 1964).

Second acid dissociation of N,N-Di-(2-hydroxyethyl)-glycine and related thermodynamic quantities from 0 to 55°, S. P. Datta, A. K. Grzybowski and R. G. Bates, J. Phys. Chem. **68,** No. 2, 275–280 (Feb. 1964).

Effects of deuteration and temperature upon the photolysis of cellulose in a vacuum with 2537 A light, J. H. Flynn and W. L. Morrow, J. Polymer Sci.: Pt. A, **2,** 91–103 (1964).

Polarons in an electric field, D. M. Larsen, Phys. Rev. **133,** No. 3A, A860–A866 (Feb. 3, 1964).

The effect of carbon-arc intensity on asphalt oxidation, J. R. Wright, P. G. Campbell, and T. L. Fridinger, J. Appl. Chem. **14,** 30–35 (Jan. 1964).

Structure beyond the ionization limit in inelastic electron scattering in the rare gases, C. E. Kuyatt and J. A. Simpson, Proc. 6th Intern. Symp. Ionization Phenomena in Gases IA11, 33–35 (Paris, 1964).

Statistics in its proper place, W. J. Youden, J. Wash. Acad. Sci. **54,** 53–57 (1964).

Spectroradiometry by means of modified spectrophotometers, H. K. Hammond III, Appl. Opt. **2,** No. 11, 1207–1208 (Nov. 1963).

Absolute oscillator strengths for Fe I, C. H. Corliss and B. Warner, Astrophys. J. Suppl. Ser. No. 83, **VIII,** 395–438 (Feb. 1964).

**Publications for which a price is indicated are available by purchase from the Superintendent of Documents, U.S. Government Printing Office, Washington, D.C., 20402 (foreign postage, one-fourth additional). Reprints from outside journals and the NBS Journal of Research may often be obtained directly from the authors.*

UNIVERSITY MICROFILMS INC
EDITORIAL DEPARTMENT
313 NORTH FIRST ST
ANN ARBOR MICH
SJR-C JUNE

UNITED STATES
GOVERNMENT PRINTING OFFICE
DIVISION OF PUBLIC DOCUMENTS
WASHINGTON, D.C. 20402

OFFICIAL BUSINESS

PENALTY FOR PRIVATE USE TO AVOID PAYMENT OF POSTAGE, $300 (GPO)

JOURNAL OF RESEARCH of the National Bureau of Standards
C. Engineering and Instrumentation

Vol. 68C, No. 3 July–September 1964

Contents

	Page
Response of highly precise balances to thermal gradients. L. B. Macurdy.	135
A direct-reading two-knife 50-pound balance of high precision suitable for State weights and measures laboratories. H. E. Almer, H. A. Bowman, M. W. Jensen, L. B. Macurdy, H. S. Peiser, and B. Wasko.	141
Wave front shearing prism interferometer. J. B. Saunders.	155
A new high resolution small-angle x-ray camera. H. Brumberger and R. Deslattes.	173
Experimental determination of air drag on a textile yarn struck transversely by a high-velocity projectile. Jack C. Smith, Carl A. Fenstermaker, and Paul J. Shouse.	177
Publications of the National Bureau of Standards.	183

Library of Congress Catalog Card Number: 62-3900

For sale by the Superintendent of Documents, U.S. Government Printing Office, Washington, D.C., 20402. Price 75 cents (single copy). Subscription price: $2.25 a year; 50 cents additional for foreign mailing.

UNITED STATES GOVERNMENT PRINTING OFFICE, WASHINGTON : 1964